

# **Control of Retrograde Signaling by Protein Import and Cytosolic Folding Stress**

**Guo-Zhang Wu<sup>1</sup>, Etienne H. Meyer<sup>1,4</sup>, Andreas Richter<sup>2</sup>, Maja Schuster<sup>1</sup>, Qihua Ling<sup>3</sup>, Mark A. Schöttler<sup>1</sup>, Dirk Walther<sup>1</sup>, Reimo Zoschke<sup>1</sup>, Bernhard Grimm<sup>2</sup>, R. Paul Jarvis<sup>3</sup>, and Ralph Bock<sup>1\*</sup>**

<sup>1</sup>Max-Planck-Institut für Molekulare Pflanzenphysiologie, Am Mühlenberg 1, D-14476 Potsdam-Golm, Germany

<sup>2</sup>Institute of Biology/Plant Physiology, Humboldt-Universität zu Berlin, Unter den Linden 6, 10099 Berlin, Germany

<sup>3</sup>Department of Plant Sciences, University of Oxford, South Parks Road, Oxford OX1 3RB, UK

<sup>4</sup>Present address: Martin-Luther-Universität Halle-Wittenberg, Institute of Plant Physiology, Weinbergweg 10, 06120 Halle, Germany

\*email: [rbock@mpimp-golm.mpg.de](mailto:rbock@mpimp-golm.mpg.de)

## ABSTRACT

Communication between organelles and the nucleus is essential for fitness and survival. Retrograde signals are cues emitted from the organelles to regulate nuclear gene expression. GENOMES UNCOUPLED1 (GUN1), a protein of unknown function, has emerged as a central integrator, participating in multiple retrograde signaling pathways that collectively regulate the nuclear transcriptome. Here we show that GUN1 regulates chloroplast protein import through interaction with the import-related chaperone cpHSC70-1. We demonstrated that overaccumulation of unimported precursor proteins (preproteins) in the cytosol causes a GUN phenotype in the wild type and enhances the GUN phenotype of the *gun1* mutant. Furthermore, we identified the cytosolic HSP90 chaperone complex, induced by over-accumulated preproteins, as a central regulator of photosynthetic gene expression that determines the expression of the GUN phenotype. Taken together, our results suggest a model in which protein import capacity, folding stress and the cytosolic HSP90 complex control retrograde communication.

Signals from plastids (chloroplasts) couple the expression of nuclear genes with plastid function<sup>1</sup>. Many of the nuclear target genes of plastid-derived retrograde signals encode photosynthesis-related proteins and metabolic enzymes, suggesting that the main purpose of retrograde communication is to inform the nucleus about changing demands for gene products to be imported into the chloroplast or gene products acting in metabolic pathways that depend upon chloroplast services. Although, in recent years, a few candidate metabolites<sup>2-6</sup> potentially involved in relaying information from the chloroplast to the nucleus have been identified, our knowledge about the signaling pathways and the molecular mechanisms of retrograde communication is still scarce. What is becoming increasingly clear is that there is not a singular linear pathway, but instead, a multitude of signals and pathways appear to interact in a complex network<sup>7-9</sup>.

Elegant genetic screens identified a number of *Arabidopsis* mutants defective in retrograde signaling as evidenced by deregulated photosynthesis-associated nuclear gene (PhANG) expression<sup>10, 11</sup>. The mutants, dubbed *gun* mutants (for *genomes uncoupled*), uncouple nuclear gene expression from proper chloroplast development or function. Identification of the mutated loci<sup>5, 11-13</sup> revealed that, with a single exception, all *GUN* genes are involved in tetrapyrrole biosynthesis (TPB), consistent with the notion that perturbations in chlorophyll and heme biosynthesis affect retrograde communication<sup>5, 14, 15</sup>. However, the chemical nature of the signaling molecule(s) has remained controversial<sup>5, 14, 16, 17</sup>. The exceptional *GUN* gene is *GUN1*, which encodes a putative pentatricopeptide repeat (PPR) protein that localizes to plastids<sup>11, 18</sup>. GUN1 is a lowly abundant protein with a very high turnover rate. It accumulates only at the very early stage of leaf development, where it likely functions in the control of chloroplast biogenesis<sup>18</sup>. While all other *GUN* gene products function only in a specific signaling

pathway, GUN1 was proposed as the central node relaying information from all three classical retrograde signaling pathways that regulate PhANG expression: (i) TPB, (ii) redox and (iii) plastid gene expression (PGE)<sup>19</sup>. GUN1 was suggested to relay information to the nucleus by targeting multiple transcription factors in the nucleus, including ABSCISIC ACID INSENSITIVE4 (ABI4), GOLDEN2-LIKE (GLK1/2) and ELONGATED HYPOCOTYL 5 (HY5)<sup>11, 20-22</sup>. Recent studies suggest that GUN1 may be involved in the regulation of chloroplast proteostasis<sup>23-25</sup>, but the mechanism underlying this suspected role and the link to retrograde signaling remain elusive. Although the first *gun1* mutant allele was isolated more than 25 years ago<sup>10</sup>, the function of GUN1 as central regulator of retrograde communication and the signaling pathway to the nucleus have remained a mystery<sup>26, 27</sup>. Here, we show that GUN1 exerts its control over retrograde signaling by regulating chloroplast protein import. Moreover, we identified the cytosolic HSP90 chaperone complex as an important regulator of PhANG expression and an essential transducer of retrograde information from chloroplasts to the nucleus.

## RESULTS

### GUN1 Interacts with cpHSC70-1

Since the GUN1 protein possesses putative RNA-binding and DNA-binding domains and had been suggested to be associated with the chloroplast nucleoid<sup>11</sup>, we first investigated possible nucleic acid-binding functions of GUN1 and obtained multiple lines of evidence



that *GUN1* is unlikely to function in the regulation of chloroplast gene expression (Supplementary Figs. 1-5 and Supplementary Data 1).

We have previously shown that GUN1 accumulates and exerts its function mainly during chloroplast biogenesis and upon stresses that affect retrograde signaling<sup>18</sup>. To identify protein interaction partners of GUN1, we used GUN1-GFP transgenic lines (OE-13)<sup>18</sup> and conducted co-immunoprecipitation (co-IP) experiments (Supplementary Tables 1 and 2) with (1) rosette leaves where chloroplast biogenesis is finished and GUN1 likely has no function, (2) de-etiolating seedlings where active chloroplast biogenesis occurs and GUN1 functions in biogenetic control<sup>18, 28</sup>, and (3) seedlings grown as in (2) but treated with lincomycin (Lin) to interfere with the PGE pathway of retrograde signaling (Fig. 1a,b). In co-IP experiments (2) and (3), under conditions where retrograde signaling can be demonstrated, cpHSC70-1 was identified as a potential interaction partner of GUN1 (Fig. 1b, Supplementary Table 2 and Supplementary Data 2). cpHSC70-1 is a chloroplast stroma-localized HSP70-type chaperone crucial for protein import. It represents the major molecular motor driving the precursor proteins (preproteins) through the import channel<sup>29-32</sup>.

Interestingly, in co-IP experiments (1), cpHSC70-1 was not identified (Supplementary Table 1). Instead, the most abundant protein in the immunoprecipitates was ClpC1 (Fig. 1a, Supplementary Table 1 and Supplementary Data 2), a protein associated with the protein import apparatus and likely acting as quality check-point of newly imported proteins<sup>30, 33</sup>. In addition to cpHSC70-1 and ClpC1, some other proteins also could be identified, including subunits of the protein import machinery and enzymes from TPB pathway (Supplementary Tables 1 and 2). The interactions of GUN1 with ClpC1 and cpHSC70-1 were further verified by bimolecular fluorescence

complementation (BiFC) assays (Fig. 1c; Supplementary Fig. 6). Considering that GUN1 probably has no function in rosette leaves under normal growth conditions and is rapidly turned over in a ClpC-dependent manner<sup>18</sup>, the physiological relevance of the ClpC1-GUN1 interaction is most likely the delivery of GUN1 to the Clp protease for degradation. It is worth noting that, in the BiFC experiments, the YFP fluorescence shows a diffuse distribution, similar to the GUN1-GFP fluorescence in differentiating plastids and in seedlings treated with Lin (Supplementary Fig. 7)<sup>18</sup>, and different from the punctate nucleoid co-localization which was reported previously by transient expression in tobacco leaves<sup>11</sup> (Supplementary Fig. 6). The diffuse GUN1-GFP distribution in stable transgenic lines (Supplementary Fig. 7) also provides evidence that the fusion protein does not get stuck in the protein import channel, as the GFP signal does not show the peripheral distribution typical of envelope-localized proteins (e.g., Tic110-GFP; Supplementary Fig. 6).

To provide further evidence for GUN1 interacting with cpHSC70-1 under conditions that affect retrograde signaling, we performed co-IP experiments in the *clpc1* knock-out mutant. Mutations affecting plastid protein import are known to also interfere with retrograde signaling<sup>22, 34</sup>. Strong interaction of GUN1 with cpHSC70-1 is also seen in the *clpc1* background, thus providing additional support for cpHSC70-1 being the functionally relevant interaction partner of GUN1 in retrograde signaling (Supplementary Fig. 8; Supplementary Table 3 and Supplementary Data 2). Furthermore, the *cphsc70-1* mutant shows a GUN phenotype, in that PhANG (*LHCB*, *RBCS* and *CAI*) expression is derepressed when chloroplast biogenesis is disturbed (Fig. 1d; Supplementary Fig. 9a), by Lin or norflurazon (NF) treatment. The *clpc1* mutant shows a GUN phenotype only under Lin treatment, which seems to be a general feature of mutants for subunits of the

Clp protease (in that *clpr1-2* also shows its GUN phenotype under Lin treatment; Supplementary Fig. 9b).

cpHSC70-1 is an important chaperone in the chloroplast that, in theory, could participate in retrograde signaling by regulating the turnover of the GUN1 protein. To investigate this possibility, we crossed the GUN1-GFP transgene (OE-13) into the *cphsc70-1* mutant background. This led to unexpected partial transgene silencing (of both *GUN1-GFP* and the hygromycin resistance gene) at the transcriptional level (Supplementary Fig. 10a,b), resulting in much lower GUN1-GFP protein accumulation (Supplementary Fig. 10c). However, GUN1-GFP transcript and protein accumulation were well correlated (Supplementary Fig. 11a,b), and the degradation rate of the GUN1-GFP protein was comparable in the wild-type background (OE-13) and the *cphsc70-1* background (OE-13*cphsc70-1*; Supplementary Fig. 11c,d). These results exclude regulation of GUN1 by the cpHSC70 chaperone at the level of protein stability.

To exclude the possibility that GUN1 is directly regulated by protein import and, in this way, produces the GUN phenotype, we tested different mutants in Tic (translocon at the inner envelope membrane of chloroplasts) and Toc (translocon at the outer envelope membrane of chloroplasts) subunits, including *ppi1*, *toc75-III* and *tic40-4*. None of these mutants showed a GUN phenotype, neither under Lin nor under NF treatment (Supplementary Fig. 12). This observation provides further evidence for a specific function of GUN1 in the regulation of protein import under conditions when retrograde signaling is affected. At least some of the various Tic-Toc subunits control the import of specific sets of plastid proteins. For example, the *ppi1* mutant is specifically defective in the import of photosynthesis-related proteins<sup>35</sup> (the unimported precursors of which are degraded so rapidly that they can be visualized only by treatment of the mutants with

proteasome inhibitors<sup>36</sup>). Under Lin or NF treatment, the expression of most of these genes is repressed at the transcript level by retrograde signaling and, hence, no accumulation of unimported preproteins can occur (and produce a GUN phenotype; see below).

Interestingly, similar to *gun1*, *cphsc70-1* also showed delayed chloroplast biogenesis and reduced PhANG expression (*LHCB* and *RBCS*) during germination and de-etiolation (Supplementary Fig. 13)<sup>18, 28</sup>, providing further evidence for GUN1 and cpHSC70-1 acting together in retrograde communication.

### **The Cytosolic Protein Quality Control (PQC) System Is Induced in Response to Precursor Accumulation in the *gun1clpc1* Double Mutant**

We next sought to obtain genetic support for the function of GUN1 in protein import. To this end, we generated double mutants of *gun1-101* with components of the Tic complex (Fig. 2a and Supplementary Fig. 14). The *clpc1-1* and *tic40-4* mutants displayed reduced chlorophyll content and also showed constitutively reduced *LHCB* expression (Supplementary Fig. 14e,f). Introduction of the *gun1* allele into single mutants for the three import-associated genes (*ClpC1*, *cpHSC70-1* and *Tic40*) drastically aggravated the growth phenotypes of *clpc1-1* and *cphsc70-1* (with *gun1cphsc70-1* plants producing no or only a few inviable seeds; Fig. 2a and Supplementary Fig. 14a), strongly reduced their photosynthetic performance (Supplementary Fig. 14g), and even resulted in embryo lethality in the *gun1tic40-4* double mutant (Supplementary Fig. 14b-d).

To understand the molecular basis of the strong phenotype of the double mutant, we analyzed the proteome of the wild type, the *gun1* and *clpc1* single mutants, and the *gun1clpc1* double mutant by mass spectrometry (Fig. 2b,c and Supplementary Data 3). In

agreement with the paler phenotype of *gun1clpc1* compared to *clpc1*, more than 86% of the down-regulated proteins in the double mutant are chloroplast localized proteins (Fig. 2b and Supplementary Data 3). By contrast, more than 60% of the up-regulated proteins in the double mutant are localized in the cytosol, indicating a strong response that takes place in the cytosol. Interestingly, cytosolic chaperones of the HSP90 and HSP70 families and their co-chaperones (HOP3 and SGTB1) are highly induced in *gun1clpc1* compared to the single mutants and the wild type (Fig. 2c and Supplementary Fig. 15a). HSP70-4 was demonstrated to mediate the degradation of unimported chloroplast preproteins through the ubiquitin–proteasome system<sup>36</sup>. HSP90 and its co-chaperones (HOP and FKBP) also interact with chloroplast precursor proteins in the cytosol<sup>37</sup>. The large increase of HSP90.1 and HSP70s in *gun1clpc1* could suggest that, because proteins cannot be efficiently imported into chloroplasts in the double mutant, the cytosolic PQC system is induced to degrade the unimported precursors, a phenomenon that also has been observed in yeast when mitochondrial precursor proteins accumulate in the cytosol<sup>38, 39</sup>. Consistent with this hypothesis, a large number of components of the 26S proteasome were up-regulated in the double mutant (Supplementary Fig. 15b). Importantly, significantly more peptides that map to transit peptide regions of chloroplast preproteins were identified in the proteome of *gun1clpc1* (Fig. 2d).

### **GUN1 Regulates Protein Import**

Having seen precursor accumulation and cytosolic PQC induction in the *gun1clpc1* double mutant, we conducted protein import assays to further investigate the function of *GUN1* in protein import (Fig. 2e). These assays revealed no significant difference in import capacity between *gun1* and the wild type. By contrast, import was significantly

reduced in *clpc1*<sup>40</sup>, and even more so in *gun1clpc1*. These findings imply that, while the loss of GUN1 has no appreciable consequence under normal growth conditions, GUN1 function becomes important when impaired protein import disturbs proteostasis (e.g., by the *clpc1* mutation) and affects retrograde signaling<sup>22</sup> (Supplementary Fig. 14f).

*gun1* mutants were recently shown to be hypersensitive to treatment with Lin and NF<sup>25, 41</sup> (Supplementary Fig. 16). To further prove that GUN1 functions in protein import under conditions that interfere with retrograde signaling, we conducted import assays with seedlings treated with low concentrations of Lin (15  $\mu$ M), where isolation of import-competent chloroplasts is still possible (Supplementary Fig. 16a). While no significant difference was observed in import capacity between *gun1* and the wild type under normal growth conditions (Fig. 2e), the import capacity of the mutant is significantly reduced upon treatment with Lin (Fig. 2f). Importantly, Tic-Toc subunits are not reduced in their abundance in *gun1* compared to the wild type (Supplementary Fig. 17), excluding the possibility that the reduced import capacity of *gun1* results from reduced levels of the Tic-Toc complex.

We next asked if import defects are also observed under classical conditions that are commonly used in retrograde signaling studies (i.e., treatments with 0.5 mM Lin or 5  $\mu$ M NF<sup>11</sup>). As the seedlings are albino under these conditions and do not provide suitable materials for *in vitro* import assays, we analyzed transgenic lines that target GFP into plastids via the RBCS transit peptide either in the wild type (C-cpGFP) or in the *gun1* (g-cpGFP) background (Fig. 3a and Supplementary Fig. 18). While GFP is correctly targeted to plastids under control conditions and also in the control line expressing cpGFP (C-cpGFP) in the presence of Lin or NF, it is not efficiently imported into plastids in the g-cpGFP line upon Lin and NF treatments (Fig. 3a and Supplementary Fig. 18).

Accumulation of the cpGFP precursor (preGFP) in the cytosol of *gun1* is not due to plastid rupture and cell death, as the bleached seedlings grown on Lin or NF medium recover after transfer to inhibitor-free medium, become green and resume growth (Supplementary Fig. 19). Also, no cell death was detectable in these seedlings (Supplementary Fig. 20), and the inhibitor treatments did not result in reduced levels of Tic-Toc subunits in *gun1* compared to the wild type (Supplementary Fig. 21).

A portion of *gun1* seedlings shows a variegated cotyledon phenotype upon growth in continuous light<sup>18</sup>. The cpGFP import defect was also observed in these variegated seedlings, as evidenced by massive accumulation of unimported GFP in the cytosol (Supplementary Fig. 22).

Taken together, the results from our protein import assays and *in vivo* GFP localization analyses clearly indicate that the function of GUN1 in protein import is revealed when retrograde signaling is altered, either by genetic perturbations, pharmacological treatments or environmental stress.

### **Precursor Proteins Accumulating in the Cytosol Function in Retrograde Signaling**

To obtain additional evidence for the function of GUN1 in protein import under the classical conditions used in retrograde signaling studies<sup>11</sup>, a series of immunoblot analyses was performed. The fate of three classes of nucleus-encoded chloroplast proteins was monitored: (1) the import chaperones themselves (ClpC and cpHSC70), (2) representative PhANGs, and (3) selected stromal proteins whose expression is not repressed by Lin and NF treatment. The import-related chaperones did not show any difference between the analyzed genotypes (Supplementary Fig. 23a,c). The analyzed PhANG gene products did not accumulate under Lin or NF treatments, due to retrograde

regulation (Supplementary Fig. 23b,c). As class (3) proteins, we chose subunits of the Clp protease, because their expression is not suppressed by Lin or NF treatment (Supplementary Fig. 24a), and therefore, is immunologically detectable under all conditions. Interestingly, we noticed that ClpD, a nucleus-encoded HSP100 chaperone, shows an additional higher molecular weight band in the *gun1* mutants upon Lin treatment (Fig. 3b). Upon NF treatment, the additional band is also seen in the wild type, but accumulates to much higher levels in the *gun1* mutants, whereas low wild-type-like levels are restored in the complemented lines (Fig. 3c).

The larger ClpD band represents the unimported precursor (preClpD), which is supported by (i) it migrating exactly at the same height as *in vitro* translated preClpD (Supplementary Fig. 24b), (ii) the band being seen in western blots with total protein extracts, but not with protein extracts from isolated chloroplasts (Fig. 3d), (iii) a peptide mapping to the transit peptide region being detected by mass spectrometry only in the *gun1* mutant under Lin treatment (Supplementary Fig. 24c), and (iv) GFP fused to the ClpD transit peptide not being efficiently imported into plastids under Lin treatment in the *gun1* background (Fig. 3e and Supplementary Fig. 24d). PreClpD accumulation positively correlated with the strength of Lin and NF treatment and started to become detectable in the partially complemented line C-10<sup>18</sup> at high concentrations of Lin (100  $\mu$ M) or NF (100 nM; Supplementary Fig. 25). Presence of preClpD further suggests that defective protein import in the *gun1* mutant also occurs under the classical conditions used in retrograde signaling studies. Moreover, *cphsc70-1* also shows preClpD accumulation under Lin or NF treatment (Fig. 3f), thus confirming the functional connection of cpHSC70-1 with GUN1.



ClpP4, a subunit of the Clp protease, also showed a specific reduction at the protein level in the two mutant alleles of *gun1* upon Lin or NF treatment (Fig. 3b and Supplementary Fig. 23c), while transcript levels are not reduced (Supplementary Fig. 24a). Since the turnover of mature ClpP4 is not GUN1-dependent (Supplementary Fig. 26), this finding may suggest that unimported preClpP4 is unstable and rapidly degraded.

To investigate the possible impact of unimported chloroplast preproteins on retrograde signaling, we overexpressed ClpD in either the wild type (C-ClpD) or in the *gun1-101* (*g*-ClpD) background (Fig. 4a). Interestingly, preClpD can already be seen under normal growth condition in *g*-ClpD lines, and causes a white cotyledon phenotype (Fig. 4b). This phenotype is not due to over-expressed ClpD disturbing the accumulation of the ClpC chaperone (Fig. 4c). The *gun1* mutant displays a similar phenotype under environmental stress as, for example, elicited by irradiation with continuous light<sup>18</sup>. PreClpD weakly accumulates in the C-ClpD lines under Lin or NF treatment, where it produces a GUN phenotype (Fig. 4d and Supplementary Table 4). Moreover, ClpD overexpression in the *gun1* mutant (*g*-ClpD) enhances the GUN phenotype of the mutant (Fig. 4d and Supplementary Table 4). Importantly, the GUN phenotype correlates with the cytosolic accumulation of preClpD, but not with the chloroplast-localized mature form of ClpD (Fig. 4d). Also, the two *clpd* mutants do not show a GUN phenotype and *gun1clpd* behaves exactly as the *gun1* single mutant (Fig. 4e,f). The GUN phenotype caused by precursor overaccumulation is not restricted to ClpD. The preGFP precursor also accumulates under Lin and NF treatments (Supplementary Fig. 27a). Although not as effective as preClpD, it also enhances the GUN phenotype of *gun1* in the presence of Lin (Supplementary Fig. 27b).

## **The Cytosolic HSP90 Chaperone Complex Regulates Retrograde Signaling**

The HSP90 chaperone participates in a wide range of signal transduction pathways in yeast, animals and plants<sup>42-45</sup>. The strong up-regulation of HSP90.1 and HSP70s observed in *gun1clp1* (Fig. 2c; Supplementary Fig. 15a and Supplementary Data 3) raises the possibility that cytosolic chaperones are components of the retrograde signaling pathway. We, therefore, compared the accumulation of HSP90.1 and HSP70s in the presence of Lin or NF in the wild type and *gun1*. Western blot analyses revealed that HSP90.1 and HSP70 contents were strongly elevated in *gun1* under these conditions (Fig. 5a,b).

To further explore the role of HSP90/70 chaperones in retrograde communication, we treated seedlings with the HSP90-specific inhibitor geldanamycin (GDA) and the HSP70 inhibitors VER155008 or PES-Cl + apoptozole (Az), and monitored the expression of PhANGs (Fig. 5c-e and Supplementary Fig. 28). Under control conditions, the expression of all three PhANGs (*LHCB1.2*, *LHCB2.2* and *RBCS2B*) investigated was significantly repressed upon HSP90 inhibition in both the wild type and two non-allelic *gun* mutants (*gun1* and *gun5*). By contrast, inhibition of HSP70 had less effect on PhANG expression (Fig. 5c and Supplementary Fig. 28a). Strikingly, inhibition of HSP90 significantly suppresses the GUN phenotype of *gun1* in the presence of Lin and NF (50  $\mu$ M GDA), and that of *gun5* in the presence of NF (Fig. 5d,e and Supplementary Fig. 28b,c). The role of HSP90 in retrograde signaling was further verified by obtaining independent genetic evidence. Knock-down of HSP90 by RNA interference (RNAi; Supplementary Fig. 29) suppressed the GUN phenotype of *gun1* (Fig. 5f) and *gun5*<sup>46</sup>. In contrast to *gun1*, overaccumulation of HSP90 and HSP70 is not seen in *gun5* (Supplementary Fig. 30). This is consistent with previous reports that *gun5* accumulates less Mg-protoporphyrin IX (Mg-ProtoIX), which potentially accounts for the GUN

phenotype of *gun5*, because Mg-ProtoIX can inhibit HSP90 activity<sup>46, 47</sup>. Taken together, these results suggest a key role of the HSP90 chaperone complex in both the PGE and TPB pathways of retrograde signaling.

GUN1-dependent control of protein import was also determined for proteins involved in the TPB pathway. Several enzymes of TPB interacted with GUN1 in our co-IP experiments (Supplementary Tables 1-3) and also in a recent study<sup>23</sup>. This might suggest that their import is regulated by GUN1. Indeed, when three enzymes of TPB were investigated (glutamyl-tRNA reductase (GluTR), GluTR-binding protein (GBP) and Mg-ProtoIX monomethyl ester cyclase (CHL27), their precursors accumulate when the *gun1* mutation had been introduced (*gun1* or *gun1gun5* double mutant) upon Lin or NF treatment (Fig. 6a). These results provide a potential link of GUN1 to TPB mediated retrograde signaling through control of the import of key TPB enzymes.

## DISCUSSION

Mitochondrial retrograde signaling pathways were demonstrated to be of fundamental importance for the tuning of nuclear gene expression in eukaryotes<sup>48, 49</sup>. Photosynthetic eukaryotes have implemented additional retrograde pathways to serve the needs of the plastids<sup>15, 50</sup>. *GUN1* was identified as a key player that participates in several retrograde signaling pathways<sup>11</sup>. Despite the central importance of GUN1 and enormous efforts to elucidate its mode of action, the molecular function has remained enigmatic. Our data provided here indicate that GUN1 likely has no direct function in the regulation of plastid gene expression (Supplementary Figs. 1-5 and Supplementary Data 1). Instead, GUN1 is

engaged in the regulation of chloroplast protein import through interaction with the chloroplast chaperone cpHSC70-1, the ATP-powered import motor that drives preproteins through the import channel<sup>29, 31, 32</sup>. In agreement with this finding, the *cphsc70-1* mutant shows a GUN phenotype (Fig. 1d and Supplementary Fig. 9a).

Interestingly, the *gun1* mutation does not affect protein import capacity under normal growth conditions (Fig. 2e). GUN1 exerts its function on protein import only during chloroplast biogenesis and when retrograde signaling is affected by genetic perturbations (mutations in protein import components such as *clpC1*<sup>22</sup>), or environmental stress (mimicked, e.g., by treatments with NF or Lin). This is well in line with the recent observation that the GUN1 protein accumulates to detectable amounts only under these conditions<sup>18</sup>. We have shown previously that GUN1 has a high turnover and its degradation is ClpC1-dependent<sup>18</sup>. It was recently reported that the ClpC1 chaperone, rather than being a motor for protein import, acts as part of a protein quality control system by associating the Clp protease with the inner envelope membrane in close proximity to the import channels, and, in this way, removes defective or otherwise unwanted proteins directly upon their arrival in the organelle<sup>30</sup>. The interaction of GUN1 with ClpC1 in rosette leaves, where the GUN1 function is dispensable, supports the idea that GUN1 is a substrate of the Clp protease and is delivered by the ClpC chaperone for degradation.

Cellular responses to stress from overaccumulation of mitochondrial precursor proteins were recently shown to be functionally important for fitness of yeast strains that suffer from import defects<sup>38, 39, 51</sup>. When preproteins accumulate in the cytosol (e.g., upon strong overexpression of chloroplast-localized proteins), they trigger a GUN phenotype in the wild-type background and enhance the GUN phenotype of the *gun1* mutant (Fig. 4

and Supplementary Fig. 27). This finding suggests a role of over-accumulated preproteins in GUN1-dependent retrograde communication. Cytosolic HSP90-HSP70 chaperone complexes participate in multiple signal transduction pathways<sup>42, 44, 45</sup>. HSP90.1 and HSP70 chaperones were found to be strongly over-accumulated in *gun1clp1*, and also in *gun1* under Lin or NF treatment (Figs. 2c, 5a,b and Supplementary Fig. 15a). Our findings identify the cytosolic HSP90 chaperone complex as a central regulator of PhANG expression that determines the GUN phenotype. Inhibition of HSP90 activity suppresses the GUN phenotype of *gun1* and *gun5* suggesting an essential role of HSP90 in both the PGE and TPB pathways of retrograde signaling (Fig. 5 and 6). Consistent with this, knock-down of HSP90s by RNAi was observed to suppresses the GUN phenotype of *gun1* (Fig. 5f) and *gun5*<sup>46, 47</sup>.

Our data suggest that GUN1 regulates the TPB pathway of retrograde signaling through control of the import of key TPB enzymes (Fig. 6a), which can also explain the observation that *gun1* mutants are hypersensitive to NF treatments (Supplementary Fig. 16b,c)<sup>25, 41</sup>. The global plastid import defects observed in the absence of GUN1 are dominant over TPB-specific *gun* mutations. Hence, in contrast to *gun1*, protein import into plastids of *gun4* and *gun5* is normal, but a GUN phenotype develops upon NF treatment. This suggests a different source of the retrograde signal arising from TPB-specific *GUN* genes (Fig. 6b).

Based on the molecular function of GUN1 discovered in this study, we propose a new model of GUN1 function and retrograde signaling (Fig. 6b). GUN1 is a lowly abundant protein that promotes early chloroplast development. In differentiated chloroplasts, GUN1 is degraded upon import by the inner envelope membrane-associated Clp protease through the action of ClpC<sup>18, 30</sup> (Fig. 1). Under environmental stress, genetic

defects and in early chloroplast biogenesis, GUN1 is required to maximize their import capacity. This occurs through interaction with the import chaperone cpHSC70-1. The overaccumulation of preproteins, which causes folding stress in the cytosol, induces up-regulation of cytosolic HSP90 and in turn sustains PhANG expression. HSP90 mediates retrograde communication by either repressing negative regulator(s) of transcription (e.g., through delivery to the 26S proteasome for degradation) or by activating a positive regulator of transcription (e.g., through promoting folding or refolding of a transcription factor). Target transcription factors (HSP90 clients) may include ABI4<sup>11</sup>, HY5<sup>20</sup> and GLK1/2<sup>21</sup>, all of which have been implicated in retrograde signaling. Future studies should be directed towards elucidating the precise molecular mechanism how the HSP90 chaperone complex regulates downstream events of retrograde signaling.

## Methods

**Plant material and growth conditions.** The Col-0 strain of *Arabidopsis thaliana* was used as the wild-type (WT) genetic background in all experiments. The *gun1-1*, *gun5-1*<sup>10</sup> and *abi4*<sup>11</sup> mutants used in this study were described previously. The *gun1-102*<sup>23</sup> mutant was kindly provided by Dr. Dario Leister (Ludwig-Maximilians-University Munich, Germany). The *ppi1*<sup>52</sup> and *toc75-III*<sup>53</sup> mutants were described previously. The *gun1-101*, *clpc1-1* mutants, GUN1-GFP overexpression (OE) and complementation (C) lines and chloroplast localized GFP lines (cpGFP, by RBCS transit peptide) in the wild-type background (C-cpGFP) were isolated and described previously<sup>18</sup>. cpGFP lines in the *gun1-101* background (g-cpGFP) were obtained by transformation of the *gun1-101*

mutant with the same construct used to produce the C-cpGFP lines. The *tic40-4* (SAIL\_92\_C10), *cphsc70-1* (SALK\_140810), *clpr1-2* (SALK\_088407C), *clpd-1* (SALK\_110649) and *clpd-2* (Sail\_77\_G05) mutants were obtained from the European Arabidopsis Stock Centre (NASC). Primers used for the verification of T-DNA insertions are listed in Supplementary Table 5.

For plant growth under aseptic conditions, seeds were surface-sterilized with 1.2% NaOCl for 15 min, washed five times with sterile water, then sown on 0.5× Murashige & Skoog (MS) medium<sup>54</sup> containing 1% (w/v) sucrose and stratified at 4°C for 48 h in the dark prior to germination. For selection of transgenic plants, the medium was supplemented with 20 µg/mL hygromycin. To alter retrograde signaling, seeds were sown on 0.5× MS medium containing 1% (w/v) sucrose and 0.5 mM lincomycin (Lin) or 5 µM norflurazon (NF)<sup>11</sup>. Seedlings were grown for 11 days in long-day conditions, or initially grown for 5 days in the dark followed by 2 days under continuous light. In order to increase the production of rosette leaves for co-immunoprecipitation (co-IP) experiments, plants were initially grown for 10 days under short day conditions (8 h light/16 h darkness). Light-stressed plant material for analysis of plastid genome stability by pulsed-field gel electrophoresis (PFGE) was produced by raising plants under low light (60 µmol m<sup>-2</sup> s<sup>-1</sup>) in long-day conditions for 3 weeks followed by adaptation to very low light (20 µmol m<sup>-2</sup> s<sup>-1</sup>) for 2 weeks and exposure to high light (1000 µmol m<sup>-2</sup> s<sup>-1</sup>) for 3 h. To produce de-etiolated seedling for analysis of PhANG expression in the wild type, *gun1-101* and *cphsc70-1*, seeds were sown on 0.5× MS medium with 1% (w/v) sucrose and stratified for 48 h at 4°C in the dark. The seeds were incubated in a growth chamber in the light for 8 h to promote germination, and then wrapped with two layers of aluminum

foil for continued growth in the dark until day 6, followed by exposure to continuous light. Material was harvested at 0, 2, 4, 8 and 24 h after irradiation.

**Construction of transformation vectors and generation of transgenic plants.** To produce ClpD overexpression lines (with and without GFP fusion) and lines expressing GFP fused to the ClpD transit peptide (ClpD-TP-GFP), the complete *ClpD* coding region (including the stop codon for the unfused ClpD, but excluding the stop codon for the ClpD-GFP fusion) or the region encoding the transit peptide (as predicted by the ChloroP1.1 server; <http://www.cbs.dtu.dk/services/ChloroP/>) were amplified from cDNA. The amplified PCR products were cloned into the pEZR(H)-LN binary vector using the In-Fusion HD Cloning kit (Clontech). Both WT and *gun1-101* mutant plants were transformed by *Agrobacterium tumefaciens* strain GV3101.

For bimolecular fluorescence complementation (BiFC) experiments, the following fusions with the N-terminal (YN) or C-terminal (YC) half of YFP were generated: GUN1-YN, ClpC1-YN, ClpC1-YC, Tic110-YC, ClpD-YC and cpHSC70-1-YC. To this end, full length cDNAs were amplified (except for ClpC1 which was amplified from genomic DNA) and cloned into the Gateway entry vector pENTR/SD/D-TOPO (Invitrogen). The final expression vectors were produced by an LR recombination reaction between the entry vector and the pBiFP1 (*GUN1* and *ClpC1*) or pBiFP4 (*ClpC1*, *Tic110*, *ClpD* and *cpHSC70-1*) vectors<sup>55</sup>. The YN (*GUN1* and *ClpC1*) or YC (*ClpC1*, *Tic110*, *ClpD* and *cpHSC70-1*) parts were fused to the C-terminus of the different genes and expressed under the control of the CaMV 35S promoter. The GUN1-GFP construct was described previously<sup>18</sup>. The ClpC1-GFP, Tic110-GFP and cpHSC70-1-GFP expression constructs were generated by an LR recombination reaction between the



Gateway entry vector obtained above and the pUC-GFP-DEST vector<sup>56</sup>. Primers used for cloning are listed in Supplementary Table 5.

**Seed germination and cotyledon greening assays.** Seeds for germination assays and cotyledon greening assays were harvested from plants grown under identical conditions. The assays were done in four independent experiments with different batches of seeds. To synchronize germination, seeds were sown on 0.5× MS medium with 1% (w/v) sucrose and stratified for 48 h at 4°C in the dark prior to incubation in a growth chamber under long-day conditions. Seed germination was analyzed with a Leica MZ12.5 stereomicroscope (and defined as visible radicle protrusion out of the testa), and the germination rate was scored at different time points. Seedlings developing green cotyledons were counted each day 1 hour after the start of the light period.

**Pulsed-field gel electrophoresis (PFGE).** Samples for PFGE analysis were prepared by isolating intact chloroplasts as described below. Sample preparation and PFGE were done according to a published protocol<sup>57</sup>. A phage lambda-derived PFGE marker (NEB) was loaded as molecular weight marker. After electrophoretic separation, the gel was stained with ethidium bromide.

**Quantification of plastid DNA.** To determine the plastid DNA (ptDNA) content per cell, total cellular DNA was extracted using a CTAB (cetyltrimethylammonium bromide)-based extraction buffer (2% CTAB (w/v), 100 mM Tris-HCl, pH 8.0, 20 mM EDTA, 1.4 M NaCl and 0.2% β-mercaptoethanol) and the ptDNA amount was quantified against nuclear DNA by qPCR. Primers used are listed in Supplementary Table 5.

**Ribosome profiling.** Ribosome footprints and total RNA were isolated as described<sup>58</sup> with a minor modification: After MNase treatment 4 mL lysate was loaded onto a 1 mL sucrose cushion (30% (w/v) sucrose, 0.1 M KCl, 40 mM Tris acetate, pH 8.0, 15 mM MgCl<sub>2</sub>, 5 mM 2-mercaptoethanol, 100 mg/L chloramphenicol, and 100 mg/L cycloheximide) and centrifuged for 1.5 h at 300,000 g at 4°C.

Ribosome footprints were further purified as follows: 60 µg of the monosome RNA was loaded onto a 12% polyacrylamide gel (acrylamide:bisacrylamide = 19:1) in 1× TBE buffer containing 8 M urea and run in 1× TBE buffer. Subsequently, the gel region between 23 and 45 nt was excised and the RNA was eluted from the gel by overnight incubation in 4 mL TESS buffer (10 mM Tris-HCl pH 8.0, 1 mM EDTA pH 8.0, 0.1 M NaCl, 0.2 % SDS) on an over-head rotator at 4°C. RNA was purified from the eluate by phenol extraction and precipitated overnight at -20°C. Subsequently, ribosome footprints were pelleted by centrifugation at 20,000×g for 1 h at 4°C and dissolved in 20 µL RNase-free water.

Total RNA samples were processed in parallel by diluting 10 µg RNA to a volume of 22.5 µL in RNase-free water. After addition of 2.5 µL RNA fragmentation buffer (400 mM Tris-OAc pH 8.3, 1 M KOAc, 300 mM Mg(OAc)<sub>2</sub>), the fragmentation was done by incubation for 12 min at 85°C and stopped by adding 225 µL of TESS buffer.

Ribosome footprints and fragmented total RNA samples were labeled according to Zoschke et al., 2013<sup>58</sup> with minor modifications: For total RNA samples, 3.5 µg RNA was used for labeling, for footprint samples of NF control (DMSO) and NF treatments, 4.2 µg purified footprints were used; for the Lin control and Lin-treated samples, 4 µg and 3.5 µg purified footprints, respectively, were used. Samples from control and

treatment experiments were labeled with Cy5 and Cy3 fluorescence dye, respectively, following the manufacturer's instructions (ULS Small RNA Labeling Kit, Kretech Diagnostics). The labeled RNA was denatured and hybridized to a custom tiling array covering the whole chloroplast genome.

Ribosome and transcriptome profiling data were analyzed as described<sup>58</sup>. In brief, all negative background-subtracted single channel signals (F635-B635 and F532-B532, respectively) were normalized to the average signal of the compared datasets, including all replicates of ribosome footprints and total RNA to remove overall differences introduced by technical variations (e.g., unequal labeling efficiencies between samples). The signal intensity of each reading frame (RF) was calculated by averaging normalized signals from all probes in the RF. RFs with weak averaged signal intensities of less than 100 were considered unreliable and excluded from the analysis (*psbK*, *psbM*, *psaI* and *petL* in Lin and NF treatment conditions; indicated as nd in Supplementary Figs. 2 and 3).

**RNA extraction, qRT-PCR, and RNA gel blot analyses.** Total RNA was extracted using the NucleoSpin® RNA Plant kit (Macherey-Nagel) and treated with DNase (TURBO DNA-free Kit; Ambion) to eliminate genomic DNA contaminations. First-strand cDNA was synthesized using the SuperScript III Reverse Transcriptase (Invitrogen). qRT-PCR analysis was performed with the ABI 7900HT system (Applied Biosystems) using SYBR Green detection (Applied Biosystems). The actin gene (AT5G09810) was used as internal standard and relative expression values were calculated for each target gene including calculation of the amplification efficiencies of the different primers<sup>59</sup>.

For northern blot analyses, RNA samples were separated in denaturing (formaldehyde-containing) 1% (w/v) agarose gels, blotted onto Hybond-XL nylon membranes (GE Healthcare) and subsequently cross-linked by UV light. To generate hybridization probes, cDNA sequences were amplified with gene-specific primers, and labeled with [ $\alpha^{32}\text{P}$ ]dCTP using the Megaprime DNA labeling system (GE Healthcare). Hybridizations were performed at 65°C. Primers used for qRT-PCR and generation of hybridization probes are listed in Supplementary Table 5.

**Protein extraction and western blot analyses.** Total cellular protein was isolated according to a published procedure<sup>60</sup>. Protein samples were separated by SDS-polyacrylamide gel (10% w/v) electrophoresis (SDS-PAGE) and blotted onto membranes. Immunoblot detection was performed with specific antibodies using the enhanced chemiluminescence system (GE Healthcare). Signals were detected with High Performance Chemiluminescence film (GE Healthcare) or the G:box Chemi Imaging System (Syngene). Antibodies against Clp proteins (ClpC, ClpP1, ClpP4 and ClpD) were kindly provided by Dr. Adrian Clarke (Gothenburg University, Sweden). Antibodies against GluTR and GBP were previously described<sup>61</sup>. All other antibodies were obtained from commercial suppliers (GFP from Clontech; actin from Sigma; Toc159, Tic110, Tic40, cpHSC70, Toc75, LHCB1, PsbO, RbcL, HSP90.1, HSP70 and CHL27 from Agrisera).

**Polysome analyses.** For isolation of polysomes, plants were germinated and grown for 5 days in the dark followed by growth for 2 days in continuous light. Polysome analysis and puromycin treatment were performed essentially as described<sup>18, 62</sup>.

**Chloroplast isolation.** For isolation of chloroplasts, leaf material was ground in chloroplast isolation buffer (0.3 M sorbitol, 5 mM MgCl<sub>2</sub>, 5 mM EGTA, 5 mM EDTA, 10 mM NaHCO<sub>3</sub>, 20 mM HEPES-KOH pH 8.0), the released chloroplasts were loaded onto a linear Percoll gradient<sup>63</sup> and centrifuged in a swing-out rotor for 10 min at 7800×g at 4°C. Intact chloroplasts were collected from the lower green band.

**Seedling re-greening assays and trypan blue staining.** To test the viability of the seedlings grown on Lin or NF-containing medium, the wild type, *gun1-101* and *cphsc70-1* seeds were germinated and then grown with 0.5 mM Lin or 5 µM NF for 7 days in long-day conditions on 0.5× MS medium containing 1% (w/v) sucrose. Afterwards, the seedlings were transferred to inhibitor-free medium and grown further (for the times indicated in the figures) to test for re-greening.

For trypan blue staining, 7-day old seedlings grown in the presence or absence of 0.5 mM Lin or 5 µM NF were stained with trypan blue solution according to standard protocols<sup>64</sup>. As a positive control, seedlings at day 6 were incubated for 4 h at 60 °C, moved back to 22 °C for 20 h and stained with trypan blue.

**Cycloheximide (CHX) chase assays.** CHX chase assays were used to determine the turnover rate of GUN1-GFP in the wild-type (OE-13) and *cphsc70-1* (OE-13*cphsc70-1*) backgrounds, and of ClpP4 in the wild type, *gun1-101* and OE-13 as described previously<sup>18</sup>. In brief, plant material for the assays was produced by germinating seeds and growing the resulting seedlings for 5 days in the dark, followed by growth for 2 days in continuous light in Petri dishes with 0.5× MS medium supplemented with 0.1% DMSO

or 5  $\mu$ M NF. Seedlings were then transferred into flasks with liquid 0.5 $\times$  MS medium and cultured under slow agitation. The liquid medium used for seedlings from 0.1% DMSO-containing Petri dishes was supplemented with 0.1% DMSO or 0.1% DMSO + 10  $\mu$ M CHX. The liquid medium used for seedlings from 5  $\mu$ M NF-containing Petri dishes was supplemented with 5  $\mu$ M NF or 5  $\mu$ M NF + 10  $\mu$ M CHX. Samples were collected at different time points and snap frozen in liquid nitrogen for further analyses.

**Co-immunoprecipitation and mass spectrometric protein analyses.** For co-immunoprecipitation (co-IP) experiments with rosette leaves, 10 g leaves per isolation were harvested. A crude chloroplast extract was isolated from freshly harvested material and used for co-IP. Leaves were homogenized with a Waring blender in chloroplast isolation medium (0.4 M sorbitol, 50 mM HEPES, 2 mM EDTA, 0.1% (w/v) BSA, 0.1% (w/v) isoascorbic acid; pH 8.0). The homogenate was filtered through 2 layers of Miracloth (Calbiochem), followed by centrifugation at 2000 $\times$ g for 2 min. The pellet was solubilized in co-IP buffer (0.5 M sucrose, 50 mM HEPES, 2 mM EDTA, 3 mM MgCl<sub>2</sub>, 1.5% n-dodecyl  $\beta$ -D-maltoside (w/v), protease inhibitor cocktail; pH 7.5) for 20 min on ice and centrifuged 2 $\times$ 20 min at 20,000 $\times$ g, 4°C. Subsequently, 50  $\mu$ L of anti-GFP beads (Miltenyl Biotec) were added to the supernatant and incubated for 1.5 h at 4°C with agitation to facilitate binding. The beads were then washed and the bound proteins released by incubation in SDS-PAGE sample buffer at 95°C. Immunoprecipitates were separated in 10% (w/v) SDS-PAGE gels and either stained with colloidal Coomassie blue for mass spectrometry or subjected to western blot analysis with specific antibodies. For the co-IP experiments with de-etiolating seedlings, seedlings were grown for 5 days in the dark followed by 2 days in continuous light with or without Lin treatment. Whole

seedlings were harvested, ground in liquid nitrogen and directly solubilized in co-IP buffer.

For mass spectrometric analysis (MS) of co-IP samples, immunoprecipitates separated in SDS-PAGE gels were stained with colloidal Coomassie blue. Each lane was cut into several gel slices followed by in-gel tryptic digestion<sup>65</sup>. The peptides were separated by reverse phase chromatography performed on a nanoflow HPLC (EASY-nLCII, Proxeon Biosystems, Odense, Denmark) using a Chromolith® CapRod® RP-18e 150-0.2 column (Merck, Darmstadt, Germany) with a 30 min linear gradient (4-48% (v/v) acetonitrile), followed by a final peptide elution step for 5 min with 64% (v/v) acetonitrile. The HPLC was coupled via a nano-ESI ion source to a high-resolution Orbitrap hybrid mass spectrometer (LTQ-Orbitrap, Thermo Fisher Scientific). Spectral acquisition for full-scan MS spectra was performed at a full-width half-maximum resolution of 30,000 in the Orbitrap section of the MS, while the data-dependent MS/MS, with up to five spectra per preceding full scan, were obtained in the linear ion trap of the LTQ. Protein identification and ion intensity quantitation were performed using the MaxQuant software (version 1.3.0.5<sup>66</sup>). The parameters were: fixed modification: carbamidomethylation of Cys; variable modification: oxidation of Met, protein N-terminal acetylation; multiplicity set to 1 for label-free quantitation; trypsin specified as protease allowing one missed cleavage; razor and unique peptides (also including modified peptides) were used for quantification; all other parameters set as default. Spectra were matched against the *Arabidopsis* proteome (TAIR10; 35,386 entries). Common contaminations (e.g., trypsin and keratin) were included in the database searches. For identification of putative interaction partners of GUN1, the following data filter criteria were used: (i) identification in the GUN1-GFP sample, but not in the cpGFP sample, or protein abundance in the

GUN1-GFP sample >50-fold higher than that in cpGFP sample (except for the de-etiolation co-IP experiments in which 20-fold was used as cut-off); (ii) protein identification in the GUN1-GFP sample with  $\geq 2$  unique peptides; (iii) protein localize in chloroplasts as predicted by ChloroP (<http://www.cbs.dtu.dk/services/ChloroP/>) or TargetP (<http://www.cbs.dtu.dk/services/TargetP/>) or according to published information.

For proteomic analysis of WT, the *gun1* and *clpc1* single mutants, and the *gun1clpc1* double mutant, seedlings were grown in long-day conditions for 11 days, except for the double mutant, which was grown for 20 days to reach a similar developmental stage. Protein extraction and on-column digestion with trypsin were conducted according to Wu et al. 2018<sup>18</sup>. For MS analysis, peptides were separated on a nonaflow HPLC (EASY-nLC 1000, Proxeon Biosystems, Odense, Denmark) using an Acclaim PepMap 100 C18, 2  $\mu$ m, 250 mm LC Column (Thermo Scientific) with a 230 min linear gradient of 4.25-51% (v/v) acetonitrile, followed by a final peptide elution step for 10 min with 76.5% (v/v) acetonitrile. A Q-Exactive Plus (Thermo Fisher Scientific) high-resolution Orbitrap hybrid mass spectrometer was used and run in positive ion mode. For full MS scans, the following settings were used: resolution: 70,000, AGC target: 3E6, maximum injection time: 100 ms, scan range: 200 to 2000 m/z. For dd-MS2, the following settings were used: resolution: 175000, AGC target: 1E5, maximum injection time: 50 ms, loop count: 15, isolation window: 4.0 m/z, NCE: 30. The following data-dependent settings were used: underfill ratio: 1%; apex trigger: off; charge exclusion: unassigned, 1, 5, 5–8, >8; peptide match: preferred; exclude isotypes: on; dynamic exclusion: 20.0 s. Protein quantification was done as in co-IP experiments with the MaxQuant software (Version 1.5.8.3). Unique peptides were used for quantification and



post-data analysis was done with the Perseus software<sup>67</sup>. A two-tailed Student's *t*-test was performed to determine the significance of differences. Proteins with a false discovery rate adjusted p value (q value, permutation-based) <0.05 and fold change >2 were considered as significantly different between genotypes. Additionally, proteins identified in all three replicates of one genotype with an averaged log<sub>2</sub> protein intensity of more than 25, but not identified in all three replicates of the comparator genotype, were also considered as differentially expressed proteins.

To identify peptides that map to transit peptide regions of proteins, the chloroplast-localized proteins (according to SUBA localization: [suba.live](http://suba.live)) were selected from all identified proteins in the experiments. Amino acid sequences of proteins were obtained from TAIR10 ([www.arabidopsis.org](http://www.arabidopsis.org)). The transit peptides and their length were predicted by ChloroP1.1 (<http://www.cbs.dtu.dk/services/ChloroP/>). Peptides that were completely localized within a transit peptide region and peptides whose N-terminus has  $\geq 3$  amino acids overlap with the C-terminus of the transit peptide were defined as transit peptide-localized peptide (P-TP in Fig. 2d). The relative P-TPs intensity (Fig. 2d) was calculated as the sum of the peptide intensities of all the P-TPs in the sample divided by the sum of all protein intensities of the sample.

For characterization of unimported ClpD precursor, total protein was extracted from WT and *gun1-101* mutant seedlings grown on 0.5 mM Lin-containing plates, separated by SDS-PAGE, and stained with colloidal Coomassie blue. The ClpD-containing gel region (around 100 kD) from each lane was excised, in-gel digested and analysed by mass spectrometry as described above.

To quantify Tic-Toc subunits in the wild type and *gun1-101* in the material used for protein import assays (15  $\mu$ M Lin treatment), seedlings were grown in long-day

conditions exactly as in the import assays and harvested. To quantify the Tic-Toc subunits upon treatment with 0.5 mM Lin or 5  $\mu$ M NF, seedlings were grown in the presence or absence of 0.5 mM Lin, or in the presence of 0.1% DMSO (control for NF treatment) or 5  $\mu$ M NF in the dark for 5 days followed by 2 days in continuous light. Total protein was extracted and separated by SDS-PAGE. The gel region from the beginning of the separation gel until 100 kD (containing Toc159, Toc132, Ycf1 and Tic110) was excised, in-gel digested and analysed by the Q-Exactive Plus (Thermo Fisher Scientific) high-resolution Orbitrap hybrid mass spectrometer as described above. Protein quantification was done as above with the MaxQuant software (Version 1.5.8.3). Unique peptides were used for quantification.

**Bimolecular fluorescence complementation (BiFC) assays.** For BiFC analyses, YN and YC fusion constructs (and the GFP fusion protein constructs as controls) were transformed into *Agrobacterium tumefaciens* strain GV3101. *Agrobacterium* cultures were grown to OD 1.0 and the cells were washed with infiltration medium (10 mM MgSO<sub>4</sub>, 10 mM MES, 150  $\mu$ M acetosyringone, pH 6.5). *Agrobacterium* strains harboring the GUN1-YN or ClpC1-YN constructs were mixed 1:1 with strains expressing YC fusions (to ClpC1, Tic110, ClpD or cpHSC70-1). The *Agrobacterium* strains harboring GUN1-GFP, ClpC1-GFP, Tic110-GFP, cpHSC70-1-GFP and ClpD-GFP constructs were washed with infiltration medium. The cultures were incubated in the dark in infiltration medium for 3 h and then infiltrated into 5-6 week-old *Nicotiana benthamiana* leaves for transient expression. GFP or YFP fluorescence was analyzed 3 days after infiltration by confocal microscopy.

**Microscopic analyses and analysis of embryo development.** Subcellular localization of GFP, YFP and chlorophyll fluorescences was determined by confocal laser-scanning microscopy (TCS SP5; Leica). For GFP fluorescence, the excitation wavelength was 488 nm and emission was detected with a 495-530 nm filter. For YFP fluorescence, excitation was at 514 nm and a 530-590 nm filter was used for detection. For detection of chlorophyll fluorescence, a 650-702 nm filter was used.

For observation of seed development, siliques were opened under a stereomicroscope (Leica MZ12.5) and photographed. For analysis of embryo development, siliques at different developmental stages were collected and embryos were visualized by clearing the siliques in Hoyer's solution<sup>68</sup> for several weeks. Embryo development was analyzed with an Olympus BX-51 microscope using a differential interference contrast (DIC) filter and the Olympus cellSens Dimension software.

**Determination of chlorophyll contents and chlorophyll fluorescence measurements.**

The chlorophyll content and the chlorophyll a/b ratio in rosette leaves were determined by pigment extraction from ground leaves (in 80% (v/v) acetone) followed by spectrophotometric measurement of the concentrations of chlorophyll a and b<sup>69</sup>. For Lin and NF treatments, whole seedlings were harvested and the chlorophyll content were determined<sup>70</sup>.

Chlorophyll fluorescence was recorded with the MAXI version of the Imaging-PAM (Heinz Walz GmbH) on intact plants at room temperature. Plants were dark adapted for 1 h prior to determination of the maximum quantum efficiency of photosystem II ( $F_v/F_m$ ). Subsequently, the light-response curves were measured and the PSII yield, the

electron transfer rate (corrected for leaf absorbance) and the quenching parameters  $q_N$  and  $q_L$  were calculated.

***In vitro* translation and protein import assays.** To produce the ClpD precursor and the mature protein, the full-length coding region and the coding region without the sequence encoding the transit peptide (predicted by ChloroP1.1) were cloned into the pF3A WG (BYDV) Flexi vector. *In vitro* translation reactions were carried out with the TNT SP6 High-Yield Wheat Germ Protein Expression System (Promega). Primers used for cloning are listed in Supplementary Table 5.

To produce the Rubisco small subunit (RBCS) precursor protein for import assays, the complete cDNA (cloned into the pBluescript vector<sup>71</sup>) was amplified with M13 primer and reverse primer, and transcribed and translated using a coupled system containing rabbit reticulocyte lysate (TNT T7 Quick for PCR DNA, Promega) and the EXPRE<sup>35</sup>S<sup>35</sup>S Protein Labeling Mix (PerkinElmer).

For each import assay,  $10^7$  isolated chloroplasts (see above) from each genotype were used and assays were performed according to published protocols<sup>63</sup>. For import assays, WT, *gun1-101* and *clpc1-1* mutant plants were grown for 10 days in long-day conditions and the *gun1clpc1* double mutant was grown for 20 days to reach a similar developmental stage. For import assays upon Lin treatment, WT and the *gun1-101* mutant were grown for 9 or 11 days, respectively, to reach similar developmental stage, with 15  $\mu$ M Lin in long-day conditions. Import was allowed to proceed for the indicated time periods, and the samples were then analyzed by SDS-PAGE and phosphorimaging. For quantification of import efficiencies, three independent experiments were conducted and band intensities were determined by GeneTools (Syngene). Mature protein bands at each

time point were quantified and the data were expressed as percentages of the value for the final time point in the wild type. Thermolysin treatments were conducted using standard procedures with a final concentration of 100 µg/ml thermolysin on ice in the dark for 30 min<sup>72</sup>.

**HSP90 and HSP70 inhibition.** For HSP90 and HSP70 inhibition experiments, WT, *gun1-101* and *gun5-1* seeds were germinated and grown on 0.5× MS medium with 1 % sucrose for 10 days in long-day conditions with 0.5 mM Lin or 5 µM NF, or 6 days with 0.1% DMSO as a control. The seedlings were then transferred to liquid 0.5× MS medium for inhibitor treatments. For the experiments shown in Fig. 5c-e, the seedlings were treated with 50 µM HSP90 inhibitor geldanamycin<sup>73, 74</sup> (GDA; InvivoGen), 50 µM HSP70 inhibitor VER155008<sup>44, 75</sup> (VER; Sigma), or GDA+VER. For the experiments in Supplementary Fig. 28, seedlings were treated with 25 µM GDA, 10 µM HSP70 inhibitor PES-Cl<sup>76</sup> (Millipore) + 0.4 µM Apoptozole<sup>77</sup> (Az; Millipore), or GDA + PES-Cl + Az. The seedlings were treated for 24 h with the inhibitors in liquid 0.5× MS medium in the presence of 0.5 mM Lin, 5 µM NF or the corresponding concentration of DMSO as control. The samples were harvested and snap-frozen in liquid nitrogen for further analyses.

**Reporting Summary.** Further information on research design is available in the Nature Research Reporting Summary linked to this article.

**Data availability**

Mass spectrometry-based proteomic data have been deposited in the PRIDE partner repository of the ProteomeXchange Consortium with the dataset identifiers PXD010730 and PXD013005. All other data are available in the main text or the supplementary materials.

## REFERENCES

1. Bradbeer, J.W., Atkinson, Y.E., Borner, T. & Hagemann, R. Cytoplasmic synthesis of plastid polypeptides may be controlled by plastid-synthesized RNA. *Nature* **279**, 816-817 (1979).
2. Ramel, F. et al. Carotenoid oxidation products are stress signals that mediate gene responses to singlet oxygen in plants. *Proc Natl Acad Sci U S A* **109**, 5535-5540 (2012).
3. Estavillo, G.M. et al. Evidence for a SAL1-PAP chloroplast retrograde pathway that functions in drought and high light signaling in Arabidopsis. *Plant Cell* **23**, 3992-4012 (2011).
4. Xiao, Y.M. et al. Retrograde signaling by the plastidial metabolite MEcPP regulates expression of nuclear stress-response genes. *Cell* **149**, 1525-1535 (2012).
5. Woodson, J.D., Perez-Ruiz, J.M. & Chory, J. Heme synthesis by plastid ferrochelatase I regulates nuclear gene expression in plants. *Curr Biol* **21**, 897-903 (2011).
6. Fang, X. et al. Chloroplast-to-nucleus signaling regulates microRNA biogenesis in Arabidopsis. *Dev Cell* **48**, 371-382.e4 (2018).
7. Martin, G. et al. Phytochrome and retrograde signalling pathways converge to antagonistically regulate a light-induced transcriptional network. *Nature Commun* **7**, 11431 (2016).
8. Jarvis, P. & Lopez-Juez, E. Biogenesis and homeostasis of chloroplasts and other plastids. *Nat Rev Mol Cell Biol* **14**, 787-802 (2013).

9. Singh, R., Singh, S., Parihar, P., Singh, V.P. & Prasad, S.M. Retrograde signaling between plastid and nucleus: a review. *J Plant Physiol* **181**, 55-66 (2015).
10. Susek, R.E., Ausubel, F.M. & Chory, J. Signal-transduction mutants of Arabidopsis uncouple nuclear CAB and RBCS gene-expression from chloroplast development. *Cell* **74**, 787-799 (1993).
11. Koussevitzky, S. et al. Signals from chloroplasts converge to regulate nuclear gene expression. *Science* **316**, 715-719 (2007).
12. Mochizuki, N., Brusslan, J.A., Larkin, R., Nagatani, A. & Chory, J. Arabidopsis genomes uncoupled 5 (GUN5) mutant reveals the involvement of Mg-chelatase H subunit in plastid-to-nucleus signal transduction. *Proc Natl Acad Sci U S A* **98**, 2053-2058 (2001).
13. Larkin, R.M., Alonso, J.M., Ecker, J.R. & Chory, J. GUN4, a regulator of chlorophyll synthesis and intracellular signaling. *Science* **299**, 902-906 (2003).
14. Strand, A., Asami, T., Alonso, J., Ecker, J.R. & Chory, J. Chloroplast to nucleus communication triggered by accumulation of Mg-protoporphyrin IX. *Nature* **421**, 79-83 (2003).
15. von Gromoff, E.D., Alawady, A., Meinecke, L., Grimm, B. & Beck, C.F. Heme, a plastid-derived regulator of nuclear gene expression in Chlamydomonas. *Plant Cell* **20**, 552-567 (2008).
16. Moulin, M., McCormac, A.C., Terry, M.J. & Smith, A.G. Tetrapyrrole profiling in Arabidopsis seedlings reveals that retrograde plastid nuclear signaling is not due to Mg-protoporphyrin IX accumulation. *Proc Natl Acad Sci U S A* **105**, 15178-15183 (2008).



17. La Rocca, N., Rascio, N., Oster, U. & Rudiger, W. Amitrole treatment of etiolated barley seedlings leads to deregulation of tetrapyrrole synthesis and to reduced expression of Lhc and RbcS genes. *Planta* **213**, 101-108 (2001).
18. Wu, G.Z. et al. Control of retrograde signaling by rapid turnover of GENOMES UNCOUPLED 1. *Plant Physiol* **176**, 2472-2495 (2018).
19. Hernandez-Verdeja, T. & Strand, A. Retrograde signals navigate the path to chloroplast development. *Plant Physiol* **176**, 967-976 (2018).
20. Ruckle, M.E., DeMarco, S.M. & Larkin, R.M. Plastid signals remodel light signaling networks and are essential for efficient chloroplast biogenesis in Arabidopsis. *Plant Cell* **19**, 3944-3960 (2007).
21. Waters, M.T. et al. GLK transcription factors coordinate expression of the photosynthetic apparatus in Arabidopsis. *Plant Cell* **21**, 1109-1128 (2009).
22. Kakizaki, T. et al. Coordination of plastid protein import and nuclear gene expression by plastid-to-nucleus retrograde signaling. *Plant Physiol* **151**, 1339-1353 (2009).
23. Tadini, L. et al. GUN1 controls accumulation of the plastid ribosomal protein S1 at the protein level and interacts with proteins involved in plastid protein homeostasis. *Plant Physiol* **170**, 1817-1830 (2016).
24. Colombo, M., Tadini, L., Peracchio, C., Ferrari, R. & Pesaresi, P. GUN1, a jack-of-all-trades in chloroplast protein homeostasis and signaling. *Front Plant Sci* **7**, 1427 (2016).
25. Llamas, E., Pulido, P. & Rodriguez-Concepcion, M. Interference with plastome gene expression and Clp protease activity in Arabidopsis triggers a chloroplast unfolded protein response to restore protein homeostasis. *PLoS Genet* **13**, e1007022 (2017).

26. Sun, X. et al. A chloroplast envelope-bound PHD transcription factor mediates chloroplast signals to the nucleus. *Nat Commun* **2**, 477 (2011).
27. Page, M.T. et al. Seedlings lacking the PTM protein do not show a genomes uncoupled (gun) mutant phenotype. *Plant Physiol* **174**, 21-26 (2017).
28. Mochizuki, N., Susek, R. & Chory, J. An intracellular signal transduction pathway between the chloroplast and nucleus is involved in de-etiolation. *Plant Physiol* **112**, 1465-1469 (1996).
29. Su, P.-H. & Li, H.-M. Stromal Hsp70 is important for protein translocation into pea and Arabidopsis chloroplasts. *Plant Cell* **22**, 1516-1531 (2010).
30. Flores-Pérez, U. et al. Functional analysis of the Hsp93/ClpC chaperone at the chloroplast envelope. *Plant Physiol* **170**, 147-162 (2016).
31. Shi, L.X. & Theg, S.M. A stromal heat shock protein 70 system functions in protein import into chloroplasts in the moss *Physcomitrella patens*. *Plant Cell* **22**, 205-220 (2010).
32. Liu, L., McNeilage, R.T., Shi, L.X. & Theg, S.M. ATP requirement for chloroplast protein import is set by the  $K_m$  for ATP hydrolysis of stromal Hsp70 in *Physcomitrella patens*. *Plant Cell* **26**, 1246-1255 (2014).
33. Nielsen, E., Akita, M., Davila-Aponte, J. & Keegstra, K. Stable association of chloroplastic precursors with protein translocation complexes that contain proteins from both envelope membranes and a stromal Hsp100 molecular chaperone. *EMBO J* **16**, 935-946 (1997).
34. Huang, P.-K., Chan, P.-T., Su, P.-H., Chen, L.-J. & Li, H.-M. Chloroplast Hsp93 directly binds to transit peptides at an early stage of the preprotein import process. *Plant Physiol* **170**, 857-866 (2016).

35. Kubis, S. et al. The Arabidopsis ppil mutant is specifically defective in the expression, chloroplast import, and accumulation of photosynthetic proteins. *Plant Cell* **15**, 1859-1871 (2003).
36. Lee, S. et al. Heat shock protein cognate 70-4 and an E3 ubiquitin ligase, CHIP, mediate plastid-destined precursor degradation through the ubiquitin-26S proteasome system in Arabidopsis. *Plant Cell* **21**, 3984-4001 (2009).
37. Fellerer, C., Schweiger, R., Schongrubner, K., Soll, J. & Schwenkert, S. Cytosolic HSP90 cochaperones HOP and FKBP interact with freshly synthesized chloroplast preproteins of Arabidopsis. *Molecular Plant* **4**, 1133-1145 (2011).
38. Wrobel, L. et al. Mistargeted mitochondrial proteins activate a proteostatic response in the cytosol. *Nature* **524**, 485-488 (2015).
39. Weidberg, H. & Amon, A. MitoCPR-A surveillance pathway that protects mitochondria in response to protein import stress. *Science* **360**, eaan4146 (2018).
40. Kovacheva, S., Bedard, J., Wardle, A., Patel, R. & Jarvis, P. Further in vivo studies on the role of the molecular chaperone, Hsp93, in plastid protein import. *Plant J* **50**, 364-379 (2007).
41. Zhao, X., Huang, J. & Chory, J. Genome uncoupled 1 mutants are hypersensitive to norflurazon and lincomycin. *Plant Physiol* **178**, 960-964 (2018).
42. Kimura, Y., Yahara, I. & Lindquist, S. Role of the protein chaperone YDJ1 in establishing Hsp90-mediated signal transduction pathways. *Science* **268**, 1362-1365 (1995).
43. Cutforth, T. & Rubin, G.M. Mutations in Hsp83 and cdc37 impair signaling by the sevenless receptor tyrosine kinase in Drosophila. *Cell* **77**, 1027-1036 (1994).

44. Zhang, X.C., Millet, Y.A., Cheng, Z., Bush, J. & Ausubel, F.M. Jasmonate signalling in Arabidopsis involves SGT1b-HSP70-HSP90 chaperone complexes. *Nat Plants* **1**, 15049 (2015).
45. Wang, R.H. et al. HSP90 regulates temperature-dependent seedling growth in Arabidopsis by stabilizing the auxin co-receptor F-box protein TIR1. *Nat Commun* **7**, 10269 (2016).
46. Kindgren, P., Noren, L., Lopez Jde, D., Shaikhali, J. & Strand, A. Interplay between Heat Shock Protein 90 and HY5 controls PhANG expression in response to the GUN5 plastid signal. *Mol Plant* **5**, 901-913 (2012).
47. Kindgren, P. et al. A novel proteomic approach reveals a role for Mg-protoporphyrin IX in response to oxidative stress. *Physiol Plant* **141**, 310-320 (2011).
48. Cardamone, M.D. et al. Mitochondrial retrograde signaling in mammals is mediated by the transcriptional cofactor GPS2 via direct mitochondria-to-nucleus translocation. *Mol Cell* **69**, 757-772 e757 (2018).
49. Quiros, P.M., Mottis, A. & Auwerx, J. Mitonuclear communication in homeostasis and stress. *Nat Rev Mol Cell Biol* **17**, 213-226 (2016).
50. Chan, K.X., Phua, S.Y., Crisp, P., McQuinn, R. & Pogson, B.J. Learning the languages of the chloroplast: retrograde signaling and beyond. *Annu Rev Plant Biol* **67**, 25-53 (2016).
51. Wang, X. & Chen, X.J. A cytosolic network suppressing mitochondria-mediated proteostatic stress and cell death. *Nature* **524**, 481-484 (2015).
52. Jarvis, P. et al. An Arabidopsis mutant defective in the plastid general protein import apparatus. *Science* **282**, 100-103 (1998).

53. Huang, W., Ling, Q., Bedard, J., Lilley, K. & Jarvis, P. In vivo analyses of the roles of essential Omp85-related proteins in the chloroplast outer envelope membrane. *Plant Physiol* **157**, 147-159 (2011).
54. Murashige, T. & Skoog, F. A revised medium for rapid growth and bio assays with tobacco tissue cultures. *Physiol Plant* **15**, 473-497 (1962).
55. Azimzadeh, J. et al. Arabidopsis TONNEAU1 proteins are essential for preprophase band formation and interact with centrin. *Plant Cell* **20**, 2146-2159 (2008).
56. Grefen, C. et al. A ubiquitin-10 promoter-based vector set for fluorescent protein tagging facilitates temporal stability and native protein distribution in transient and stable expression studies. *Plant J* **64**, 355-365 (2010).
57. Scharff, L.B. & Koop, H.U. Linear molecules of tobacco ptDNA end at known replication origins and additional loci. *Plant Mol Biol* **62**, 611-621 (2006).
58. Zoschke, R., Watkins, K.P. & Barkan, A. A rapid ribosome profiling method elucidates chloroplast ribosome behavior in vivo. *Plant Cell* **25**, 2265-2275 (2013).
59. Pfaffl, M.W. A new mathematical model for relative quantification in real-time RT-PCR. *Nucleic Acids Res* **29**, e45 (2001).
60. Cahoon, E.B., Shanklin, J. & Ohlrogge, J.B. Expression of a coriander desaturase results in petroselinic acid production in transgenic tobacco. *Proc Natl Acad Sci U S A* **89**, 11184-11188 (1992).
61. Czarnecki, O. et al. An Arabidopsis GluTR binding protein mediates spatial separation of 5-aminolevulinic acid synthesis in chloroplasts. *Plant Cell* **23**, 4476-4491 (2011).
62. Barkan, A. Approaches to investigating nuclear genes that function in chloroplast biogenesis in land plants. *Methods Enzymol* **297**, 38-57 (1998).

63. Aronsson, H. & Jarvis, R.P. Rapid isolation of Arabidopsis chloroplasts and their use for in vitro protein import assays. *Methods Mol Biol* **774**, 281-305 (2011).
64. Mou, Z., He, Y., Dai, Y., Liu, X. & Li, J. Deficiency in fatty acid synthase leads to premature cell death and dramatic alterations in plant morphology. *Plant Cell* **12**, 405-418 (2000).
65. Walz, C., Juenger, M., Schad, M. & Kehr, J. Evidence for the presence and activity of a complete antioxidant defence system in mature sieve tubes. *Plant J* **31**, 189-197 (2002).
66. Cox, J. & Mann, M. MaxQuant enables high peptide identification rates, individualized p.p.b.-range mass accuracies and proteome-wide protein quantification. *Nat Biotechnol* **26**, 1367-1372 (2008).
67. Tyanova, S. et al. The Perseus computational platform for comprehensive analysis of (prote)omics data. *Nat Methods* **13**, 731-740 (2016).
68. Patton, D.A. et al. An embryo-defective mutant of arabidopsis disrupted in the final step of biotin synthesis. *Plant Physiol* **116**, 935-946 (1998).
69. Porra, R.J., Thompson, W.A. & Kriedemann, P.E. Determination of accurate extinction coefficients and simultaneous-equations for assaying chlorophyll-a and chlorophyll-b extracted with 4 different solvents: verification of the concentration of chlorophyll standards by atomic-absorption spectroscopy. *Biochim Biophys Acta* **975**, 384-394 (1989).
70. Moran, R. Formulae for determination of chlorophyllous pigments extracted with n,n-dimethylformamide. *Plant Physiol* **69**, 1376-1381 (1982).

71. Huang, W., Ling, Q., Bédard, J., Lilley, K. & Jarvis, P. In vivo analyses of the roles of essential Omp85-related proteins in the chloroplast outer envelope membrane. *Plant Physiol* **157**, 147-159 (2011).
72. Froehlich, J. Studying Arabidopsis envelope protein localization and topology using thermolysin and trypsin proteases. *Methods Mol Biol* **774**, 351-367 (2011).
73. Queitsch, C., Sangster, T.A. & Lindquist, S. Hsp90 as a capacitor of phenotypic variation. *Nature* **417**, 618-624 (2002).
74. Stebbins, C.E. et al. Crystal structure of an Hsp90-geldanamycin complex: targeting of a protein chaperone by an antitumor agent. *Cell* **89**, 239-250 (1997).
75. Massey, A.J. et al. A novel, small molecule inhibitor of Hsc70/Hsp70 potentiates Hsp90 inhibitor induced apoptosis in HCT116 colon carcinoma cells. *Cancer Chemother Pharmacol* **66**, 535-545 (2010).
76. Balaburski, G.M. et al. A modified HSP70 inhibitor shows broad activity as an anticancer agent. *Mol Cancer Res* **11**, 219-229 (2013).
77. Cho, H.J. et al. A small molecule that binds to an ATPase domain of Hsc70 promotes membrane trafficking of mutant cystic fibrosis transmembrane conductance regulator. *J Am Chem Soc* **133**, 20267-20276 (2011).

**Correspondence and requests for materials** should be addressed to R.B.

## **Acknowledgements**

We thank the MPI-MP GreenTeam for help with plant transformation. We are grateful to Dario Leister (Ludwig-Maximilians-University Munich, Germany) for providing *gun1-102* seeds, Åsa Strand (Umeå University, Sweden) for providing seeds of *HSP90* RNAi

lines, Adrian Clarke (Gothenburg University, Sweden) for providing antibodies against Clp proteins and Michal Gorka from MPI-MP for running the mass spectrometry samples to quantify the Toc-Tic subunits. This research was financed by the Max Planck Society, grants from the Deutsche Forschungsgemeinschaft to R.B. (FOR 804; SFB-TRR 175 A04), R.Z. (ZO 302/4-1; SFB-TRR 175 A04) and B.G. (SFB-TRR 175 C04), and a grant from the Biotechnology and Biological Sciences Research Council (BBSRC) to R.P.J. (research grant number BB/N006372/1).

### **Author contributions**

R.B. and G.Z.W. conceived and designed this research. G.Z.W. performed most of the experiments. E.H.M. performed the mass spectrometry-based proteomics. A.R. and B.G. investigated the import of TPB enzymes. M.S. performed the ribosome profiling experiments, analyzed and discussed the results with G.Z.W. and R.Z. Q.L. and G.Z.W. conducted protein import assays and analyzed the results with P.J. M.A.S. performed the photosynthesis measurements. D.W. mapped peptides to transit peptide regions of chloroplast proteins. R.B. and G.Z.W. wrote the manuscript, with input from the co-authors.

**Competing interests:** The authors declare no competing interests.



## Figure legends

### **Fig. 1 | GUN1 physically interacts with the ClpC1 and cpHSC70-1 chaperones.**

**a**, Co-IPs performed with rosette leaves from GUN1-GFP transgenic lines in the *gun1-101* (C-1) or wild-type (OE-13) background. An RBCS transit peptide-fused GFP in the wild type background (C-cpGFP) line was used as co-IP control. Tic40, which cannot be detected by mass spectrometry in co-IPs, was included as a negative control. 10% of the total input was loaded in a separated lane and analyzed as input control. Four independent immunoprecipitation experiments were performed with anti-GFP antibodies, and the immunoprecipitates were subjected to western blotting with anti-GFP antibodies (detecting cpGFP and GUN1-GFP) or antibodies against proteins associated with the Tic (anti-ClpC, anti-Tic110, anti-Tic40) and Toc (anti-Toc159) complexes.

**b**, Co-IP performed with de-etiolating seedlings grown without (control) or with 0.5 mM Lin. 10% of the total input was loaded in a separated lane as input control. Two independent co-IP experiments were performed and showed similar results. The anti-ClpC and anti-cpHSC70 antibodies (in **a** and **b**) do not distinguish between different isoforms of ClpC (ClpC1 and ClpC2) and cpHSC70 (cpHSC70-1 and cpHSC70-2).

**c**, BiFC assays verifying the specific interaction of GUN1 with ClpC1 and cpHSC70-1. GUN1-YN co-expressed with ClpD-YC served as negative control. ClpC1-YN co-expressed with Tic110-YC served as positive control. For additional controls expressing the individual proteins as GFP fusions, see Supplementary Fig. 6. Three independent experiments were performed and showed similar results. Scale bars: 10  $\mu$ m.

**d**, The *cphsc70-1* mutant shows a GUN phenotype. Expression of *LHCBI.2* was determined by qRT-PCR and the relative gene expression is compared to that in the wild

type (WT) grown under identical conditions. Data are presented as means  $\pm$  s.d. ( $n=3$  biologically independent samples, indicated as open circles). In contrast to *cphsc70-1*, the *clpc1* mutant shows a GUN phenotype only upon Lin (0.5 mM) treatment, but not upon NF (5  $\mu$ M) treatment. See Supplementary Fig. 9a for expression data for additional PhANGs and non-PhANG control genes.

**Fig. 2 | GUN1 regulates protein import under conditions that interfere with retrograde signaling.**

**a**, Four week-old plants grown in long-day conditions. Representative photographs from four independent experiments with similar results are shown. Scale bars: 1 cm.

**b**, Subcellular distributions of differentially expressed proteins (as percentages) between *clpc1* and *gun1clpc1*, as determined by proteomic analysis. Numbers in parentheses indicate the total number of proteins identified as differentially expressed between the two genotypes.

**c**, Heat map showing strong up-regulation of cytosolic HSP70, HSP90 and their co-chaperones (HOP3 and SGT1B) in the *gun1clpc1* double mutant. The heat map shows  $\log_2$  fold changes (means of three biological replicates) in protein abundance of different mutants relative to the wild type.

**d**, Histogram showing intensity-based percentages of peptides mapping to transit peptide regions (P-TP, indicating precursor accumulation in the cytosol) relative to the total protein intensity in each sample. Data are means  $\pm$  s.d. ( $n=3$  biologically independent samples, indicated as open circles). A two-tailed Student's *t*-test was performed to determine the significance of differences between the *gun1clpc1* double mutant and the *gun1* single mutant or the wild type. Note that, due to the TP being only a small part of

the full-length protein, the relative P-TP intensity strongly underrepresents the relative precursor protein intensity. Also, because of the fast degradation of unimported precursors by the cytosolic PQC, only a small proportion of the precursors can eventually be detected by mass spectrometry.

**e,** Protein import assays show reduced import capacity of the *gun1clpc1* double mutant by quantifying maturation (Mat) of *in vitro* translated (IVT) Rubisco small subunit (RBCS) precursors (Pre). The image from a representative experiment (upper panel) and the quantitation of import efficiencies from three independent experiments (lower panel; means  $\pm$  s.e.) are shown. A two-tailed Student's *t*-test was performed to determine the significance of differences between the wild type and *clpc1*, and between *clpc1* and *gun1clpc1*.

**f,** Protein import assays show reduced import capacity of the *gun1* mutant grown in the presence of 15  $\mu$ M Lin. Seedlings were grown in the presence of 15  $\mu$ M Lin for 9 days (wild type) or 11 days (*gun1-101*) to reach a similar developmental stage. *In vitro* protein import assays were conducted as in (e) and import efficiencies are shown as means  $\pm$  s.e. from three independent experiments. A two-tailed Student's *t*-test was performed to determine the significance of differences between the wild type and *gun1*. Th: import for 4 min followed by treatment with thermolysin.

**Fig. 3 | Unimported precursor proteins accumulate in the cytosol of *gun1* upon Lin or NF treatment.**

**a,** cpGFP cannot be efficiently targeted to plastids in the *gun1* background (*g*-cpGFP) compared to in the wild-type background (*C*-cpGFP) upon Lin or NF treatment. Representative images from three independent experiments with similar results are

shown. Seedlings were germinated and grown for 5 days in the dark followed by 2 days in continuous light in the presence of 0.5 mM Lin or 5  $\mu$ M NF. For Lin and NF treatments, bright-field (BF) images are shown instead of the chlorophyll (Chl) fluorescence images, because chlorophyll fluorescence is not visible. See also Supplementary Fig. 18. Scale bars: 10  $\mu$ m.

**b,** Immunoblot analyses to determine the accumulation of ClpD and ClpP4 in *gun1* and overexpression (OE) lines without or with 0.5 mM Lin treatment. Four independent experiments were performed with similar results. Seedlings were germinated and grown for 5 days in the dark followed by 2 days in continuous light. A larger band for ClpD (arrow) is seen in the Lin treatment of both alleles of *gun1*. Chloroplast-encoded ClpP1 is repressed as Lin inhibits chloroplast translation. Actin served as loading control.

**c,** Immunoblot analyses to compare the accumulation of ClpD upon NF (5  $\mu$ M) treatment. Four independent experiments were performed with similar results. C: complemented line. Note that the shifted ClpD bands in the *gun1* mutants are much stronger than in the wild type and the complemented lines. C-1 and C-10 were on the same blot as the other genotypes, but not directly adjacent to them (indicated by space separation).

**d,** Immunoblot analysis of isolated chloroplasts demonstrates that the larger ClpD form in *gun1* accumulates outside chloroplasts, as chloroplast samples do not show this band. Two independent experiments were performed with similar results. Seedlings were grown in long-day conditions with 15  $\mu$ M Lin for 9 days. Actin and ClpP4 served as cytosolic and chloroplast protein controls, respectively.

**e,** Defective import of ClpD transit peptide-fused GFP in the *gun1* (*g*-ClpD-TP-GFP), but not in the wild-type background (C-ClpD-TP-GFP) under 0.5 mM Lin treatment. In the *g*-ClpD-TP-GFP line, unimported GFP aggregates in the cytosol upon Lin treatment.

Representative images from two independent experiments with similar results are shown. Note that, under control condition, not all *gun1* mesophyll cells express ClpD-TP-GFP. The GFP, chlorophyll fluorescence and bright-field images were overlaid. For the individual images, see Supplementary Fig. 24d. Scale bars: 10  $\mu$ M.

**f**, Immunoblot analyses demonstrate accumulation of the preClpD band in the *cphsc70-1* mutant upon Lin or NF treatment. *gun1-101* was included as a positive control. Two independent experiments were performed with similar results. Seedlings of the different genotypes were grown in long-day conditions for 7 days in control conditions or for 11 days with Lin (0.5mM) and NF (5  $\mu$ M) treatment.

**Fig. 4 | Precursors accumulating in the cytosol function in retrograde regulation of PhANG expression.**

**a**, Immunoblots to identify ClpD overexpression lines in the wild-type (C-ClpD-) and the *gun1-101* (g-ClpD-) background. PreClpD accumulates in the *gun1* background causing a white cotyledon phenotype (see panel **b**). The precursor band is only seen in white seedlings (line 11, 11w), but not in green seedlings of the same line (11g). Seedlings were grown for 7 days in long-day conditions. Three independent experiments were performed with similar results. The *clpd-1* and *clpc1-1* mutants were included as controls to identify ClpD-specific bands. Actin served as loading control.

**b**, Overexpression of ClpD causes a white-cotyledon phenotype in g-ClpD, but not in C-ClpD lines. Representative photographs of seven-day-old seedlings from four independent experiments with similar results are shown. Scale bar: 2 cm and 5 mm for the whole plates and inset images, respectively.

**c,** The ClpC chaperone and the ClpP4 subunit of the Clp protease accumulate to similar levels in the wild type, *gun1-101*, C-ClpD and g-ClpD lines. The immunoblots were conducted using 7-day-old seedlings grown in long-day conditions as shown in **b**. cpHSC70 and actin served as loading controls. Two independent experiments were performed with similar results. The anti-ClpC and anti-cpHSC70 antibodies do not distinguish between different isoforms of ClpC and cpHSC70.

**d,** Accumulation of preClpD interferes with retrograde communication between chloroplasts and the nucleus. Immunoblots reveal that preClpD weakly accumulates in C-ClpD lines upon Lin (0.5 mM) or NF (5  $\mu$ M) treatments, which is not seen in the untreated control (panel **a**). As a consequence, C-ClpD lines show a weak GUN phenotype in both Lin and NF treatments (lower panel). g-ClpD lines show an even stronger GUN phenotype than *gun1* (see qRT-PCR results in Supplementary Table 4). Three independent experiments were performed with similar results. Actin served as loading control for immunoblots.

**e,f,** Northern blot analyses demonstrate that *clpd* mutants do not show a GUN phenotype. *gun1clpd* double mutants respond exactly as the *gun1* single mutant to both Lin (**e**) and NF (**f**) treatments. Two independent experiments were performed with similar results. In (**d-f**), seedlings were grown in the presence of 0.5 mM Lin or 5  $\mu$ M NF for 7 days in long-day conditions. Methylene blue staining of rRNAs served as loading control. The *LHCBI* probe used for hybridization does not distinguish between different isoforms of *LHCBI*.

**Fig. 5 | The HSP90 chaperone complex functions as a component of retrograde signaling.**

**a,b,** Western blots demonstrate strong induction of cytosolic HSP90.1 and HSP70 in the *gun1-101* mutant in response to Lin and NF treatments. Seedlings were grown for 7 days in long-day conditions in the presence of the indicated concentration of Lin or NF. Three independent experiments were performed with similar results, and representative images are shown. Actin served as loading control.

**c,** PhANG expression is positively correlated with HSP90 activity. qRT-PCR shows that expression of *LHCB1.2*, *LHCB2.2* and *RBCS2B* is repressed when seedlings were treated with 50  $\mu$ M HSP90 inhibitor GDA (HSP90 i), whereas HSP70 inhibition (HSP70 i) by VER155008 (50  $\mu$ M) has less effects. Combined inhibition of HSP90 and HSP70 (HSP90/70 i) has only minor additive effects. Relative gene expression is compared to the wild type (WT) under control conditions (DMSO). The non-PhANG gene *PDH1* was used as negative control.

**d,** Inhibition of HSP90 activity suppresses the PGE pathway of retrograde signaling in *gun1-101*. Inhibition of HSP70 has much less effect on PhANG expression, and combined inhibition of both HSP90 and HSP70 has similar effects as inhibition of HSP90 alone. Gene expression relative to the wild type (with 0.5 mM Lin, without HSP90 and HSP70 inhibitors) is shown.

**e,** Inhibition of HSP90 activity suppresses the TPB pathway of retrograde signaling in both *gun1* and *gun5* mutants. Gene expression relative to the wild type (with 5  $\mu$ M NF, without HSP90 and HSP70 inhibitors) is shown. In (c-e), the data are presented as means  $\pm$  s.d. ( $n=4$  biologically independent samples, indicated as open circles).

**f,** The GUN phenotype of *gun1* is suppressed in *HSP90* RNAi lines. Three independent *HSP90* RNAi (*HSP90i*) lines in the wild-type background<sup>46</sup> were crossed into the *gun1-101* background. The expression of three PhANGs (*LHCB1.2*, *LHCB2.2* and *RBCS2B*)

was suppressed in *gun1HSP90i* lines upon both Lin (0.5 mM) and NF (5  $\mu$ M) treatment. *PDHI* was used as a negative control. Relative gene expression is compared to the wild type grown under the same condition and presented as means  $\pm$  s.d. ( $n=6$ , of three biologically independent samples, with two technical replicates performed for each biologically independent sample; all replicates are indicated as open circles).

**Fig. 6 | Control of the import of TPB enzymes by GUN1 and working model of the GUN1/GUN5-HSP90 retrograde signaling pathway.**

**a,** Immunoblot analyses reveal that the import efficiency of TPB enzymes depends on *GUN1* under Lin (0.5 mM) or NF (5  $\mu$ M) treatment. Arrows indicate the preproteins. Two independent experiments were performed with similar results, and representative images are shown. Ponceau S staining of the membranes served as loading control. GluTR: glutamyl-tRNA reductase; GBP: GluTR-binding protein; CHL27: Mg-ProtoIX monomethyl ester cyclase.

**b,** Working model of the GUN1/GUN5-HSP90 retrograde signaling pathway. While GUN1 has no function in differentiated chloroplasts and is degraded (dashed oval) by the Clp protease through the action of ClpC1 (ClpC), GUN1 interacts with cpHSC70-1 (HSC70) and regulates protein import when chloroplast biogenesis is inhibited (e.g., by Lin or NF treatment). Overaccumulation of preproteins in the cytosol of *gun1* induces the accumulation of cytosolic HSP90, which in turn sustains PhANG expression. HSP90 regulates PhANG expression by either repression of a negative (yellow) or activation of a positive (green) transcriptional regulator (transcription factor, TF). Lower accumulation of Mg-ProtoIX in *gun5* maintains high activity of the HSP90 chaperone complex<sup>46</sup>, thus



resulting in the GUN phenotype of this mutant. GUN1 participates in the TPB-mediated retrograde signaling pathway through control of the import of key TPB enzymes.

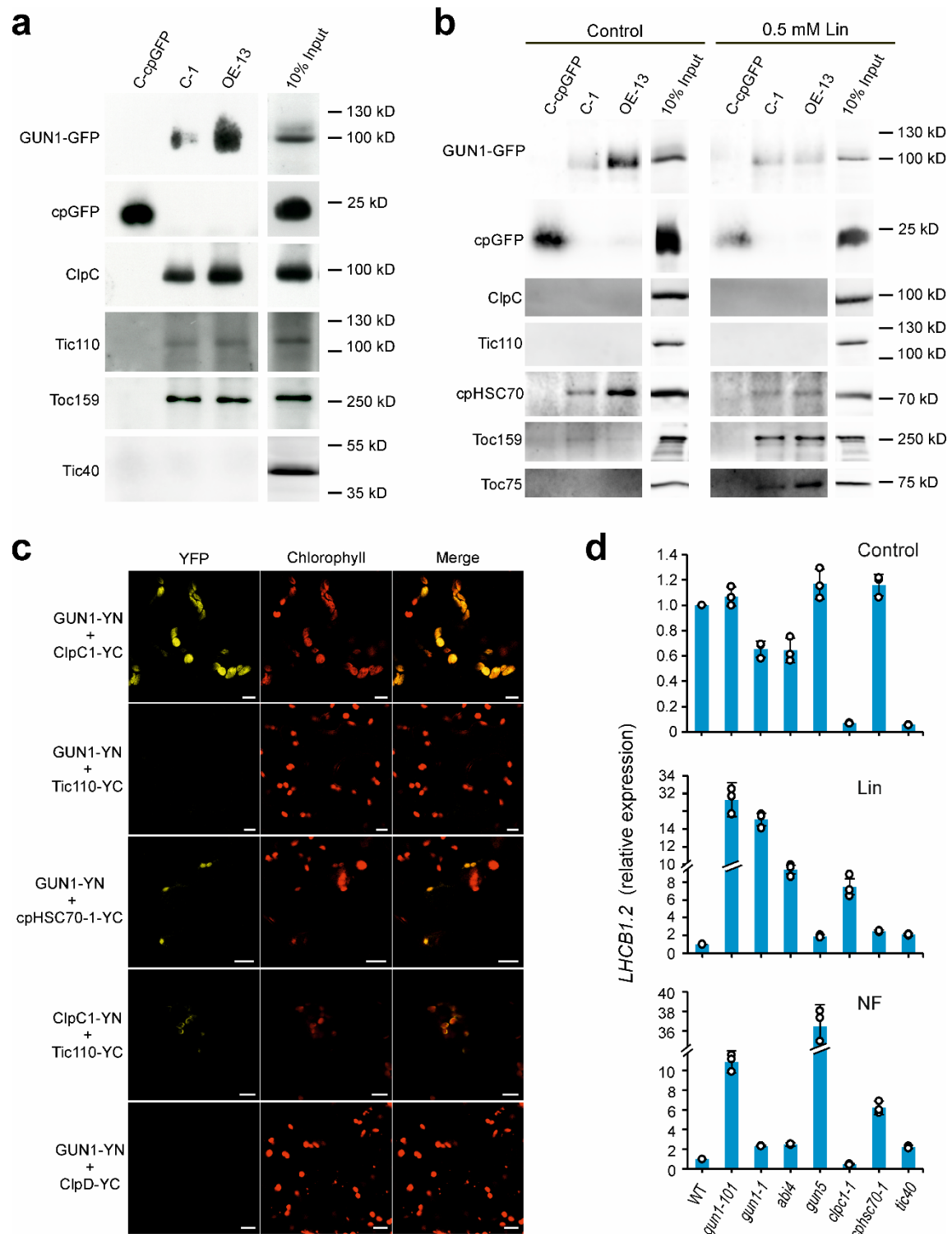


Figure 1

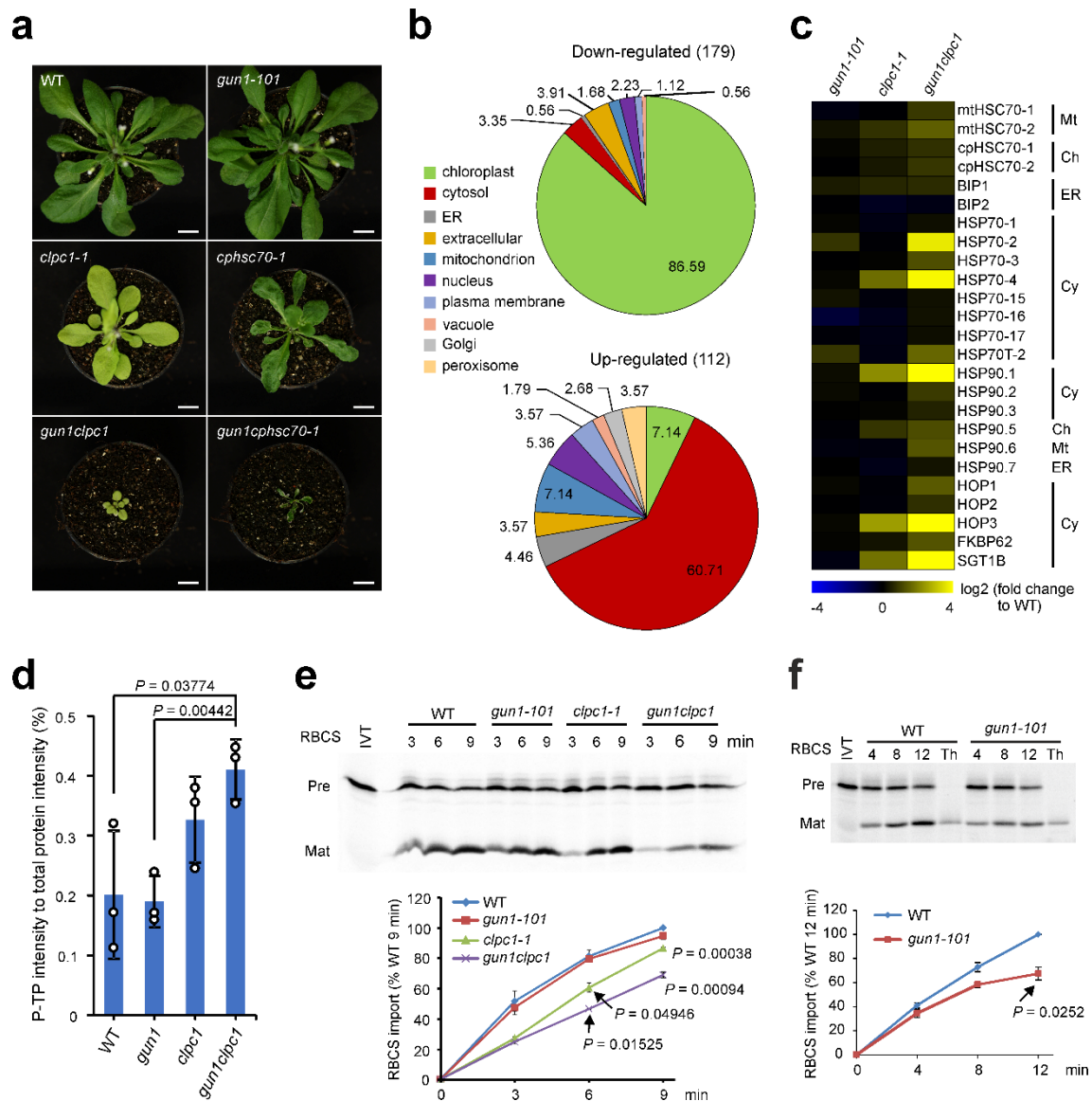


Figure 2

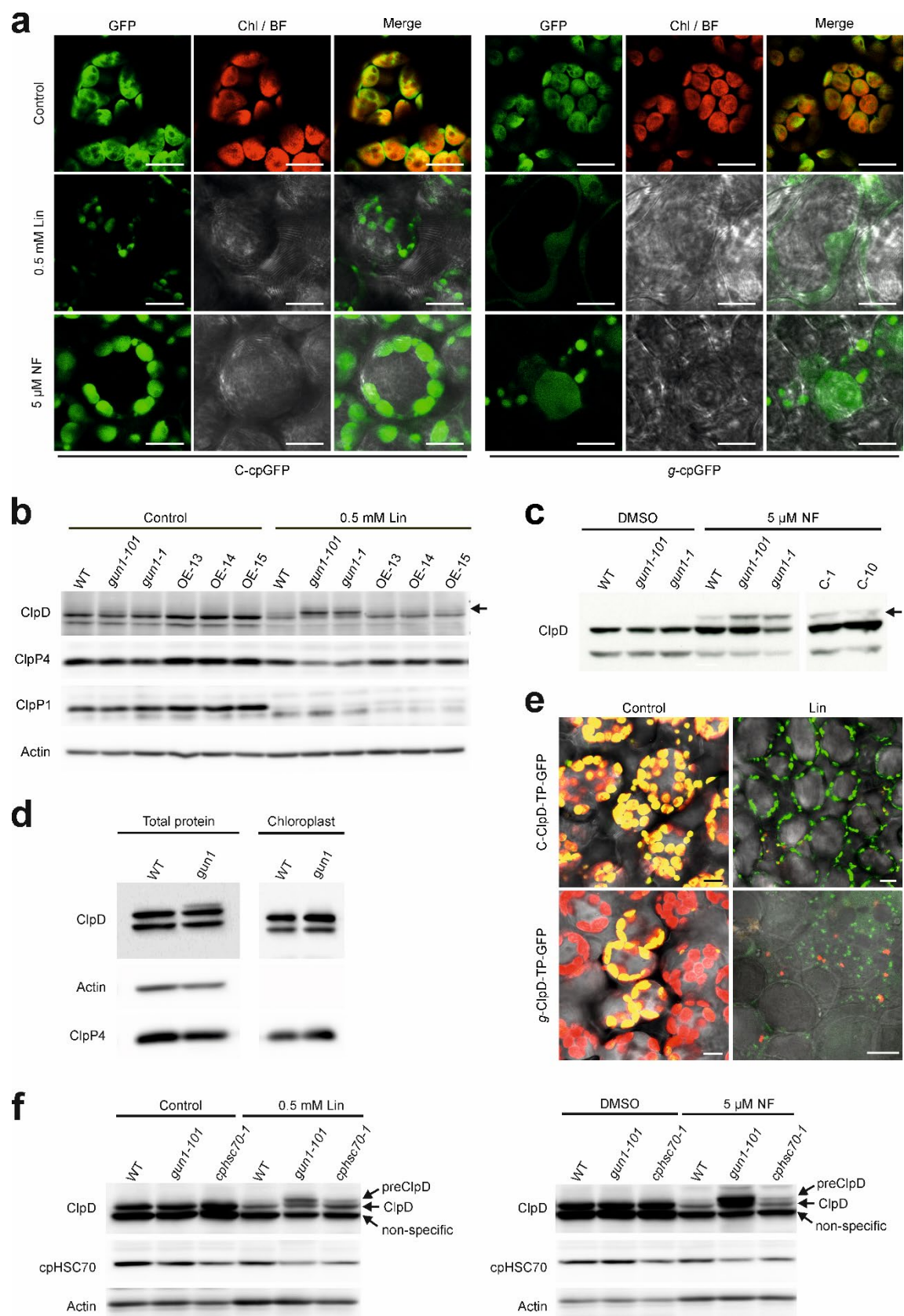


Figure 3

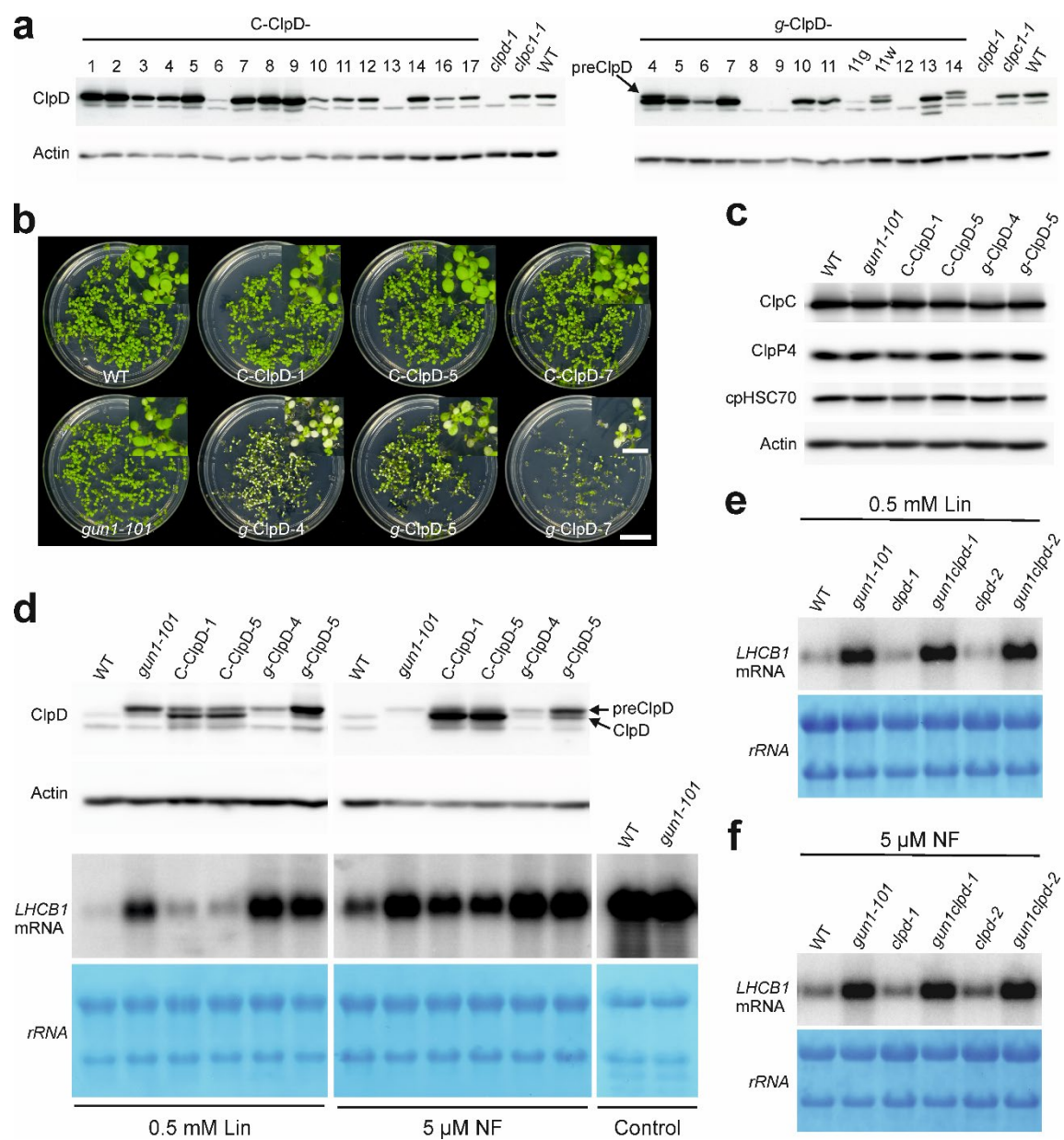


Figure 4



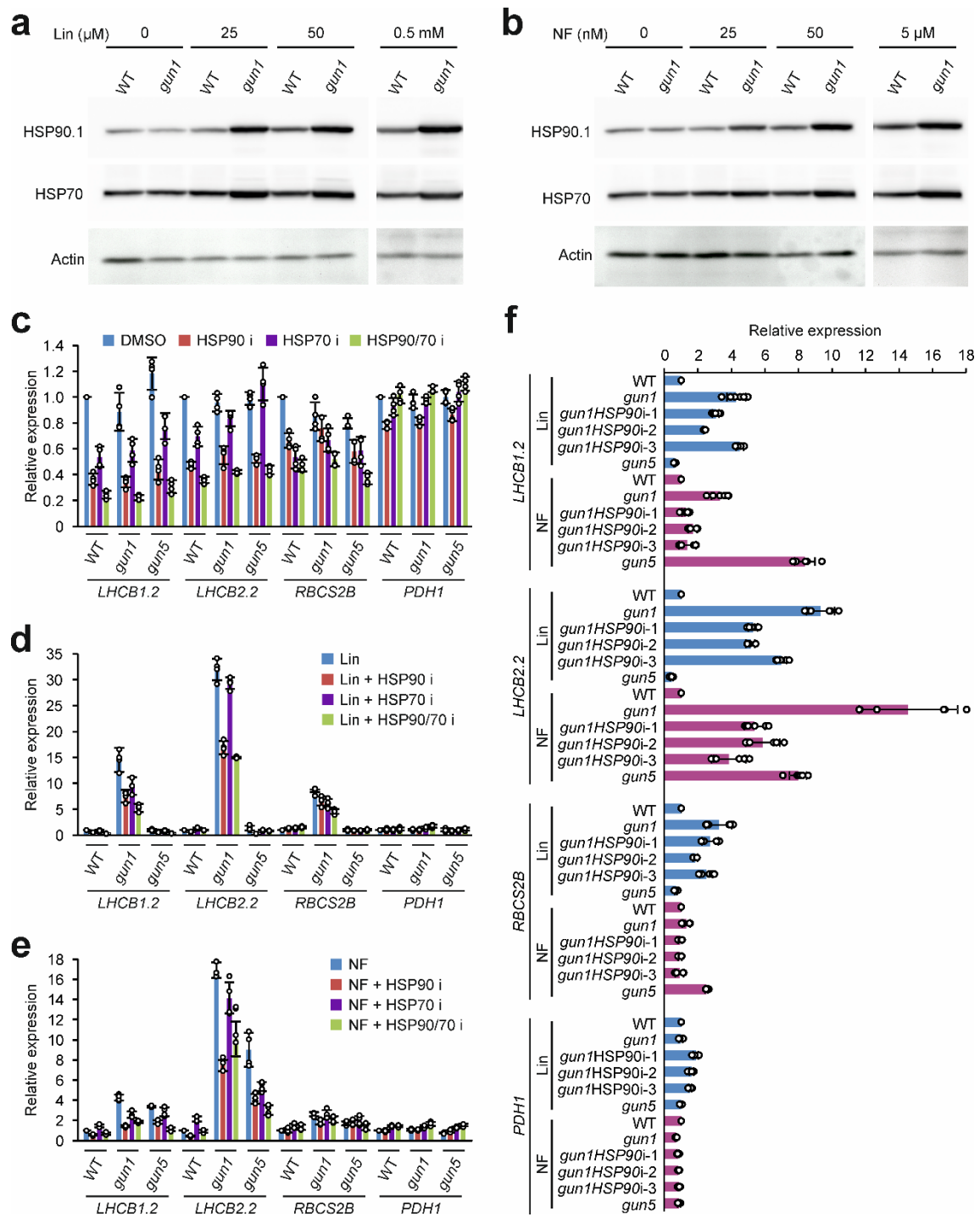


Figure 5

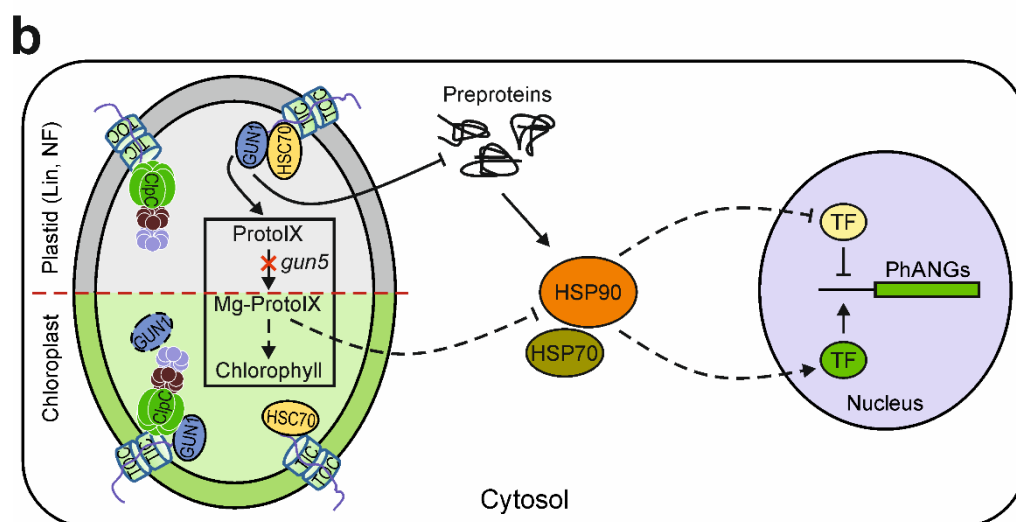
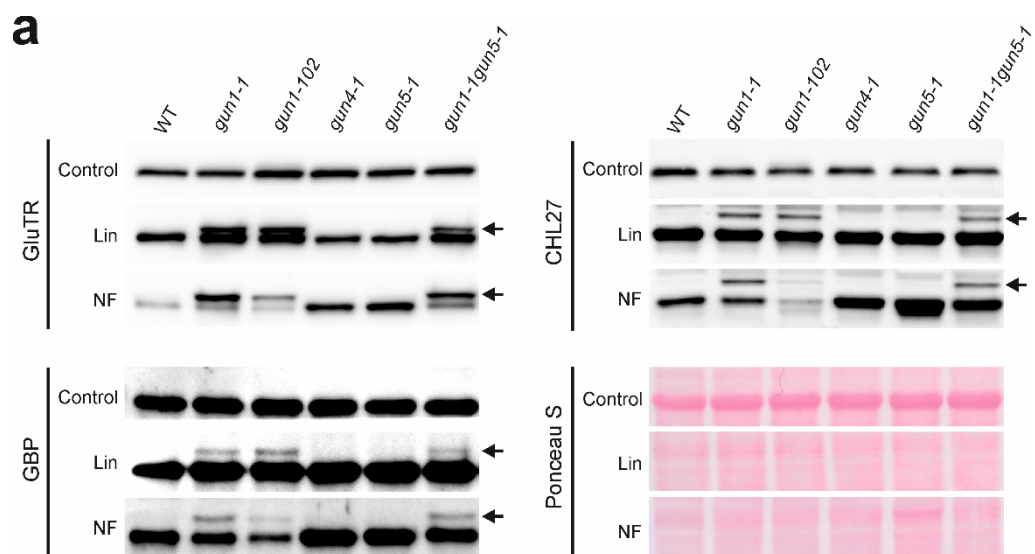


Figure 6

## **SUPPLEMENTARY FILES**

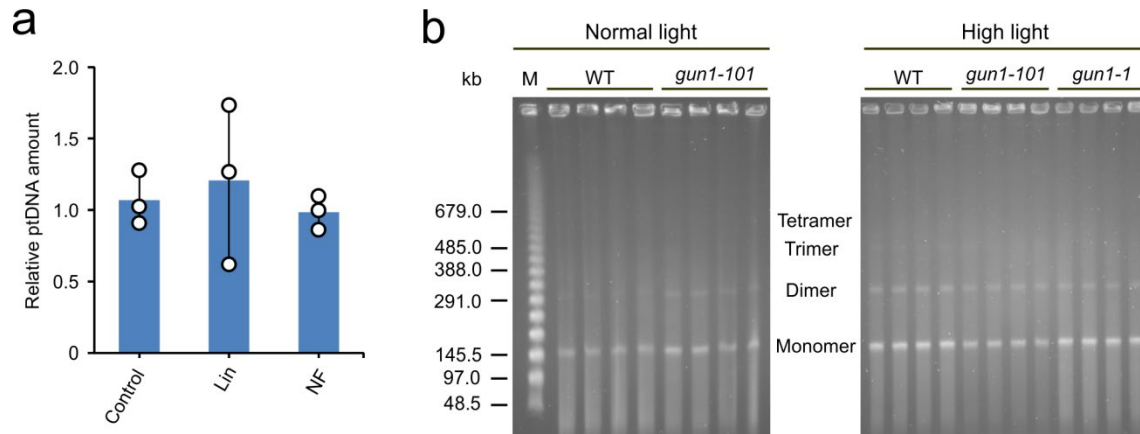
**Supplementary Information** (pdf; 7.89 MB): Contains Supplementary Figures 1-30 and Supplementary Tables 1-5.

**Supplementary Data 1** (xlsx; 7.55 MB): Data from array-based ribosome profiling experiments.

**Supplementary Data 2** (xlsx; 369 kB): Mass spectrometry data from co-IP experiments.

**Supplementary Data 3** (xlsx; 786 kB): Mass spectrometry data of proteomic analyses of the wild type, the *gun1* and *clpcl* single mutants, and the *gun1clpcl* double mutant.

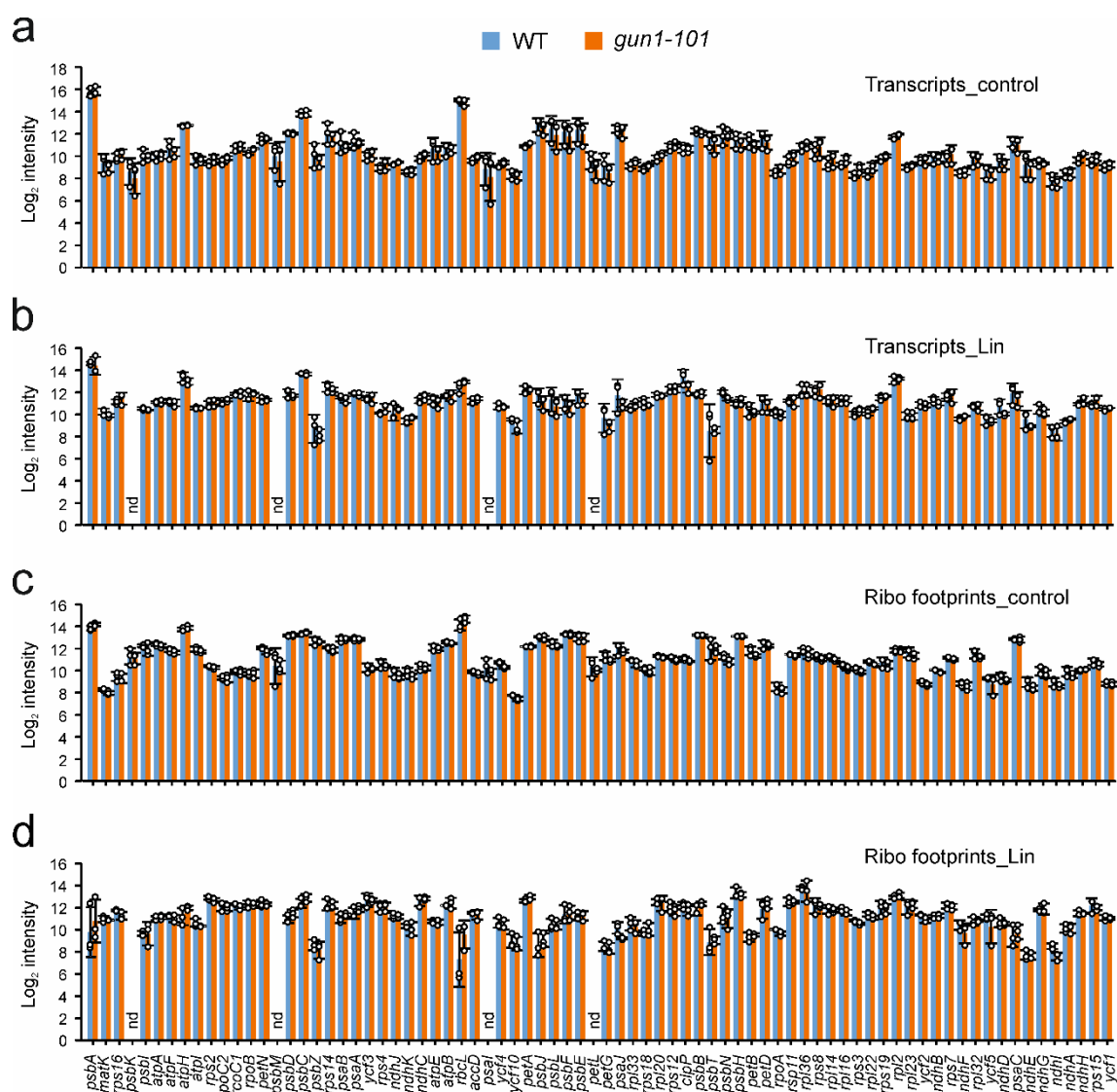




**Supplementary Figure 1. Test for association of GUN1 with chloroplast DNA metabolism.**

**a**, qPCR assays reveal similar plastid DNA (ptDNA) amounts in the wild type (WT) and *gun1-1* in the presence or absence of Lin (0.5 mM) or NF (5  $\mu$ M). The ratio between wild type and the *gun1-1* mutant is presented as means  $\pm$  s.d. ( $n=3$  biologically independent samples, indicated as open circles).

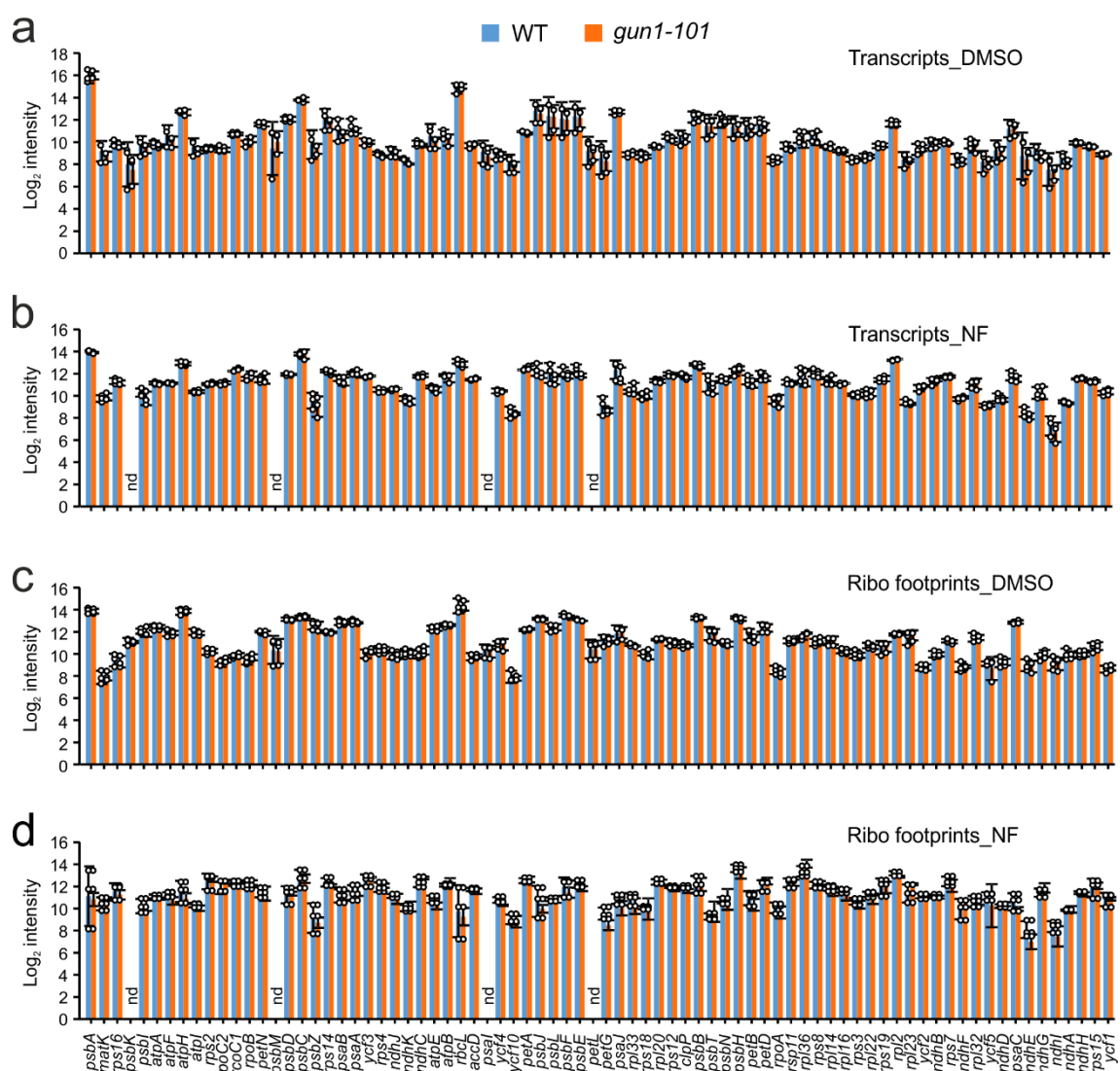
**b**, Pulsed-field gel electrophoresis (PFGE) shows identical amounts and conformations of the ptDNA in the wild type (WT) and *gun1* grown under normal light conditions (left panel) and after high-light treatment (right panel). Four biologically independent samples were analyzed for each genotype. M: molecular weight marker.



**Supplementary Figure 2. Ribosome profiling of chloroplast mRNAs in the wild type and *gun1* under control condition and upon Lin treatment.**

**a,b,** Microarray analysis of transcripts accumulation in the wild type (WT) and the *gun1-101* mutant in control condition or upon Lin (0.5 mM) treatment. Log<sub>2</sub> total RNA signals (Transcripts) of all plastid protein-coding genes were plotted along the genome as means  $\pm$  s.d. ( $n=3$  biologically independent samples, indicated as open circles). The signals from all probes for each gene were averaged.

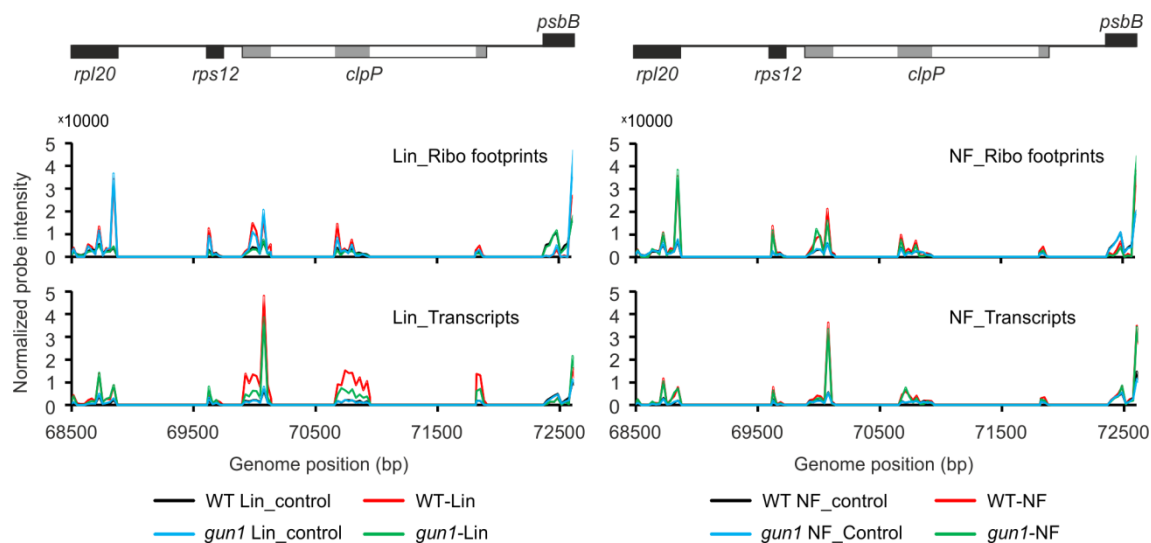
**c,d**, Ribosome profiling of chloroplast mRNAs in control condition or upon Lin treatment (0.5 mM) in the wild type and the *gun1-101* mutant. Log<sub>2</sub> of ribosome footprint signals (Ribo footprints) were plotted for all protein-coding genes along the genome as means  $\pm$  s.d. ( $n=3$  biologically independent samples, indicated as open circles). Signals from all probes for each gene were averaged. Lowly expressed genes that did not pass the data filtering criteria are marked as nd (not determined).



**Supplementary Figure 3. Ribosome profiling of chloroplast mRNAs in the wild type and *gun1* without or with NF treatment.**

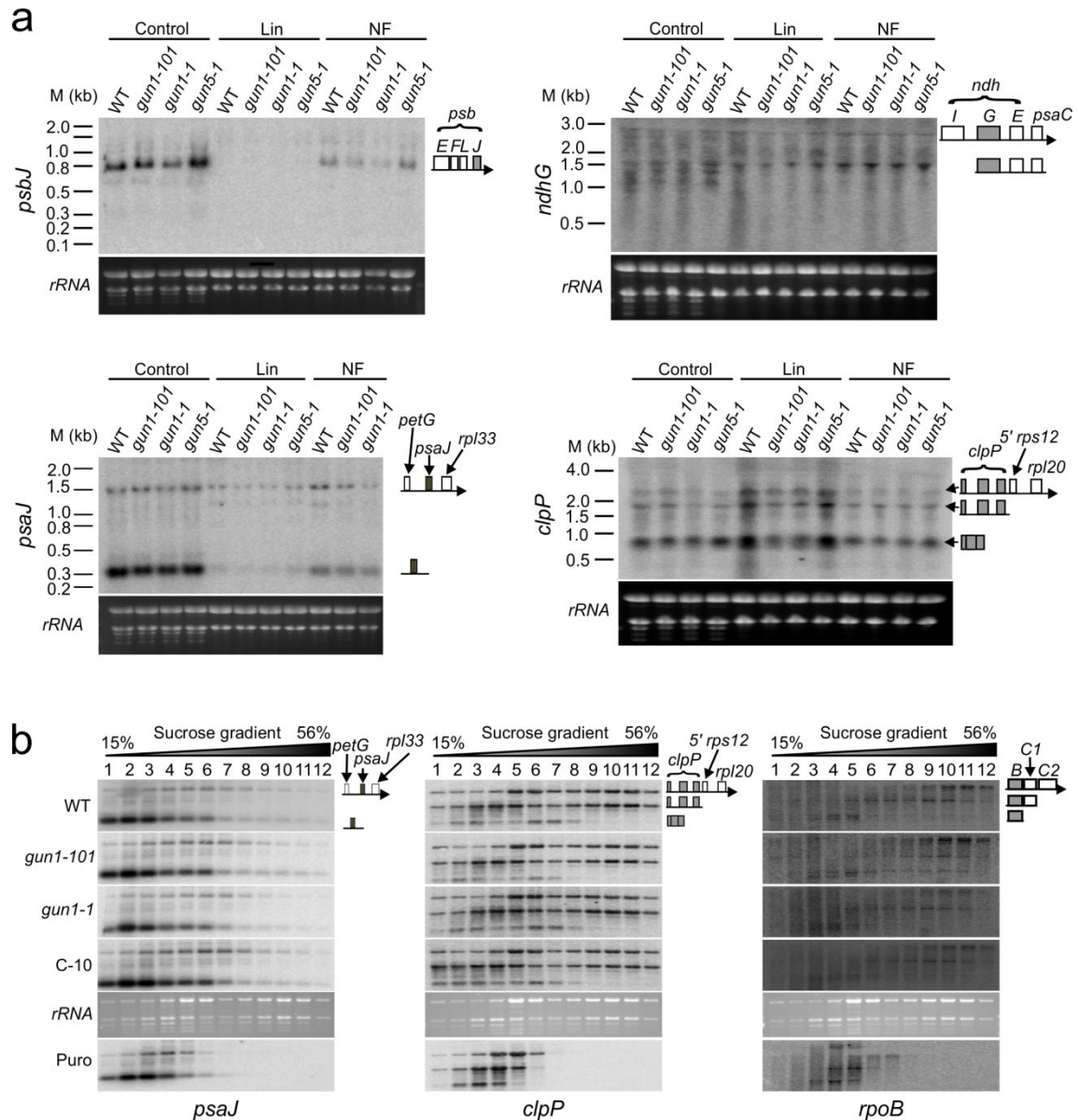
**a,b,** Microarray analysis of transcripts accumulation in the wild type (WT) and the *gun1-101* mutant in control condition (DMSO) or upon NF treatment (5  $\mu$ M). Log<sub>2</sub> total RNA signals (Transcripts) of all plastid protein-coding genes were plotted along the genome as means  $\pm$  s.d. ( $n=3$  biologically independent samples, indicated as open circles). The signals from all probes for each gene were averaged.

**c,d**, Ribosome profiling of chloroplast mRNAs in control condition (DMSO) or upon NF treatment (5  $\mu$ M) in the wild type and the *gun1-101* mutant. Log<sub>2</sub> of ribosome footprint signals (Ribo footprints) were plotted for all protein-coding genes along the genome as means  $\pm$  s.d. ( $n=3$  biologically independent samples, indicated as open circles). Signals from all probes for each gene were averaged. Lowly expressed genes that did not pass the data filtering criteria are marked as nd (not determined).



**Supplementary Figure 4. The up-regulation of the *clpP* mRNA in the Lin treatment is more pronounced in the wild type than in the *gun1* mutant.**

The normalized single channel probe intensities averaged from three biological replicates of the coding region of each gene were plotted for the genome region between 68,500 and 72,600, which includes the *clpP* operon and part of the *psbB* gene. The up-regulation of *clpP* is only seen at the mRNA level upon Lin treatment, but not upon NF treatment. There is also no up-regulation in the ribosome footprints for both treatments. The top part shows the gene models in this region, the *clpP* gene is shown as grey (exons) and white bars (introns). The genes below the horizontal line are transcribed from right to left, genes above the line are transcribed from left to right.



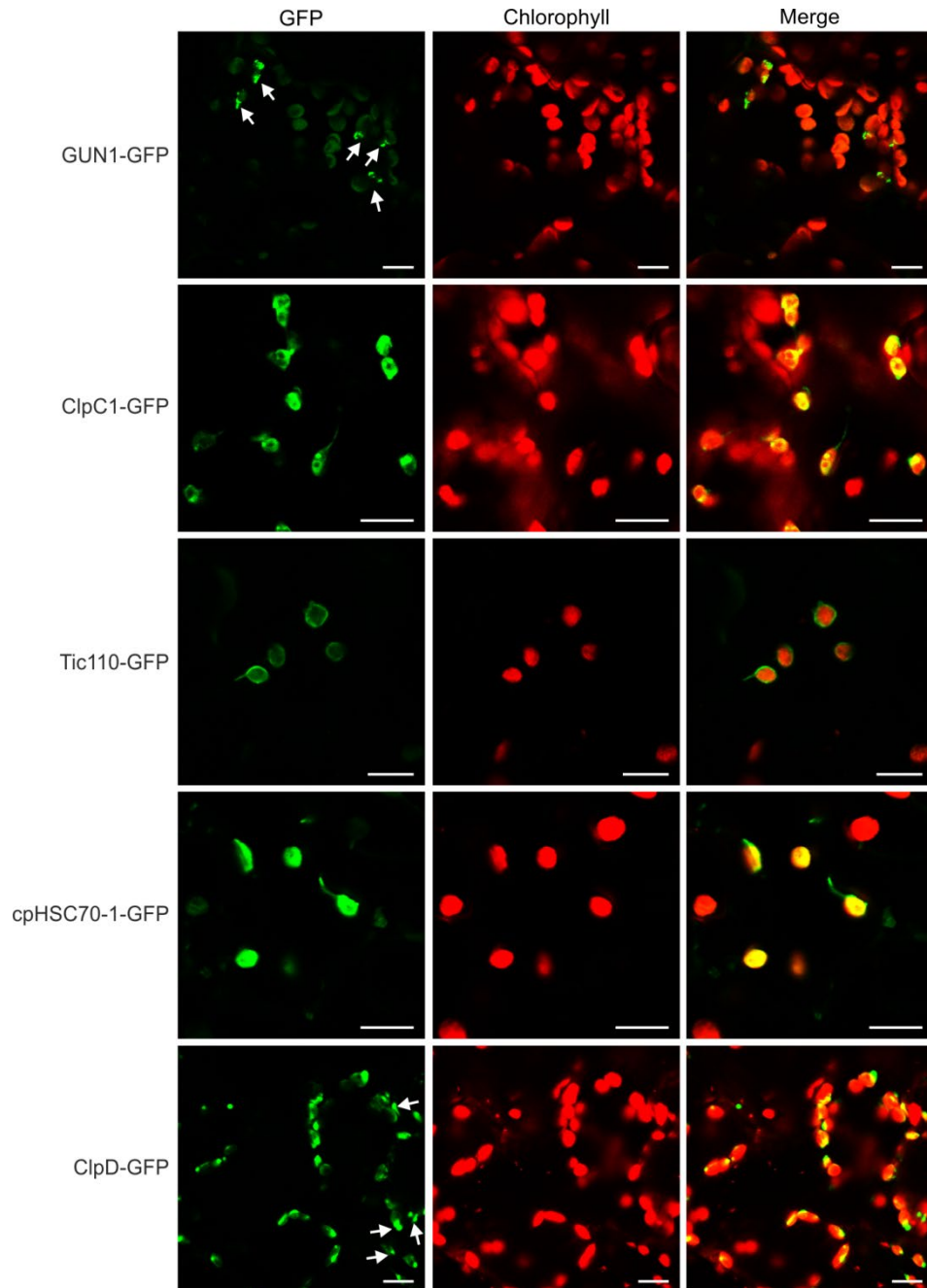
**Supplementary Figure 5. Northern blot analysis and polysome profiles of chloroplast-encoded transcripts.**

**a**, Northern blot analyses show no difference in RNA accumulation and processing of the chloroplast-encoded transcripts *psbJ*, *psaJ* and *ndhG* in two mutant alleles of *gun1* compared to *gun5* and the wild type (WT) in control conditions and upon treatment with 0.5 mM Lin or 5  $\mu$ M NF. *clpP* is up-regulated at the transcript level in the WT under Lin treatment, and to a lesser extent also in the *gun1* mutant. However, this difference was

only seen at the transcript level and not at the level of protein synthesis (as reflected by ribosome footprints), and therefore, cannot cause an altered ClpP protein accumulation (cf. Supplementary Figs. 2-4). To control for equal loading, the ethidium bromide-stained agarose gels prior to blotting are shown below each blot. The precursor transcripts, relevant processing intermediates and mature transcripts are schematically depicted at the right. The coding regions used as hybridization probes are represented as grey boxes. White boxes indicate other genes in the same operon and the arrow indicates the direction of transcription.

**b**, Polysome profiles show no difference in translation of the chloroplast-encoded transcripts *psaJ*, *clpP* and *rpoB* between wild type and *gun1* mutants. A puromycin-treated wild-type (Puro) sample was used as a control to identify polysome-containing gradient fractions. Complemented line C-10 was included for comparison. The wedges above the blots indicate the increasing sucrose concentration across the gradient. Representative images of rRNAs visualized by ethidium bromide staining (of samples not treated with puromycin) are also shown. In **a** and **b**, representative images from two independent experiments with similar results are shown.

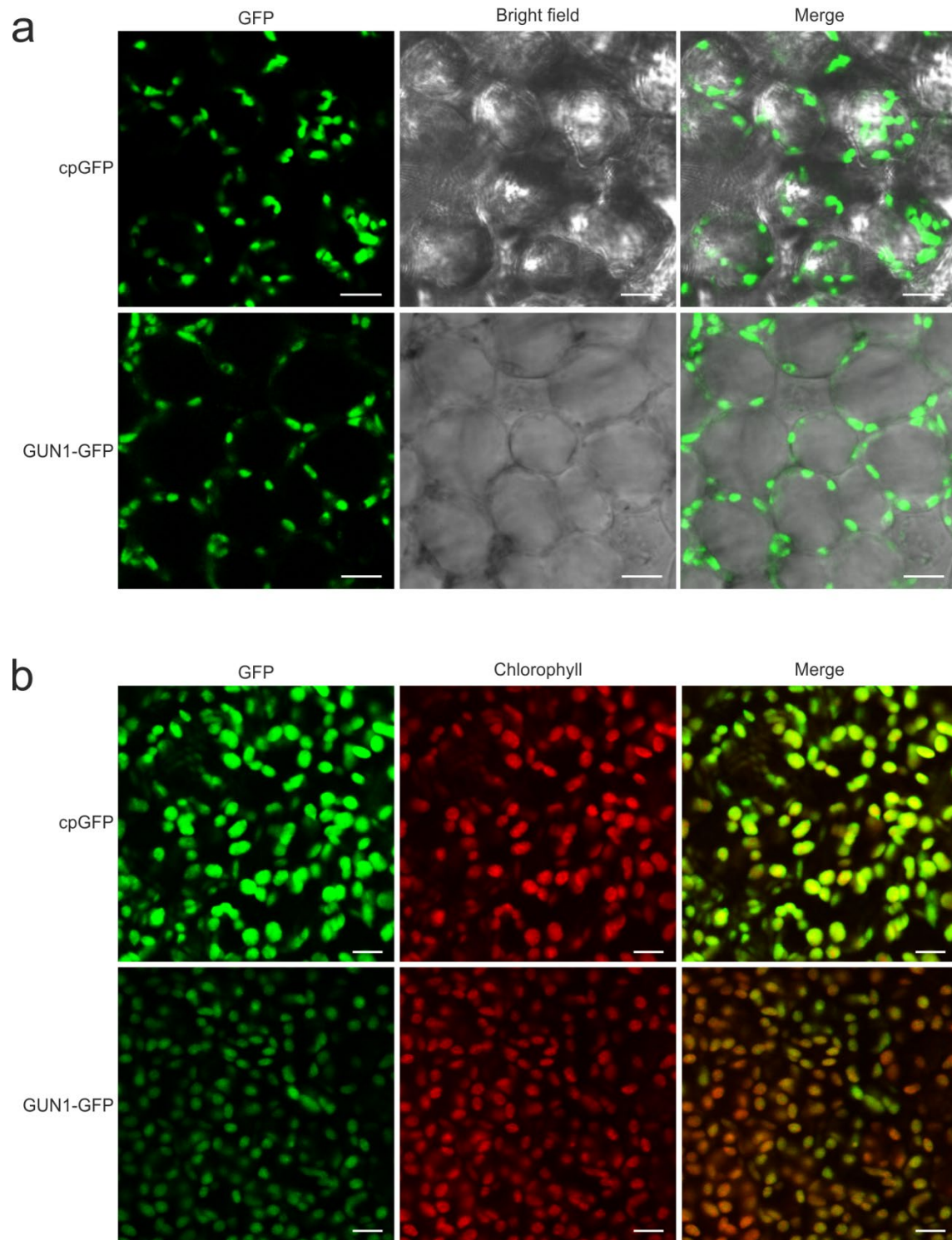




**Supplementary Figure 6. Transient expression of GUN1-GFP, ClpC1-GFP, Tic110-GFP, cpHSC70-1-GFP and ClpD-GFP in *Nicotiana benthamiana* leaves as controls for the BiFc assays shown in Fig. 1c.**

Some GUN1-GFP and ClpD-GFP signals show a spot-like pattern (arrows) which likely reflects aggregates of strongly overexpressed GFP-fusion proteins upon transient

expression in *Nicotiana benthamiana*. Note that this pattern is not seen in stable transgenic *Arabidopsis* lines (Supplementary Fig. 7). Five to six-week-old plants were infiltrated with *Agrobacterium* strains harboring the individual expressing vectors. The GFP signal was analyzed 3 days after infiltration by confocal microscopy. Three independent experiments were performed and showed similar results. Scale bars, 5  $\mu$ m.

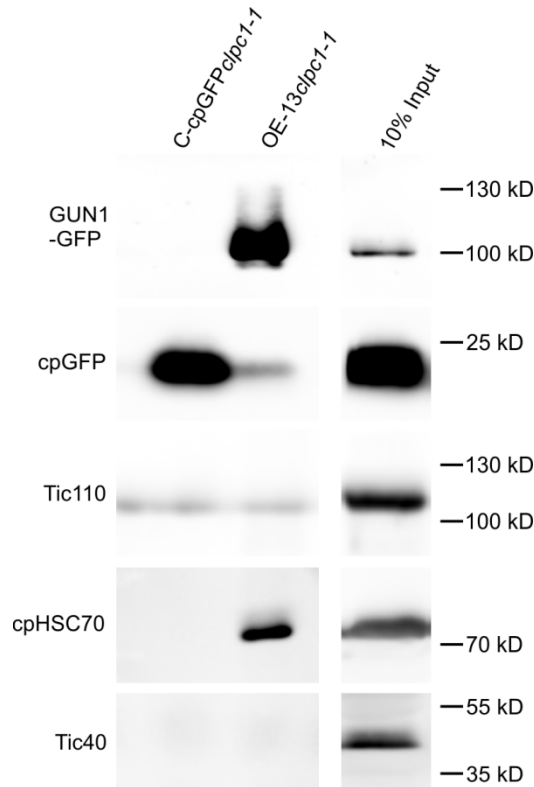


**Supplementary Figure 7. GUN1-GFP shows a diffuse distribution in plastids.**

**a**, GUN1-GFP expression in seedlings grown in the presence of 0.5 mM Lin. The seedlings were grown in the dark for 5 days prior to 2 days of growth in continuous light.

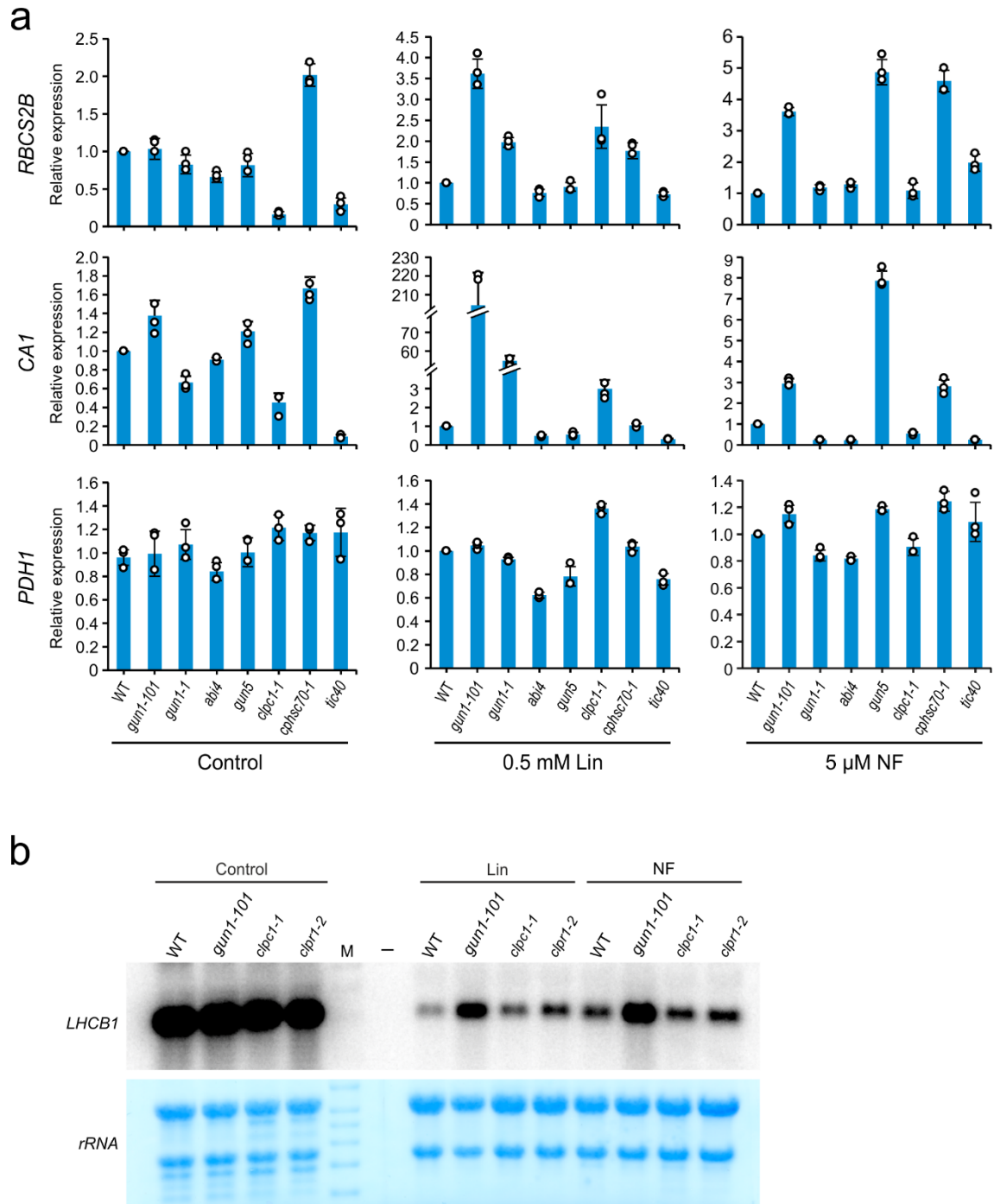
The cpGFP transgenic line was included as control. Note that the GUN1-GFP and cpGFP images were not taken with the same parameters (cpGFP was taken with a lower gain value), because the cpGFP signal is very strong. Scale bars, 5  $\mu$ m.

**b**, GUN1-GFP expression in newly emerging true leaf. True leaves that are less than 1 mm in length were analyzed by confocal microscopy<sup>18</sup>. The cpGFP transgenic line was included as control. Scale bars, 5  $\mu$ m. In **a** and **b**, representative images from three independent experiments with similar results are shown.



**Supplementary Figure 8. Co-IP performed with the OE-13 line crossed into the *clp1-1* mutant background.**

The C-cpGFP line crossed into *clp1-1* was used as co-IP control. The weak Tic110 band is a non-specific cross-reaction that is present also in the cpGFP control. 10% of the total input was loaded in a separated lane and analyzed as input control. Two independent immunoprecipitation experiments were performed with anti-GFP antibodies and showed similar results. The immunoprecipitates were subjected to western blotting with anti-GFP antibodies (detecting cpGFP and GUN1-GFP) or antibodies against Tic110, cpHSC70 and Tic40. The anti-cpHSC70 antibody does not distinguish between different isoforms of cpHSC70 (cpHSC70-1 and cpHSC70-2).

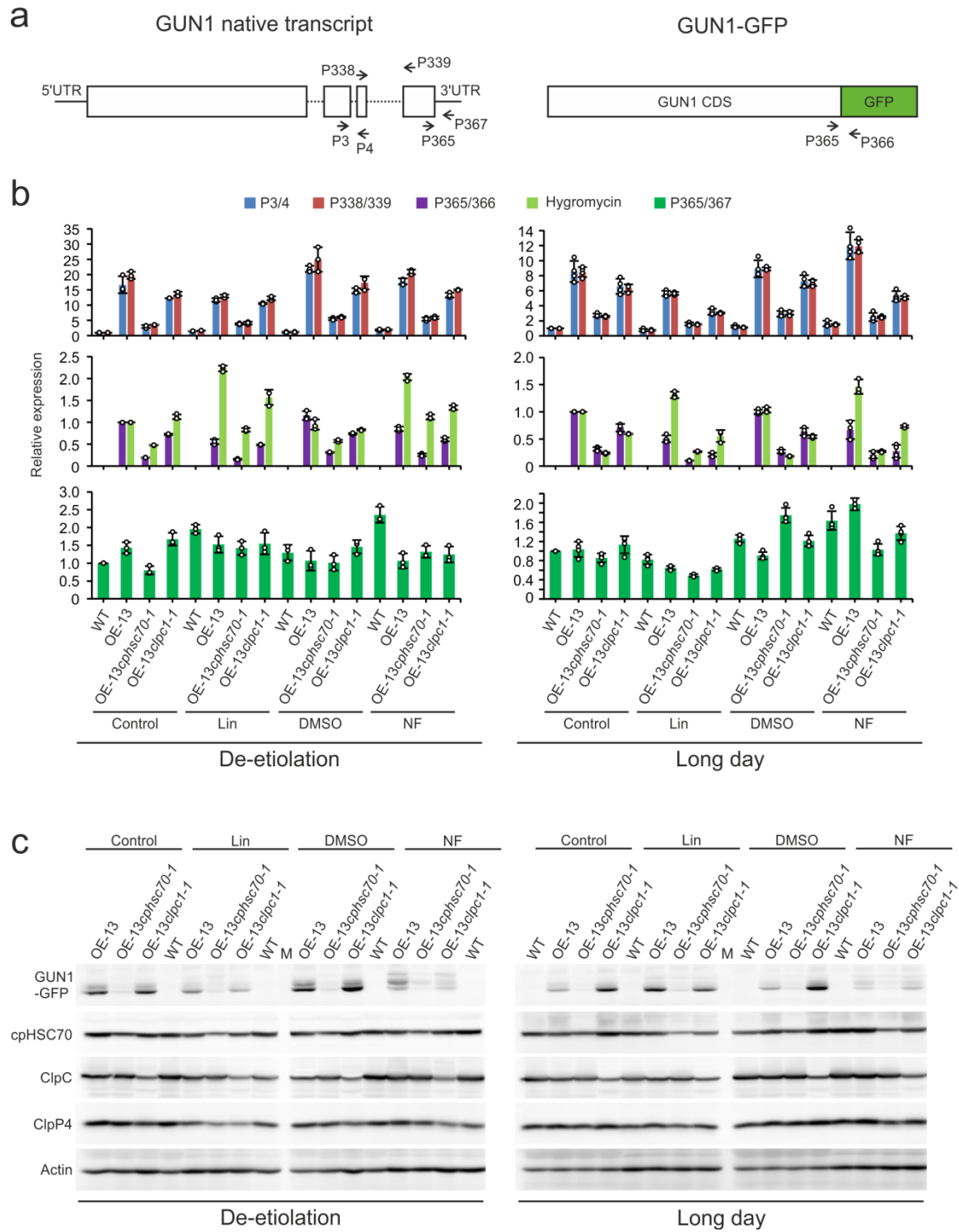


**Supplementary Figure 9. The *cphsc70-1* mutant shows a GUN phenotype.**

**a**, Expression of *RBCS2B* and carbonic anhydrase 1 (*CA1*) in the *cphsc70-1* and *clpc1* mutants compared to classical *gun* mutants. Compared to *cphsc70-1*, the *clpc1* mutant shows a GUN phenotype only upon Lin (0.5 mM) treatment, but not upon NF (5  $\mu$ M)

treatment. Gene expression was determined by qRT-PCR, and the relative gene expression is compared to that in the wild type (WT) grown under the same conditions. Data are presented as means  $\pm$  s.d. ( $n=3$  biologically independent samples, indicated as open circles). Pyruvate dehydrogenase E1 $\beta$  (*PDHI*) was used as a negative control (i.e., a gene whose expression is not regulated by retrograde signaling).

**b,** Northern blot analyses of *LHCB1* expression in mutants of Clp protease subunits under Lin or NF treatment. The GUN phenotype of *clpc1* seems to be a common property of Clp protease subunits in that the *clpr1-2* mutant also shows a weak GUN phenotype under Lin treatment (0.5 mM), but not under NF treatment (5  $\mu$ M). The expression of *LHCB1* (the hybridization probe does not distinguish between different *LHCB1* isoforms) was analyzed by northern blotting. Representative images from two independent experiments with similar results are shown. Methylene blue staining of rRNAs was used as loading control. M: RNA size marker; -: empty lane.



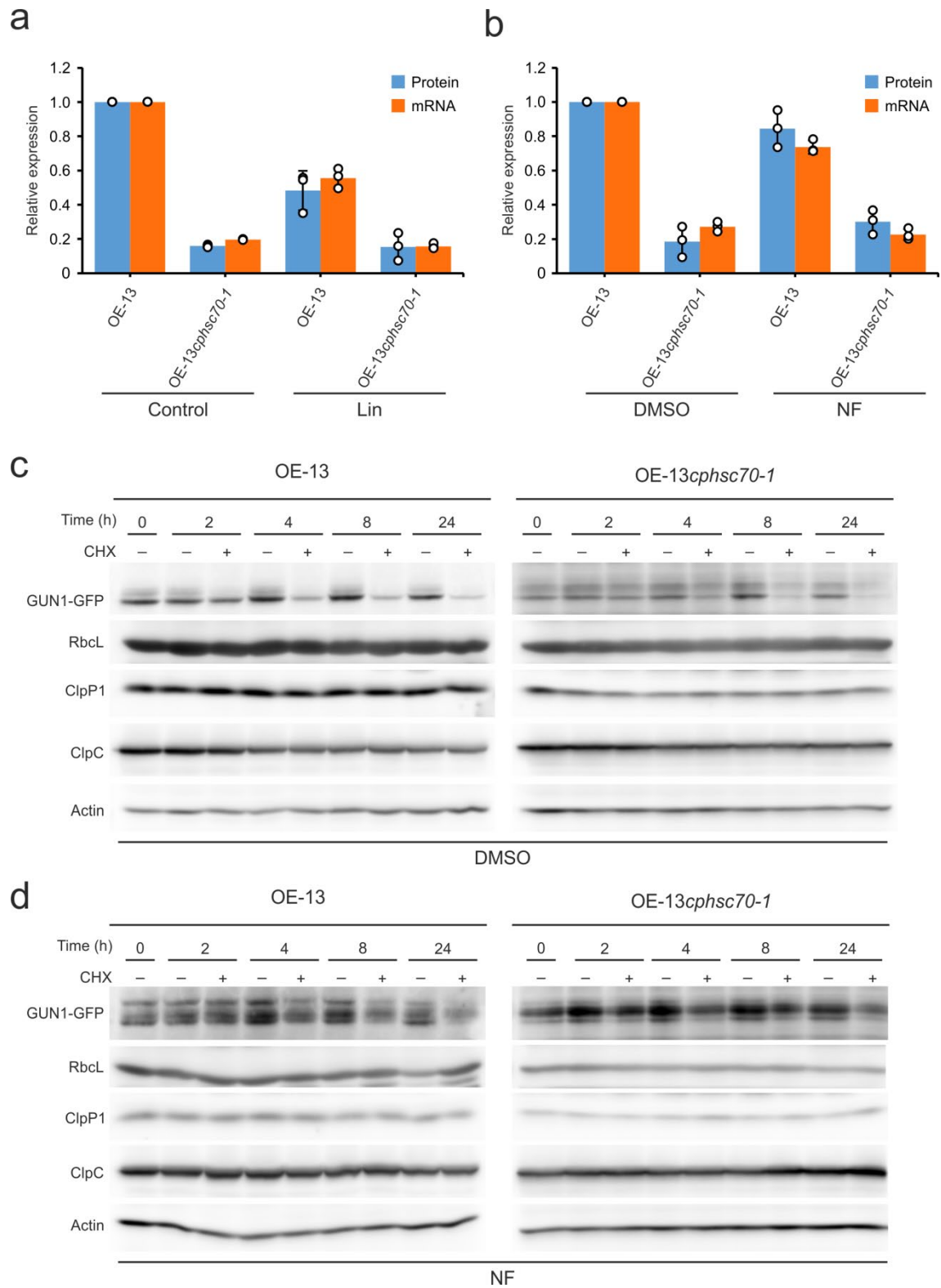
**Supplementary Figure 10. Transgenes undergo partial silencing when the *GUN1-GFP* expression line (OE-13) was crossed to the *cphsc70-1* mutant.**



**a,** Schematic representation of the native *GUNI* transcript and the transgenic *GUNI-GFP* transcript. The primers used for qRT-PCR analyses (**b**) are indicated. The untranslated regions (UTRs), exons, introns and GFP coding region are represented as solid lines, white boxes, dashed lines and green box, respectively. CDS, coding sequence.

**b,** qRT-PCR analyses demonstrate that the *GUNI-GFP* and the hygromycin resistance gene are partially silenced when the *GUNI-GFP* expression line (OE-13) was crossed to the *cphsc70-1* mutant (OE-13*cphsc70-1*). The cross of OE-13 to the *clpc1-1* mutant was included as an additional control. Compared to the native *GUNI* transcripts (amplified by primer pair P365/367), the *GUNI-GFP* (amplified by primer pair P365/366) and the hygromycin resistance gene transcripts were strongly suppressed in the *cphsc70-1* background (OE-13*cphsc70-1*) compared to in the wildtype background (OE-13) or the *clpc1* background (OE-13*clpc1-1*). Primer pairs P3/4 and P338/339 recognize exons to allow detection of all *GUNI* transcripts (native and transgenic). Seedlings were germinated and grown for 5 days in the dark followed by 2 days in continuous light (left, de-etiolation), or in long-day conditions (right, long day) for 7 days (Control and DMSO) or 11 days (Lin and NF treatment). Silencing of the transgenes was unrelated to the growth conditions or treatments, in that it was detected in all conditions investigated. Relative expression of *GUNI* (normalized to actin) is compared to that in the wild type under control conditions for primer pairs P3/4, P338/339 and P365/367. The OE-13 line was used for normalization of the expression of *GUNI-GFP* (primer pair P365/366) and the hygromycin resistance gene. Data are presented as means  $\pm$  s.d. from biologically independent samples (indicated as open circles;  $n=3$  in the de-etiolation experiment,  $n=4$  in the long-day experiment).

**c**, Immunoblot analyses demonstrate strong down-regulation of GUN-GFP protein accumulation in OE-13*cpHSC70-1*. The untransformed wild type (WT) was included to identify GUN1-GFP bands. The OE-13*clpC1-1* line was included as an additional control. Representative images from three independent experiments with similar results are shown. The seedlings were grown as in **b**. The blots were stripped and re-probed with antibodies against cpHSC70 and ClpC to confirm the transgene specificity of the silencing by analyzing the cpHSC70 and ClpC proteins in related genetic backgrounds. Actin served as loading control. M, molecular weight marker. In **b** and **c**, the concentration of Lin and NF is 0.5 mM and 5  $\mu$ M, respectively.



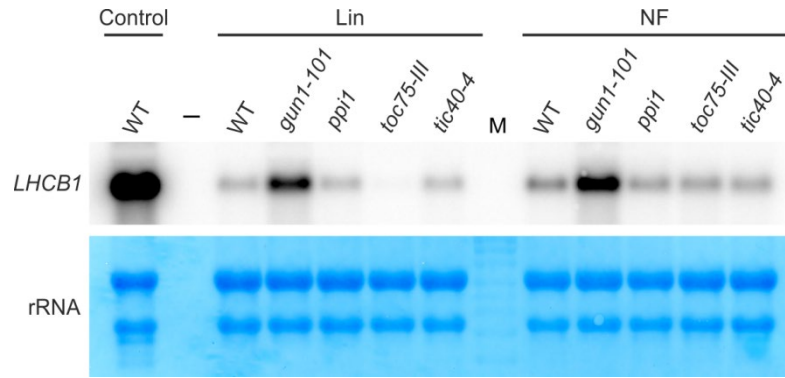
**Supplementary Figure 11. The turnover of the GUN1 protein is unchanged in the *cphsc70-1* mutant.**

**a,b,** GUN1-GFP mRNA and protein are well correlated in the *cphsc70-1* mutant, indicating no strong post-transcriptional regulation of GUN1 protein stability by the cpHSC70 chaperone. Seedlings were germinated and grown for 5 days in the dark followed by two days in continuous light without (Control and DMSO) or with 0.5 mM Lin (**a**) or 5  $\mu$ M NF (**b**). The band intensities in the western blots were quantified and are presented as means  $\pm$  s.d. ( $n=3$  biologically independent samples, indicated as open circles, from two independent experiments). The mRNA data are from Supplementary Fig. 10b (primer pair P365/366) and plotted together with the protein data for better comparison.

**c,** Cycloheximide (CHX) chase assays show that GUN1 protein turnover is comparable in the wild type background (OE-13) and in the *cphsc70-1* background (OE-13*cphsc70-1*) under control conditions (DMSO). Seeds were germinated and grown for 5 days in the dark followed by 2 days in continuous light and transferred to liquid medium with or without 10  $\mu$ M CHX. Samples were collected at different time points. As CHX inhibits only cytosolic, but not plastid translation, plastid genome-encoded proteins (RbcL and ClpP1) serve as loading controls. The nucleus-encoded chloroplast protein ClpC and a cytosolic housekeeping protein (actin) were also analyzed in comparison with GUN1-GFP.

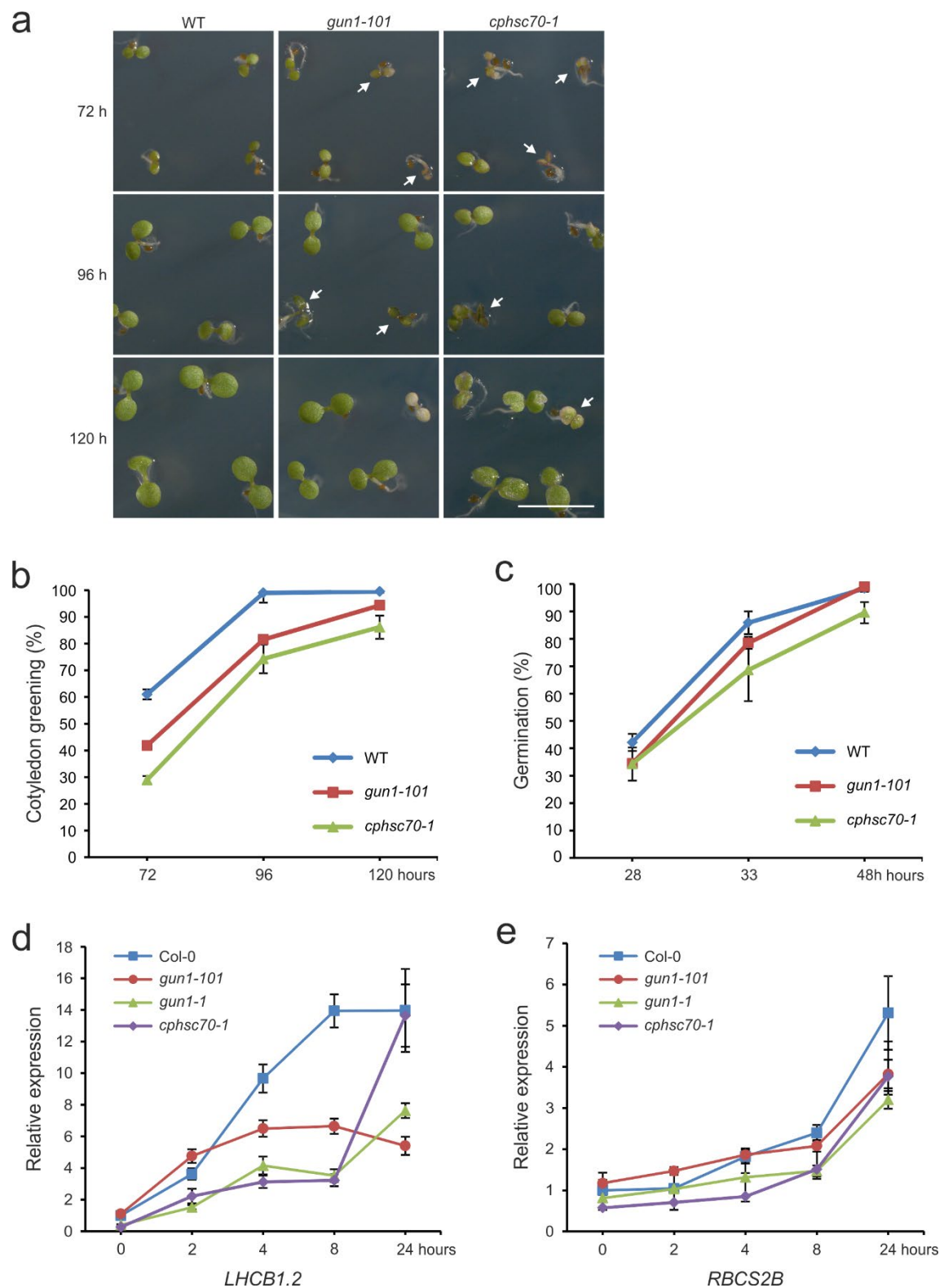
**d,** CHX chase assays show that GUN1 protein turnover is comparable in OE-13 and OE-13*cphsc70-1* under NF treatment conditions. Seeds were germinated and grown for 5 days in the dark followed by 2 days in continuous light with 5  $\mu$ M NF, and then transferred to liquid medium supplemented with 5  $\mu$ M NF and with or without 10  $\mu$ M CHX for the times indicated. Chloroplast genome-encoded proteins (RbcL, ClpP1) serve as loading

control. ClpC and actin were also analyzed for comparison. In **c** and **d**, representative images from two independent experiments with similar results are shown.



**Supplementary Figure 12. Northern blot analysis of *LHCBI* expression in mutants of subunits of the Tic-Toc apparatus under Lin or NF treatment.**

Mutants of subunits of the Tic (*tic40-4*) and Toc (*ppl1* and *toc75-III*) apparatus do not express a GUN phenotype. The *gun1-101* mutant was included as positive control. Wild-type seedlings grown without Lin (0.5 mM) or NF (5  $\mu$ M) were included for comparison. Two independent experiments were performed and showed similar results. Methylene blue staining of rRNAs was used as loading control. M: molecular marker; -: empty lane.



**Supplementary Figure 13. The *cphsc70-1* mutant shows delayed cotyledon greening during germination and reduced PhANG expression during de-etiolation.**

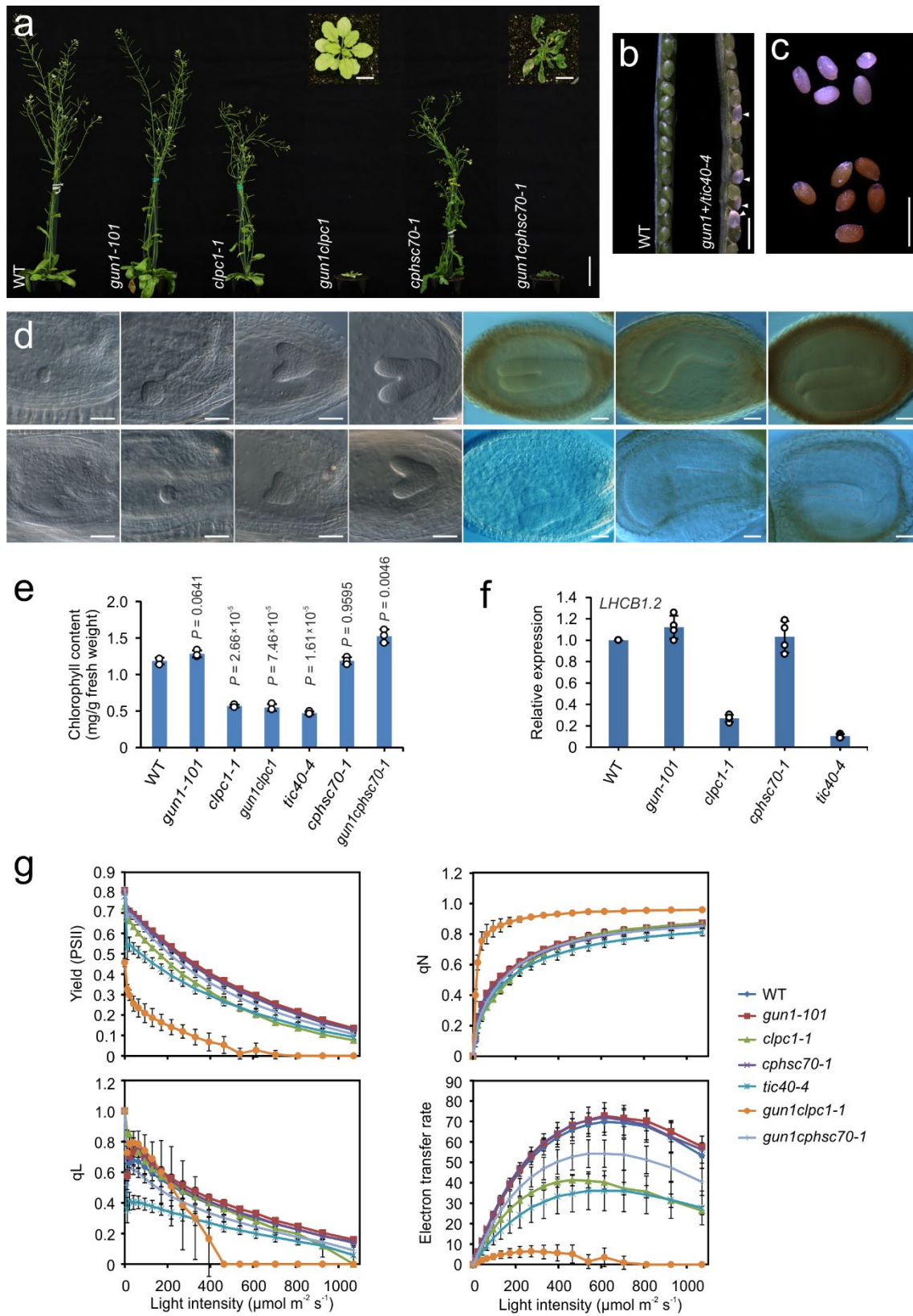
**a,** Delayed cotyledon greening in the *cphsc70-1* and *gun1-101* mutants compared to the wild type. Germination of *gun1-101* and *cphsc70-1* is slightly delayed relative to the wild type (see panel **c**), but cotyledon greening is much delayed in both mutants. Wild type, *cphsc70-1* and *gun1-101* seedlings at 72, 96 and 120 h after germination are shown. Seedlings with delayed greening of the cotyledons in the *cphsc70-1* and *gun1-101* mutants are indicated by white arrows. The experiments were performed four times independently and showed similar results. Scale bars, 5 mm.

**b,** Quantitation of cotyledon greening in **a** by four independent experiments with ~100 seeds per experiment and genotype. Data represent means  $\pm$  s.d. ( $n=4$  independent experiments).

**c,** Germination assay of wild type, *gun1-101* and *cphsc70-1* seeds. Germination rates were scored after 28, 33 and 48 h of incubation in the growth chamber. Data are presented as means  $\pm$  s.d. ( $n=4$  independent experiments), with ~100 seeds in each experiment.

**d,e,** Reduced expression of PhANGs in *cphsc70-1* compared to the wild type. *gun1-101* and *gun1-1* were included as controls. Seeds were germinated and grown for 6 days in the dark prior to expose to the light. The relative expression of *LHCBI.2* (**d**) and *RBCS2B* (**e**) was analyzed by qRT-PCR. Expression was normalized to actin and is presented as relative expression to the wild type (at the 0 h time point). The data are presented as means  $\pm$  s.d. ( $n=3$  biologically independent samples).





**Supplementary Figure 14. Phenotypes of the *gun1-101*, *clpc1* and *cphsc70-1* single mutants and the *gun1-101clpc1* and *gun1-101cphsc70-1* double mutants.**

**a,** Phenotypes of 6 week-old mutants grown in long-day conditions in comparison to the wild type (WT). The top view of the two double mutants is shown in the insets. Scale bars: 5 cm, and 1 cm in the insets.

**b,** Synthetic lethality of the *gun1-101tic40-4* double mutant. The double mutant that is homozygous for the *gun1-101* mutation and heterozygous for the *tic40-4* mutation (*gun1-101+/tic40-4*) segregates 25% inviable seeds (pigment-deficient seeds, marked by white arrowheads). Scale bar: 1 mm.

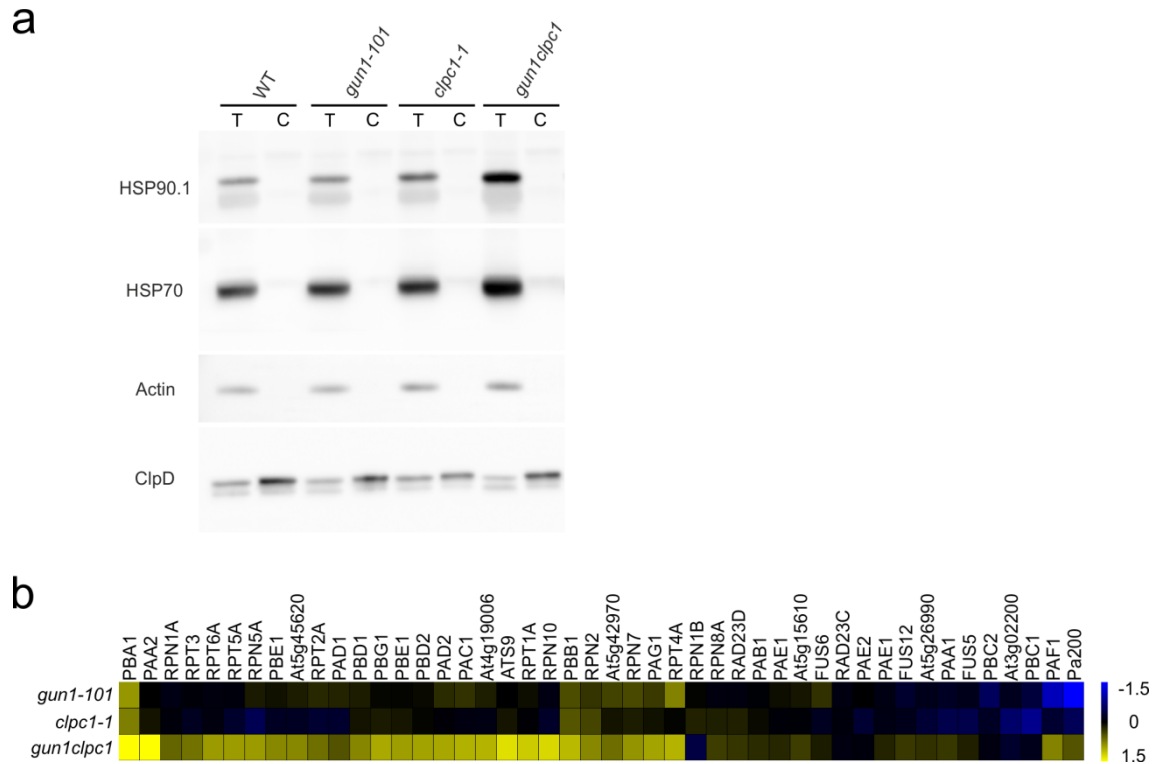
**c,** Comparison of normal seeds (brown color; lower half of the picture) and aborted seeds (white; upper half) from a ripe silique of a *gun1-101+/tic40-4* mutant. Scale bar: 1 mm.

**d,** Comparison of embryo development in viable (brown; upper panel) and inviable (white; lower panel) seeds from *gun1-101+/tic40-4*. Note that, starting from the heart-shaped stage, embryos in the white seeds are severely deficient in chlorophyll accumulation. Red dotted lines mark the embryos in the walking-stick and cotyledon stages. Scale bars: 50  $\mu$ m. In **a-d**, three independent experiments were performed and showed similar results.

**e,** Chlorophyll contents of the WT and different mutants. The data are presented as means  $\pm$  s.d ( $n=3$  biologically independent samples, indicated as open circles). A two-tailed Student's *t*-test was performed to determine the significance of differences between the wild type and the various mutants.

**f,** qRT-PCR analysis of *LHCB1.2* expression in different mutants. The relative gene expression (normalized to actin) is compared to that in the WT. The data are presented as means  $\pm$  s.d. ( $n=4$  biologically independent samples, indicated as open circles).

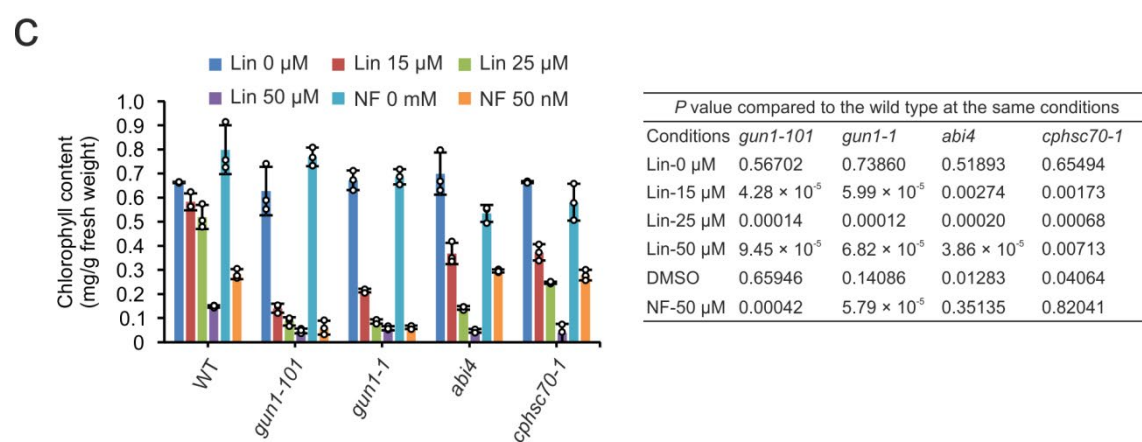
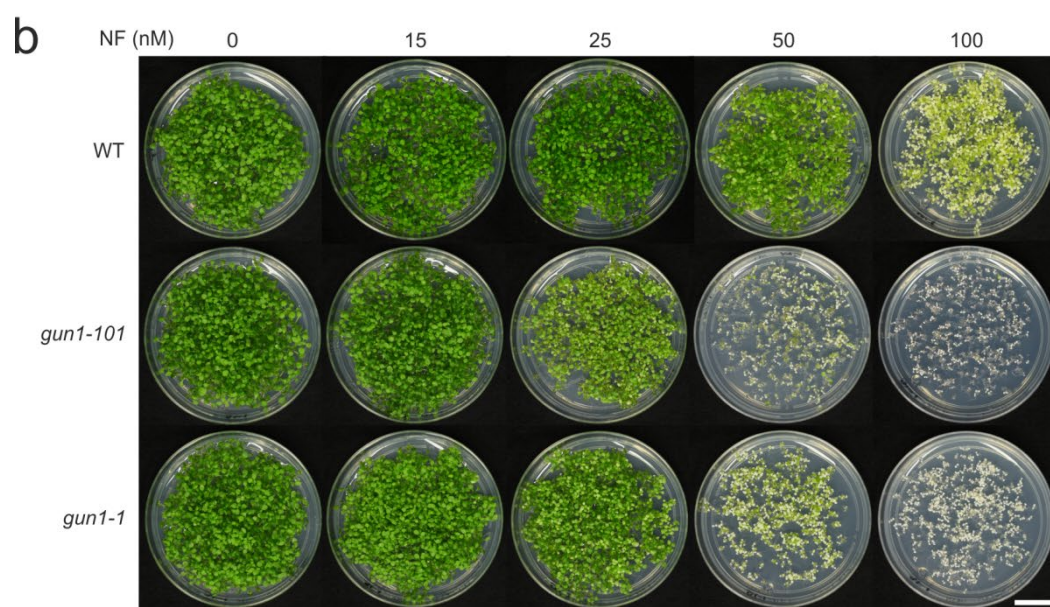
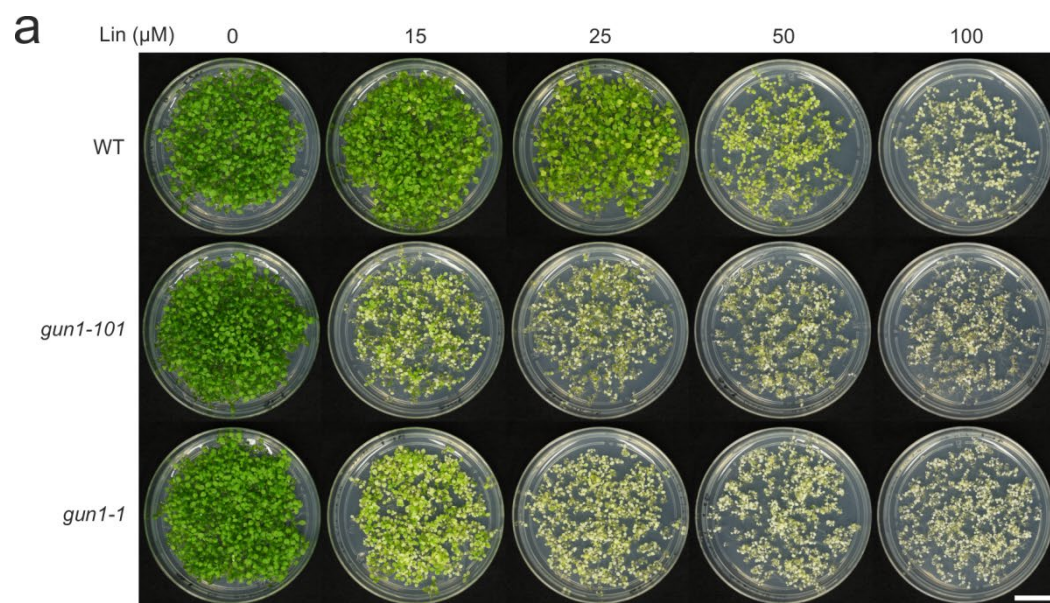
**g**, Imaging-PAM measurement of light-response curves of chlorophyll a fluorescence parameters. Photosystem II (PSII) yield, non-photochemical quenching (qN), the fraction of PSII reaction centers that are open (qL), and the electron transfer rate (given in  $\mu\text{mol electrons m}^{-2} \text{ s}^{-1}$ ) were determined for the wild type and the various mutants. The values represent the means  $\pm$  s.d. ( $n=6$  individual plants for each genotype from two independent experiments).



**Supplementary Figure 15. The cytosolic PQC system is induced in the *gun1clpc1* double mutant.**

**a**, Immunoblot analyses indicate strong up-regulation of cytosolic HSP90.1 and HSP70 in the *gun1clpc1* double mutant. T: total protein extract, C: protein extracts from isolated chloroplasts. Two independent experiments were performed and showed similar results. Actin served as loading control and cytosolic protein control. The chloroplast protein ClpD served as chloroplast protein control that is present in both T and C samples.

**b**, Heat map showing up-regulation of 26S proteasome subunits in the *gun1clpc1* double mutant. The heat map shows means of fold changes ( $\log_2$ ) in protein abundance of the mutants to the wild type from three biological replicates.

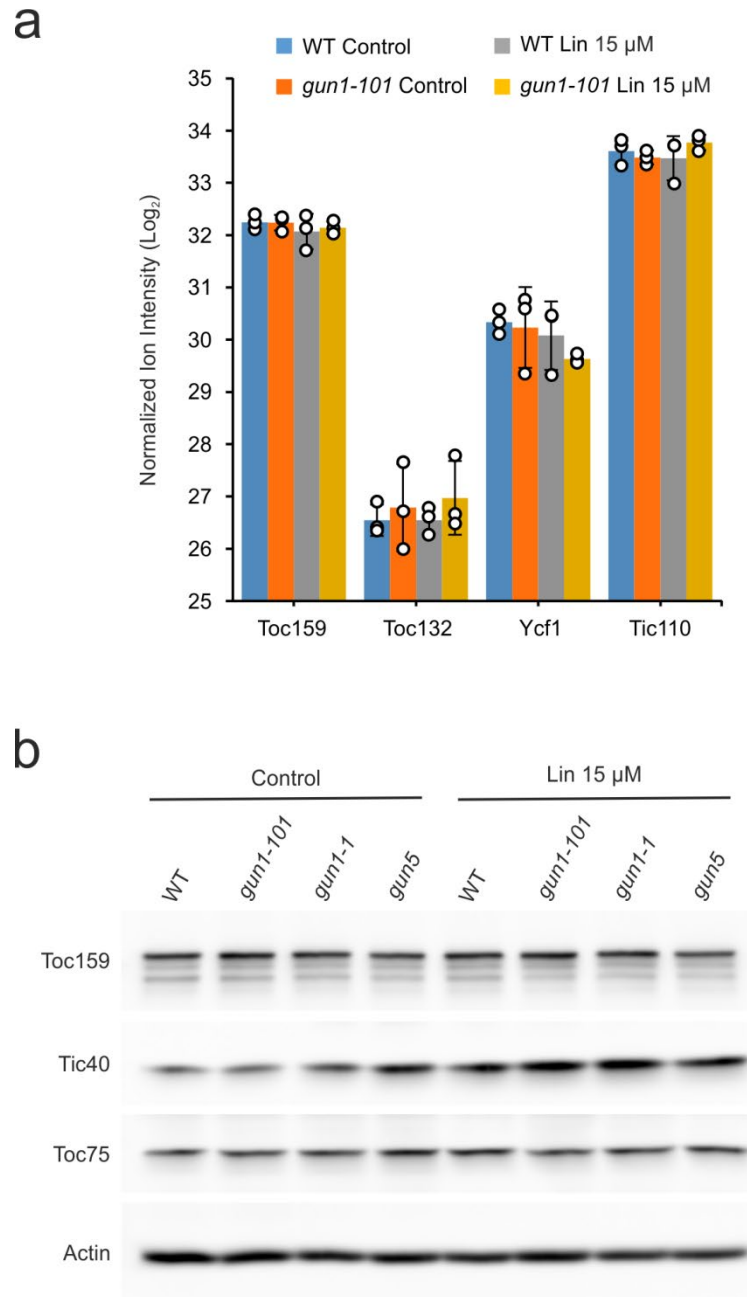


**Supplementary Figure 16. Hypersensitivity of *gun1* mutants to Lin and NF treatments.**

**a,b,** Phenotype of two alleles of the *gun1* mutants compared to the wild type (WT) on different concentration of Lin (**a**) or NF (**b**). Seeds from different genotypes were germinated and grown for 11 days in long-day conditions in the presence of different concentrations of Lin or NF. Two independent experiments were performed and showed similar results. Scale bars: 2 cm.

**c,** Chlorophyll contents of the wild type (WT) and various mutants grown on different concentrations of Lin or NF. Note that the *cphsc70-1* mutant shows a similar response as the *abi4* mutant, but is less sensitive than the *gun1* mutants. The data are presented as means  $\pm$  s.d. ( $n=3$  biologically independent samples, indicated as open circles). A two-tailed Student's *t*-test was performed to determine the significance of differences between the wild type and different mutants at the same conditions. The *p* values are shown in the table.





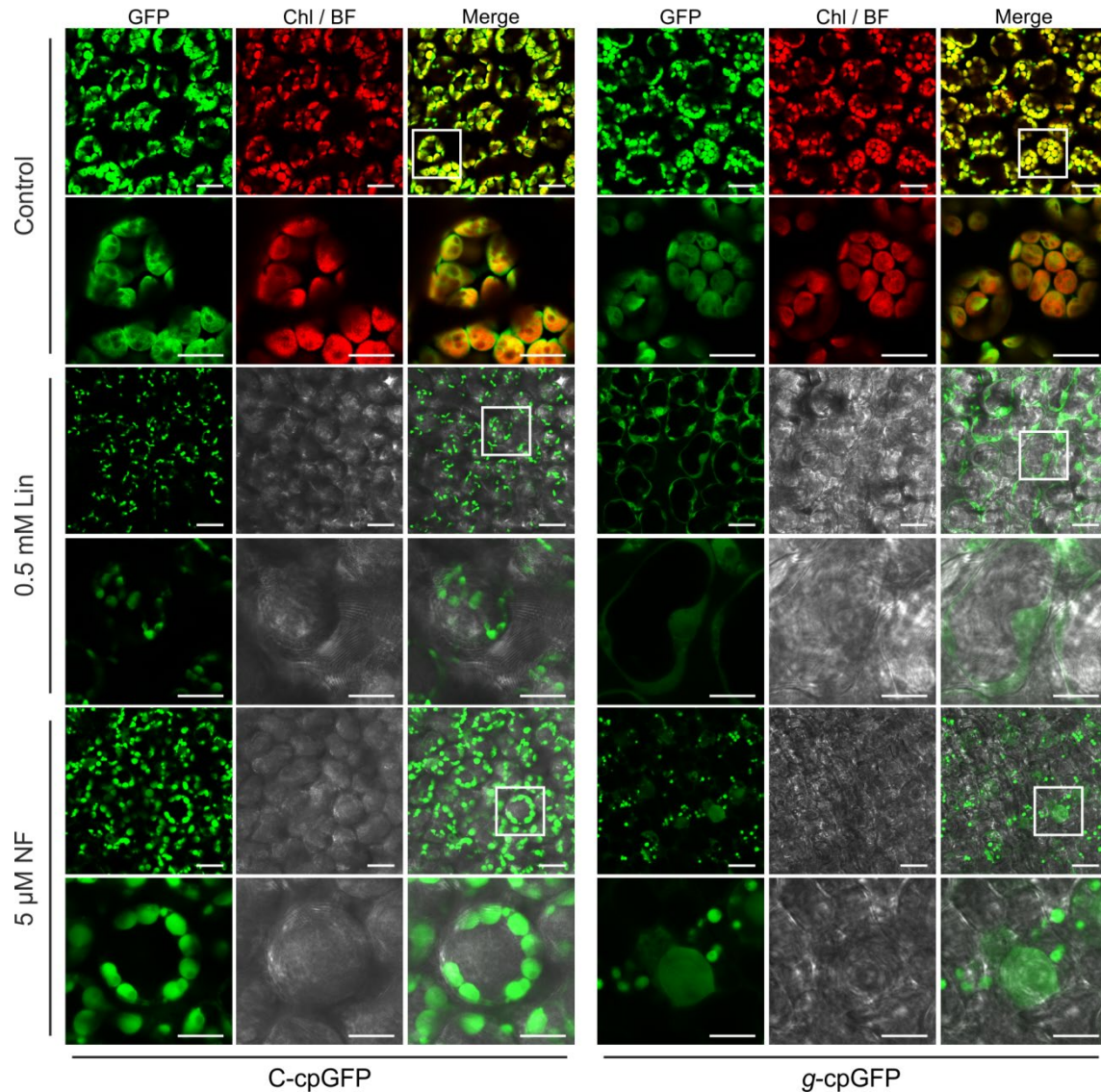
**Supplementary Figure 17. The protein levels of subunits of the Tic-Toc apparatus are comparable between the wild type and *gun1* mutants in the materials used for protein import assays.**

**a**, Label-free quantification by mass spectrometry demonstrates that protein accumulation of Tic (Ycf1 and Tic110) and Toc (Toc159 and Toc132) subunits does not show

significant differences between the wild type and *gun1-101* grown in control conditions or treated with 15  $\mu$ M Lin. Seedlings were grown without (control) or with 15  $\mu$ M Lin exactly as the material used for protein import assays. The data are presented as means  $\pm$  s.d. ( $n=3$  biologically independent samples, indicated as open circles).

**b,** Immunoblot analyses verified that Toc159, Toc75 and Tic40 accumulation is not reduced in *gun1* mutants compared to the wild type. The *gun5* mutant was included for comparison. Seedlings were grown without (control) or with 15  $\mu$ M Lin exactly as the material used for protein import assays. Two independent experiments were performed and showed similar results. Actin served as loading control.

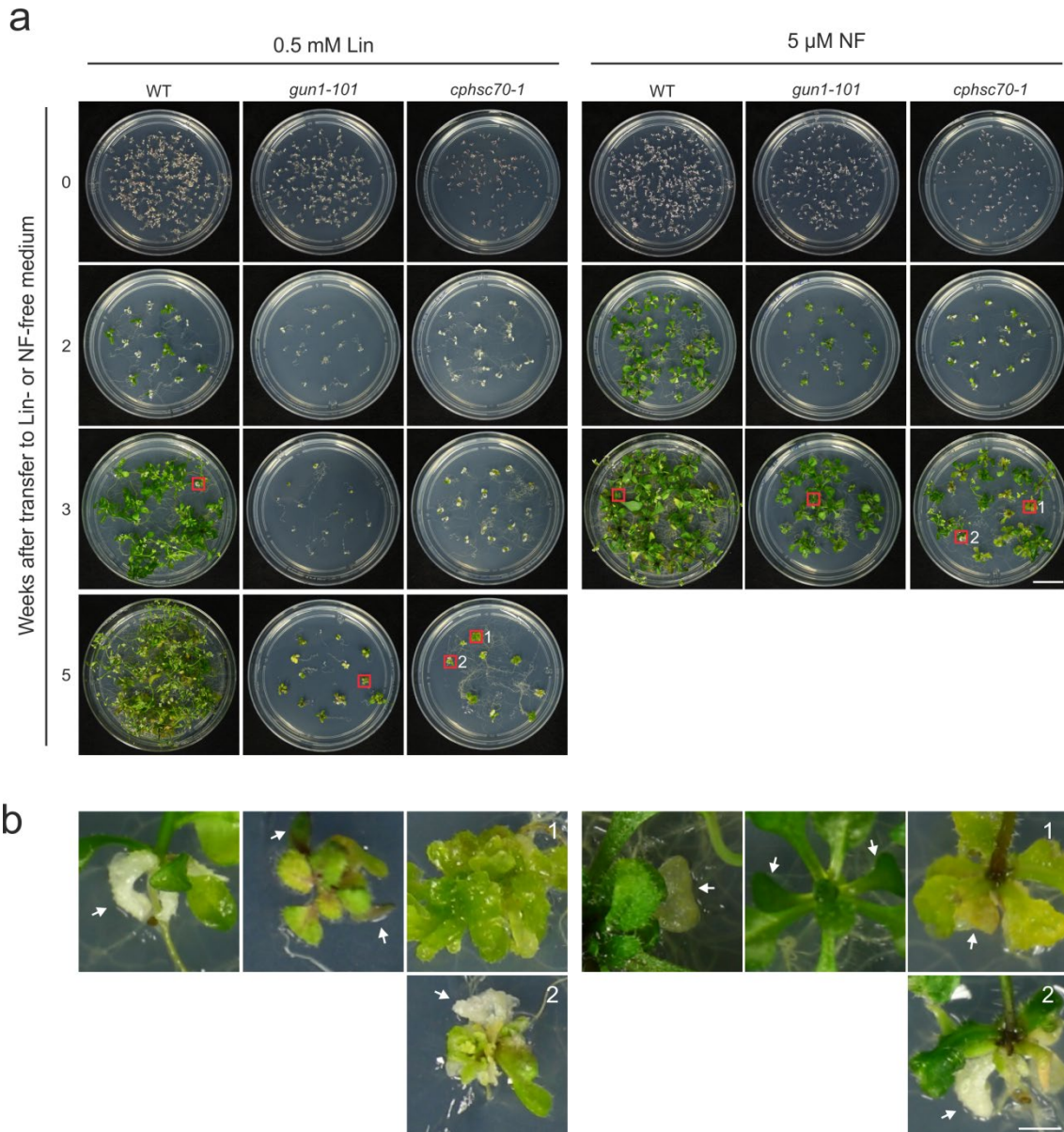




**Supplementary Figure 18. cpGFP cannot be efficiently targeted to plastids in the *gun1* background upon Lin or NF treatment.**

While cpGFP can be efficiently targeted to plastids in the wild-type background (C-cpGFP) under control conditions and also upon treatment with Lin or NF, import is inefficient in the *gun1* background (g-cpGFP) in the presence of Lin or NF. Representative images from three independent experiments with similar results are shown. The boxed regions are enlarged below to show the subcellular distribution of the GFP signal in a single mesophyll cell. Scale bars: 20  $\mu\text{m}$  in the upper panels and 10  $\mu\text{m}$

in the enlarged panels. The enlarged panels are also shown in Fig. 3a. Seedlings were germinated and grown for 5 days in the dark followed by 2 days in continuous light in the presence of 0.5 mM Lin or 5  $\mu$ M NF. For Lin and NF treatments, bright-field images are shown instead of the chlorophyll fluorescence images, because chlorophyll fluorescence is not visible.



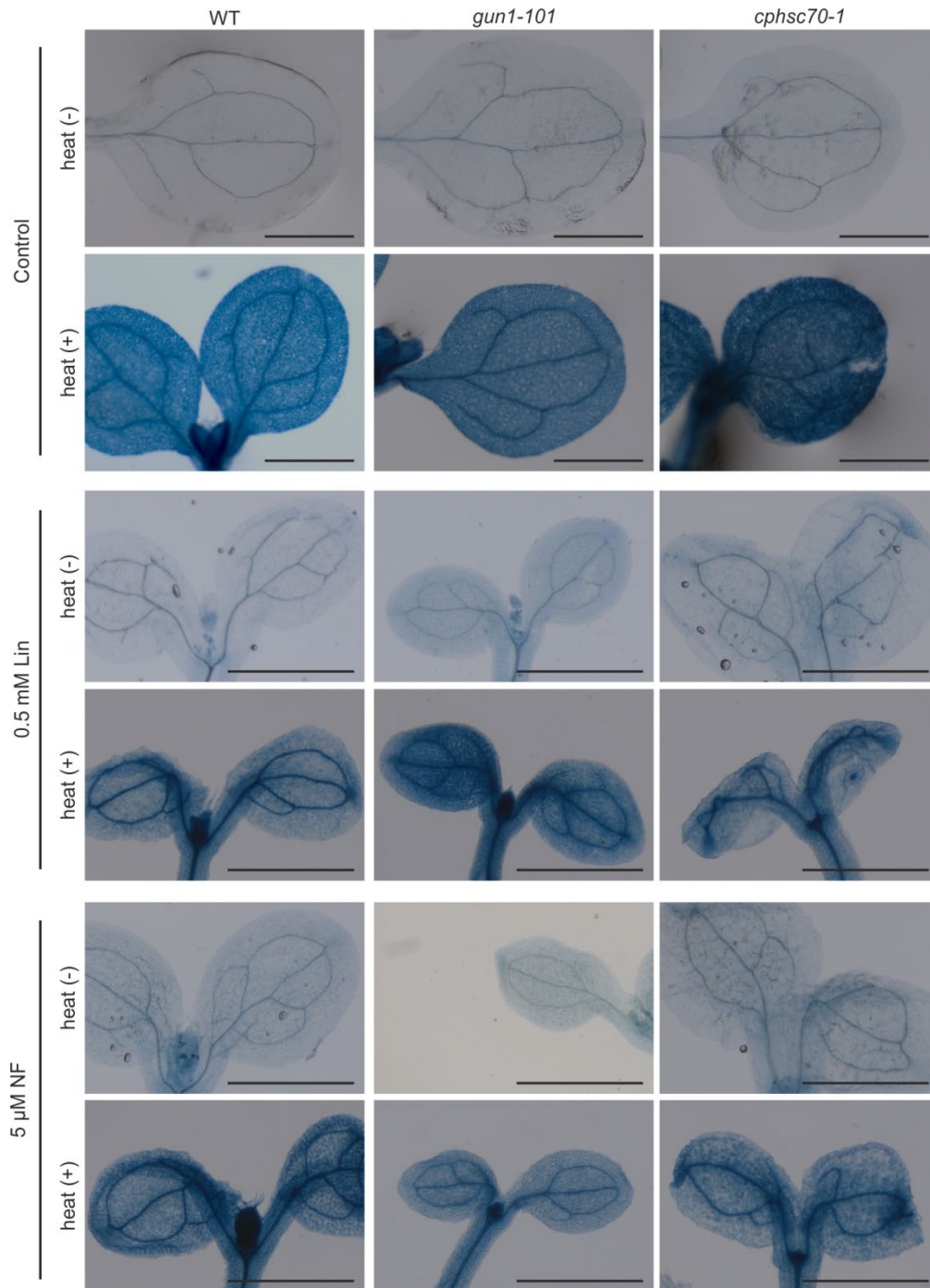
**Supplementary Figure 19. Re-greening assay of the wild type, *gun1-101* and *cphsc70-1* transferred from Lin-containing or NF-containing medium to inhibitor-free medium.**

**a**, Seedlings growing on Lin or NF-containing medium and after transfer to Lin- and NF-free medium for the weeks indicated. Seeds of the wild type, *gun1-101* and *cphsc70-1* were germinated and grown for 7 days in long-day conditions with 0.5 mM Lin or 5  $\mu$ M NF. The seedlings were then transferred to inhibitor-free medium, grown for the time

periods indicated and photographed. Because of the hypersensitivity of *gun1* and *cphsc70-1* to Lin and NF treatment, the growth of these seedlings is much delayed compared to the wild type after the transfer. The wild-type plants transferred from Lin and NF medium and part of the *cphsc70-1* plants (well-recovered individuals) transferred from NF medium flowered three weeks after transfer. Boxed seedlings were enlarged and shown in **b**. Scale bars, 2 cm.

**b**, Enlarged seedlings boxed in **a** to show the re-greened cotyledons. Compared to the re-greened cotyledons of *gun1*, pronounced greening of wild-type cotyledons did not occur, likely because the wild-type plants recovered quickly after transfer and developed new true leaves (making the cotyledons dispensable for further plant development). However, these white wild-type cotyledons were still alive (Supplementary Fig. 20) and grew bigger compared to the plants before transfer. The same phenomenon was also seen in the *cphsc70-1* mutant: the better the recovery of *cphsc70-1* individuals, the weaker the re-greening of the cotyledons (lower panel). Scale bars, 2 mm. In **a** and **b**, two independent experiments were performed and showed similar results.

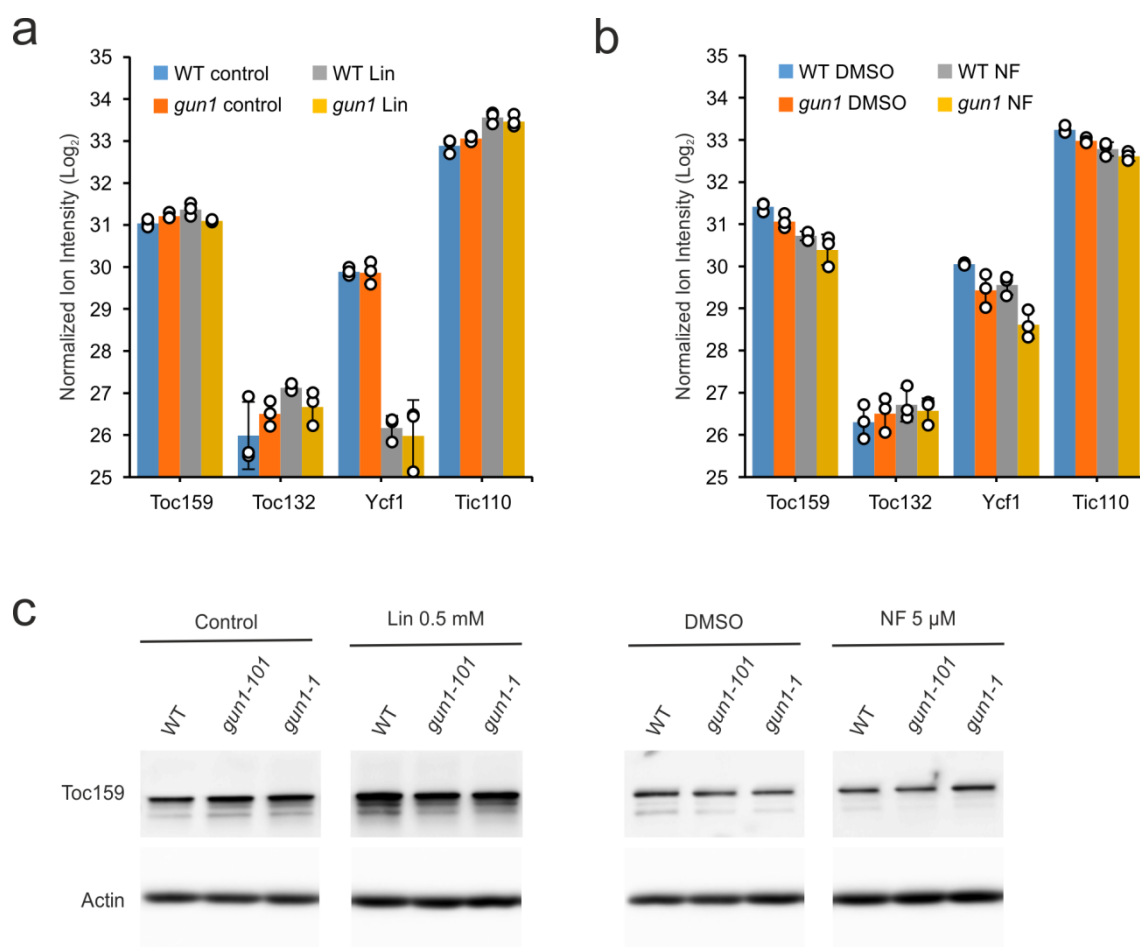




**Supplementary Figure 20. Trypan blue staining demonstrates viability of the cells in Lin and NF-treated seedlings.**

Seeds from the different genotypes were germinated, grown for 7 days in long-day conditions without (control) or with 0.5 mM Lin or 5 μM NF, and then stained with trypan

blue. To generate a stained positive control, six-day-old seedlings were incubated at 60 °C for 4 h and transferred back to 22 °C for 20 h prior to staining. Cell death in the heat-treated seedlings was revealed by dark blue staining. Two independent experiments were performed and showed similar results. Scale bars, 1 mm.



**Supplementary Figure 21. The protein levels of subunits of the Tic-Toc apparatus is comparable between the wild type and *gun1* mutants upon treatment with 0.5 mM Lin or 5 μM NF.**

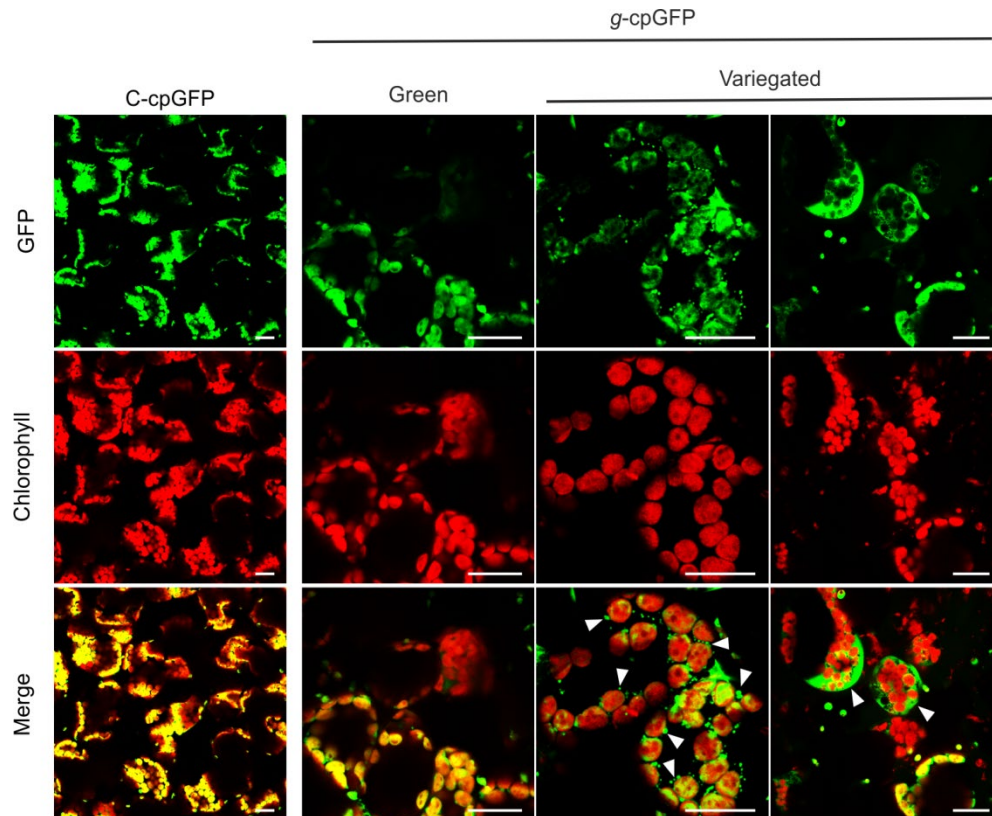
**a**, Label-free quantification by mass spectrometry demonstrates that protein accumulation of Tic (Ycf1 and Tic110) and Toc (Toc159 and Toc132) subunits shows no significant differences between the wild type and *gun1-101* grown in control conditions or treated with 0.5 mM Lin. The data are presented as means  $\pm$  s.d. ( $n=3$  biologically independent samples, indicated as open circles).

**b**, Label-free quantification by mass spectrometry demonstrates that accumulation of Tic110, Toc159 and Toc132 is not significantly different between the wild type and *gun1*-

*101* grown in control conditions (DMSO) or treated with 5  $\mu$ M NF. Ycf1 shows a small decrease in *gun1* under NF treatment compare to the wild type. The data are presented as means  $\pm$  s.d. ( $n=3$  biologically independent samples, indicated as open circles).

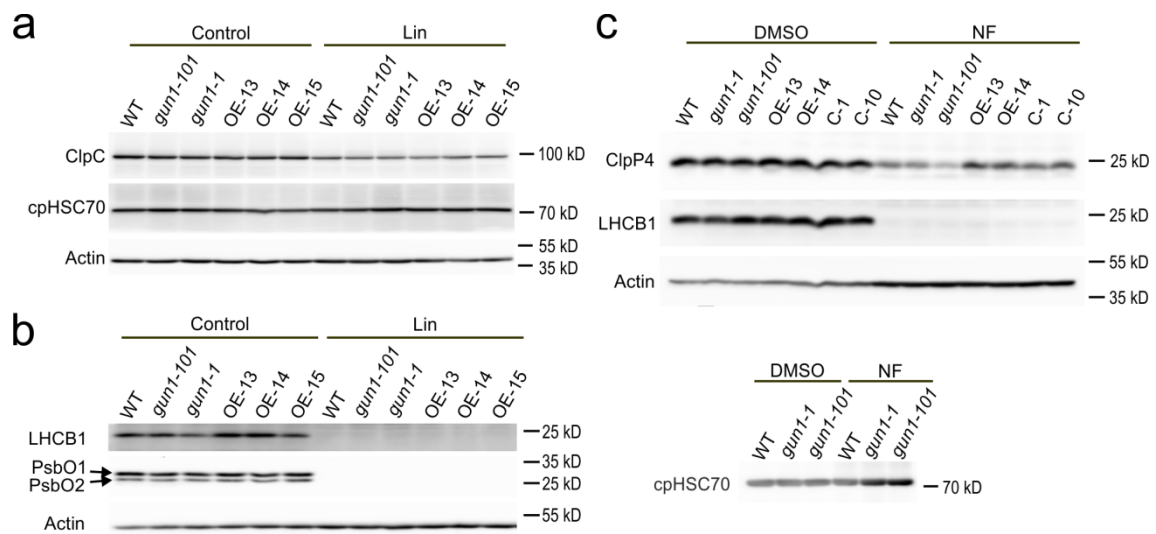
**c**, Immunoblot analyses verified that Toc159 accumulation is not reduced in *gun1* mutants compared to the wild type in control conditions (control or DMSO) or upon treatment with 0.5 mM Lin or 5  $\mu$ M NF. Two independent experiments were performed and showed similar results. Actin served as loading control.





**Supplementary Figure 22. Inefficient plastid targeting of cpGFP in *gun1* under continuous light.**

cpGFP cannot be efficiently translocated into chloroplasts in the variegated cotyledons of *gun1* (*g-cpGFP*) that grow in continuous light. By contrast, cpGFP is correctly targeted to chloroplasts in the wild-type background (*C-cpGFP*) and also to a large extent in green seedlings of *gun1*. The middle panel of the *g-cpGFP* images shows relatively mildly affected cells in which chloroplasts are surrounded by areas and dots of unimported GFP (arrowheads). The right panel shows more severely affected cells in which the vast majority of GFP remains unimported and accumulates in the cytosol. Seeds of the different genotypes were germinated and grown for 7 days in continuous light. Representative images from two independent experiments with similar results are shown. Scale bars: 20  $\mu\text{m}$ .



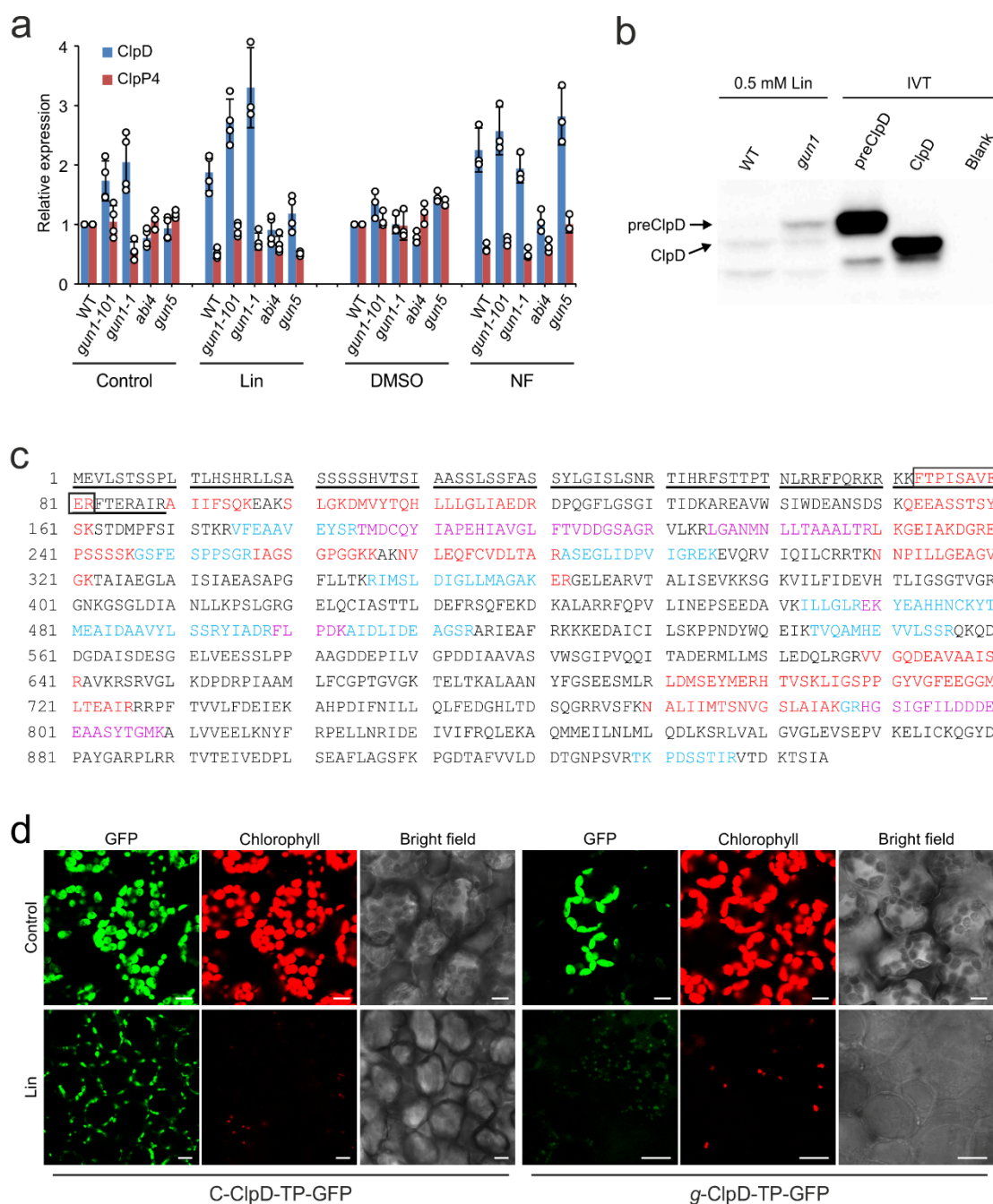
**Supplementary Figure 23. Accumulation of selected chloroplast proteins under Lin or NF treatment.**

**a**, Western blot analysis of the chloroplast chaperones ClpC and cpHSC70. Protein accumulation levels are very similar in the wild type (WT), the *gun1* mutants and the OE lines both under control conditions and upon Lin treatment (0.5 mM). This result also excludes the possibility that reduced protein import in *gun1* is caused by reduced protein levels of ClpC or cpHSC70. Actin served as loading control.

**b**, Western blot analysis of the accumulation of the photosynthesis proteins LHCb1 and PsbO. Accumulation of both proteins is completely abolished in all genotypes upon Lin treatment (0.5 mM).

**c**, Western blot analysis shows that the ClpP4 protein is reduced in *gun1* mutants compared to the wild type, the complemented lines and the overexpression lines upon NF treatment (5  $\mu$ M). LHCb1 was included as a control protein which is fully repressed by NF treatment. The lower panel shows accumulation of the chloroplast cpHSC70 in the wild type and the *gun1* mutants as an additional control confirming that the reduction of

ClpP4 is specific. In **a-c**, representative images from three independent experiments with similar results are shown.



**Supplementary Figure 24. *ClpD* and *ClpP4* expression, preClpD migration behavior, ClpD peptides identified by mass spectrometry, and individual images for Figure 3e.**

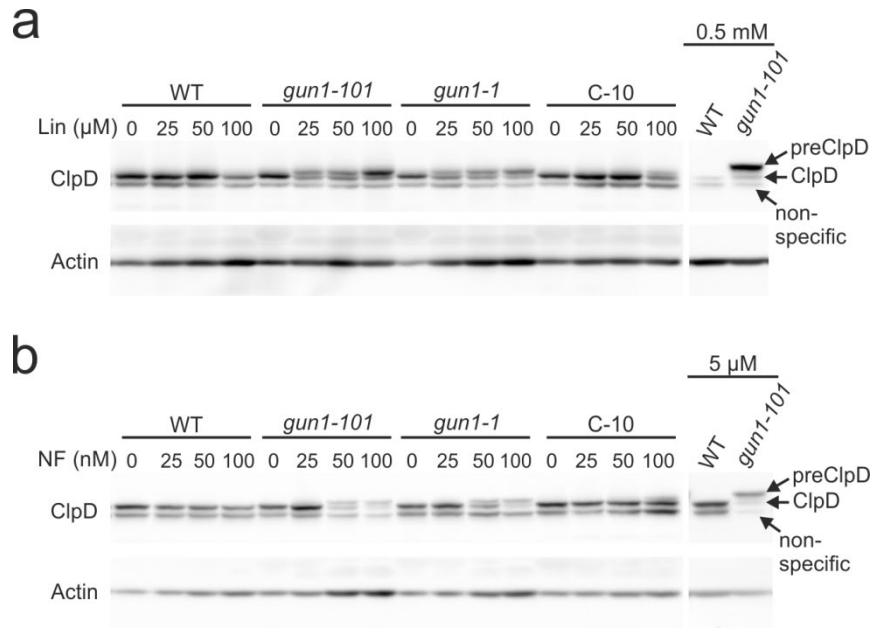
**a**, qRT-PCR analysis shows that the expression of *ClpD* and *ClpP4* is not repressed by Lin (0.5 mM) or NF (5  $\mu$ M) treatment. Relative gene expression in the different mutants is compared to that in the wild type under control conditions (Control and DMSO for Lin

and NF treatments, respectively). The data are presented as means  $\pm$  s.d. ( $n=3$  biologically independent samples, indicated as open circles).

**b**, Immunoblot analysis demonstrating that the larger ClpD band migrates exactly as preClpD generated by *in vitro* translation (IVT). Blank: IVT without the *ClpD* template. Two independent experiments were performed and showed similar results.

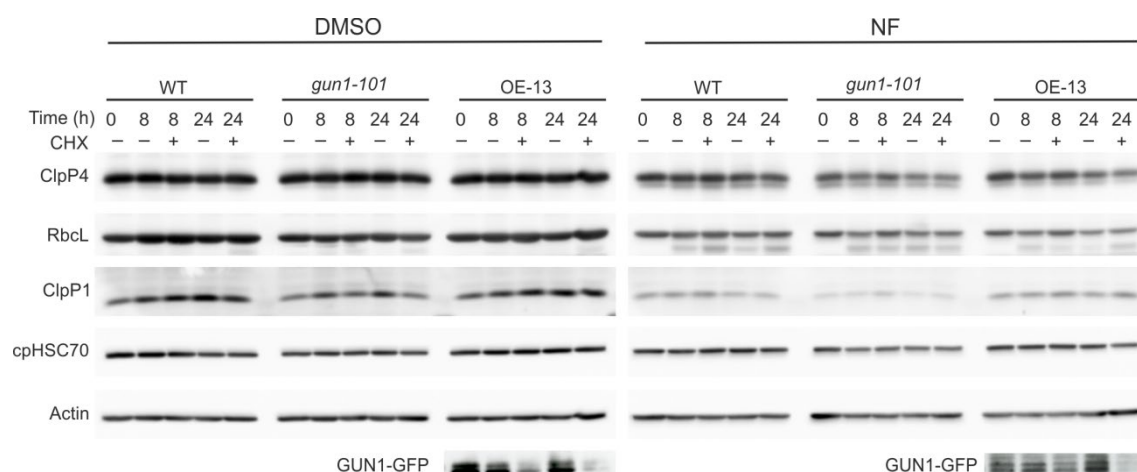
**c**, Peptides of ClpD that were identified by mass spectrometry-based proteomics in the wild type and the *gun1-101* mutant upon Lin treatment. The unique peptides that were identified only in the wild type or only in the *gun1* mutant are indicated in purple and red, respectively. Peptides identified in both genotypes are shown in blue. The transit peptide region as predicted by ChloroP1.1 (<http://www.cbs.dtu.dk/services/ChloroP/>) is underlined. Note the peptide derived from the transit peptide region that was only identified in the *gun1* mutant (boxed).

**d**, Individual images for the overlaid images shown in Fig. 3e. Scale bars, 10  $\mu$ m.



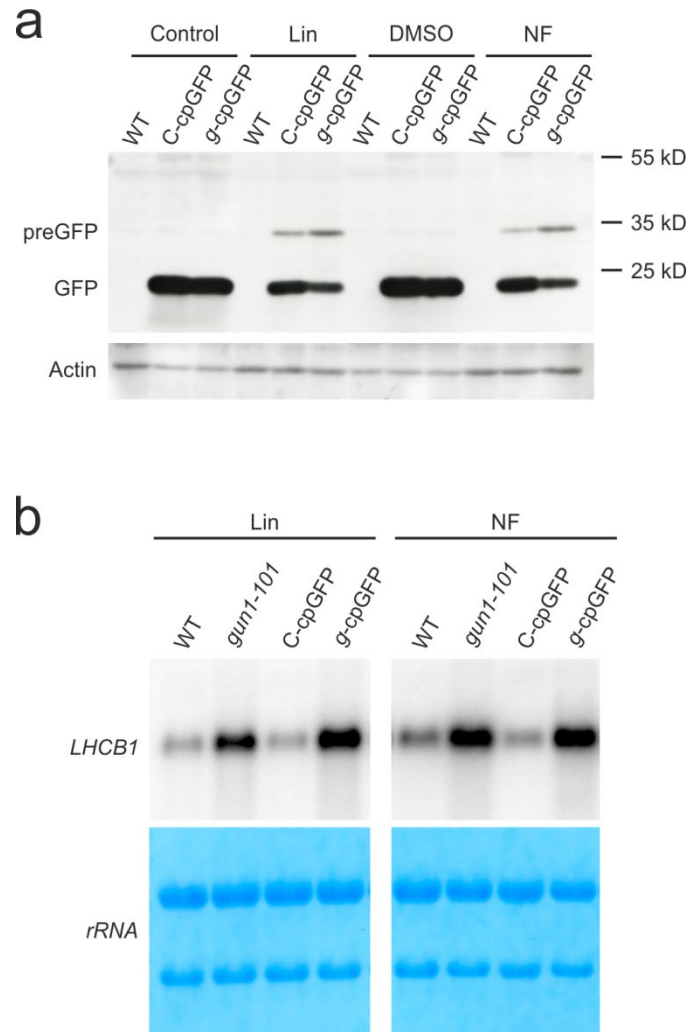
**Supplementary Figure 25. Immunoblots showing that PreClpD accumulation is positively correlated with the strength of the Lin (a) and NF (b) treatments.**

The partially complemented line C-10 also starts to accumulate preClpD at 100  $\mu$ M Lin or 100 nM NF. Seedlings were germinated and grown for 7 days in long-day conditions. Two independent experiments were performed and showed similar results. Actin served as loading control.



**Supplementary Figure 26. CHX chase assays showing that the turnover of ClpP4 is comparable in the wild type, *gun1-101* and the GUN1-GFP overexpression line (OE-13).**

Seven-day-old seedlings grown on plates with 0.1% DMSO or 5  $\mu$ M NF were transferred to liquid medium with (+) or without (-) CHX and with DMSO or 5  $\mu$ M NF. Samples were collected at different time points as indicated. The accumulation of ClpP4 was then analyzed by immunoblots. Plastid genome-encoded proteins RbcL and ClpP1 served as loading control, as CHX inhibits only cytosolic translation but not protein synthesis in the chloroplast. The nucleus-encoded chloroplast protein cpHSC70 and a cytosolic housekeeping protein (actin) were also analyzed. GUN1-GFP turnover was analyzed in OE-13 lines and showed fast turnover as described previously<sup>18</sup>. It served as control for a rapidly turned-over protein. Two independent experiments were performed and showed similar results.

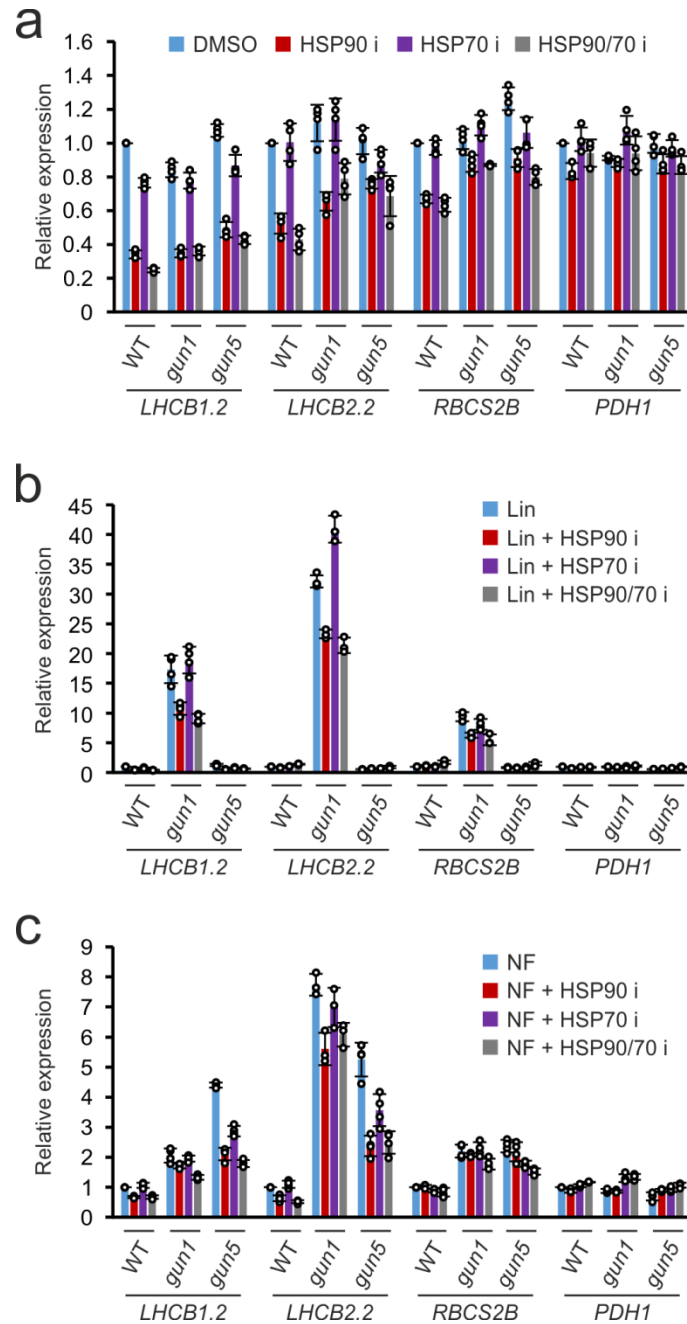


**Supplementary Figure 27. Accumulation of the cpGFP precursor upon treatment with Lin or NF, and analysis of its effects on retrograde signaling.**

**a**, Western blot analysis of cpGFP transgenic lines reveals precursor accumulation in the presence of Lin or NF. The cpGFP lines in the wild-type background (C-cpGFP) or the *gun1-101* background (g-cpGFP) were grown without (control or DMSO) or with 0.5 mM Lin or 5  $\mu$ M NF for 11 days. Actin was used as loading control.



**b**, Northern blot analysis of *LHCBI* expression upon treatment with 0.5 mM Lin or 5  $\mu$ M NF of cpGFP lines, the wild type and *gun1-101*. Whereas the C-cpGFP line does not show a GUN phenotype, the *g*-cpGFP line shows an enhanced GUN phenotype compared to the untransformed *gun1-101* in the presence of Lin, but not NF. Methylene blue staining of rRNAs served as loading control. In both **a** and **b**, two independent experiments were performed and showed similar results.



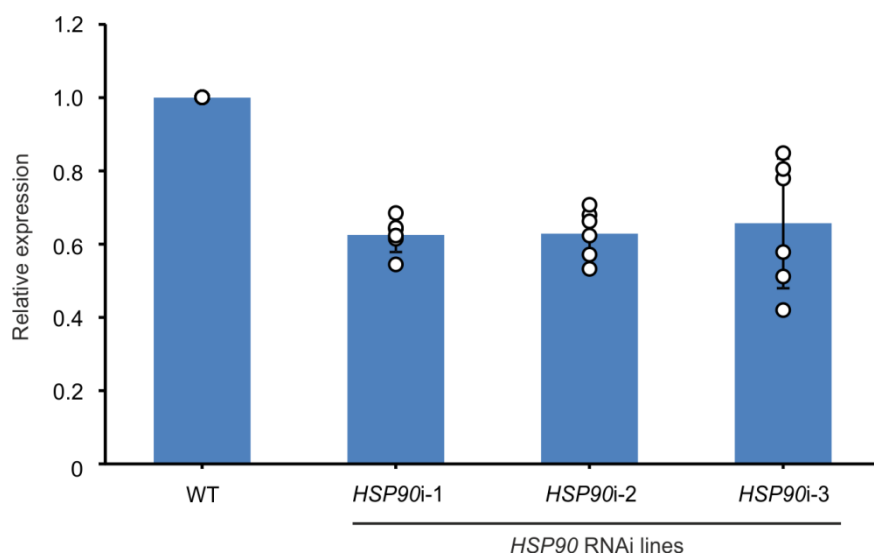
**Supplementary Figure 28. HSP90 and HSP70 inhibitor treatments as shown in Figure 5c-e, but using the HSP70 inhibitor PES-Cl+Az and 25  $\mu$ M of the HSP90 inhibitor GDA.**

**a**, PhANG expression is positively correlated with HSP90 activity. qRT-PCR shows that expression of *LHCBI.2*, *LHCBI.2* and *RBCS2B* is repressed when seedlings were treated

with 25  $\mu$ M HSP90 inhibitor GDA (HSP90 i), whereas HSP70 inhibition (HSP70 i) by PES-Cl (10  $\mu$ M) + Az (0.4  $\mu$ M) has much less effects. Combined inhibition of HSP90 and HSP70 (HSP90/70 i) has only minor additive effects. Relative gene expression is compared to expression in the wild type (WT) under control conditions (DMSO). *PDHI* was used as negative control.

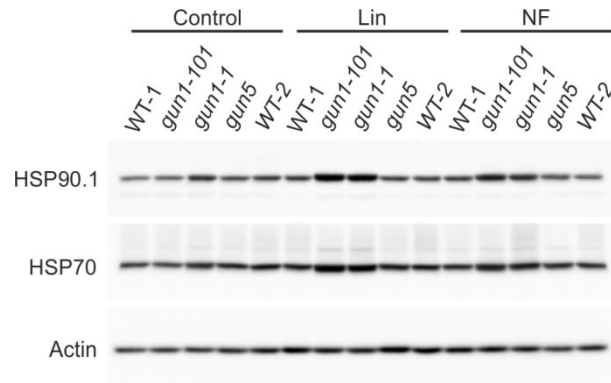
**b,** Inhibition of HSP90 activity suppresses the PGE pathway of retrograde signaling. The GUN phenotype of the *gun1* mutant (*gun1-101*) in the presence of 0.5 mM Lin is suppressed by GDA treatment (HSP90 i) inhibiting HSP90 activity. Inhibition of HSP70 (by PES-Cl + Az, HSP70 i) has no effect on PhANG expression, and combined inhibition of both HSP90 and HSP70 (HSP90/70 i) has similar effects as inhibition of HSP90 alone. Relative gene expression is compared to the expression of the wild type in the Lin treatment without HSP90 and HSP70 inhibitors. *PDHI* was used as negative control.

**c,** Inhibition of HSP90 activity affects the TPB pathway of retrograde signaling. The GUN phenotype of the *gun5* mutant (to a less extent in *gun1* mutant) in the presence of 5  $\mu$ M NF is suppressed by HSP90 inhibition (HSP90 i). Combined inhibition of both HSP90 and HSP70 (HSP90/70 i) has only minor additive effects on suppression of the GUN phenotype. Relative gene expression is compared to the expression of the wild type in the NF treatment without HSP90 and HSP70 inhibitors. *PDHI* was used as negative control. In **a-c**, the data are presented as means  $\pm$  s.d. ( $n=4$  biologically independent samples, indicated as open circles).



**Supplementary Figure 29. qRT-PCR analysis confirms the knock-down of *HSP90* in three independent RNAi lines (*HSP90i*).**

Three independent RNAi lines of *HSP90* published previously<sup>43</sup> were obtained and the relative expression of *HSP90* was analyzed by qRT-PCR. The relative expression of *HSP90* was normalized to actin and is presented as means  $\pm$  s.d. ( $n=6$ , from three biologically independent samples, with two technical replicates performed for each biologically independent sample; all replicates are indicated as open circles). Young rosette leaves ( $\sim 1$  cm) from 4 week-old soil-grown plants were used for RNA extraction.



**Supplementary Figure 30. Western blots show that cytosolic HSP90.1 and HSP70 do not over-accumulate in *gun5* upon Lin or NF treatment.**

Seedlings were grown in the absence (control) or presence of 0.5 mM Lin or 5  $\mu$ M NF for 7 days (control) and 11 days (Lin and NF treatments), respectively. Two independent experiments were performed and showed similar results. Actin was used as loading control.

**Supplementary Table 1. Summary of mass spectrometry data from four independent comparative co-IP experiments (Exp-1 to Exp-4) performed with the GUN1-GFP-Expressing (OE-13) transgenic lines in rosette leaves.**

The chloroplast localized GFP line in wild type background (by RBCS transit peptide, C-cpGFP) was used as co-IP control. Genes that were identified in all four experiments and passed the data quality criteria and filtering thresholds (see Methods) are shown in this list (cf. Supplementary Data 2).

	Exp-1			Exp-2			Exp-3			Exp-4			
AGI code	Protein ion intensity	Unique peptide number	Sequence coverage	Protein ion intensity	Unique peptide number	Sequence coverage	Protein ion intensity	Unique peptide number	Sequence coverage	Protein ion intensity	Unique peptide number	Sequence coverage	Annotation
AT2G31400	2.56E+08	38	46.6	3.16E+09	51	69.4	1.36E+08	16	24	3.04E+07	15	19	GUN1
AT5G50920	1.92E+07	8	35.7	1.99E+08	34	47.9	2.44E+08	23	34	3.18E+07	9	37	ClpC1
AT5G64940	1.74E+07	14	24.2	7.56E+08	30	38.4	3.53E+07	7	11	1.50E+07	10	14	ATH13
AT1G06950	1.72E+07	19	23.5	5.82E+07	14	21.7	1.41E+08	17	21	2.93E+07	17	19	Tic110
AT4G18480	5.69E+06	5	16.3	2.29E+07	7	27.6	4.65E+07	6	19	2.23E+06	2	8	CHL11
AT2G40100	4.87E+06	2	18.1	1.46E+07	2	15.9	1.77E+08	4	31	1.76E+07	4	24	LHCB4.3
AT1G80030	2.92E+06	4	10.2	1.15E+08	12	38.6	5.15E+07	8	23	8.61E+05	2	4	Hsp40/DnaJ-like protein

AT1G79600	2.33E+06	7	12	2.37E+06	2	3	1.48E+07	4	6	9.91E+06	11	17	ABC1-like kinase 3
AT5G12470	2.30E+06	4	10.4	1.49E+07	3	10.9	9.99E+06	4	15	1.48E+06	2	4	Unknown
AT5G03940	2.02E+06	4	9.4	6.02E+06	2	3.7	1.01E+07	2	4	7.95E+06	7	15	cpSRP54
ATCG00740	1.05E+06	2	8.5	4.74E+07	6	29.5	3.40E+07	3	10	5.07E+06	4	14	RpoA
ATCG01130	4.93E+05	4	2.6	1.10E+08	37	23.3	1.29E+07	3	2	1.14E+06	2	1	Ycf1
AT4G02510	3.46E+05	3	3.2	7.52E+06	5	4.9	5.49E+06	3	2	2.31E+06	4	3	Toc159

**Supplementary Table 2. Proteins identified in Co-IP experiments performed with de-etiolating seedlings of OE-13 and complemented line C-1 grown in the presence or absence of Lin.**

C-cpGFP was used as control. Genes that passed the data quality criteria and filtering thresholds (see Methods) and were identified in both OE-13 and C-1 are listed (cf. Supplementary Data 2).

		OE-13			C-1			
	AGI code	Protein ion intensity	Unique peptide number	Sequence coverage	Protein ion intensity	Unique peptide number	Sequence coverage	Annotation
Control	AT2G31400	2.80E+08	33	42	1.22E+08	32	42	GUN1
	AT4G24280	1.67E+07	2	13.6	9.06E+06	2	13.6	cpHSC70-1
	AT3G26650	1.12E+07	5	23	2.07E+07	6	31.1	GAPA
	AT1G42970	2.59E+06	3	14.8	4.12E+06	3	16.3	GAPB
	AT3G12780	1.50E+06	3	8.1	3.57E+06	5	12.7	PGK1
	AT3G11630	1.02E+06	3	16.5	8.23E+06	5	28.2	2-Cys peroxiredoxin
	AT1G61520	4.92E+05	2	9.2	3.67E+06	3	13.6	LHCA3
	AT3G46740	4.36E+05	3	7.1	7.44E+05	4	8.3	TOC75-3
	AT5G63570	3.05E+05	2	6.8	2.88E+06	2	6.8	GSA1
	ATCG00130	1.55E+05	2	11.4	1.78E+06	3	16.3	AtpF



Lincomycin	AT2G31400	1.42E+08	29	38.2	6.68E+07	32	41	GUN1
	AT3G46740	2.31E+07	9	16.4	9.27E+06	9	16.4	TOC75-3
	AT4G24280	8.39E+06	2	13.6	3.93E+06	2	13.6	cpHSC70-1
	AT4G02510	7.25E+06	5	4.6	2.23E+06	4	3.3	TOC159
	AT1G02280	2.60E+06	4	19.5	2.11E+06	3	16.2	TOC33
	AT5G26742	1.99E+06	2	2.8	8.25E+05	2	2.8	DEAD-box RNA helicase 3

**Supplementary Table 3. Summary of mass spectrometry data from two independent comparative co-IP experiments (Exp-1 and Exp-2) performed with OE-13 lines crossed into the *clpC1-1* background.**

C-cpGFP crossed into the *clpC1-1* background was used as control. Genes that were identified in both experiments and passed the data quality criteria and filtering thresholds (see Methods) are included in the list. Ribosomal proteins identified as general contaminants were removed (cf. Supplementary Data 2).

AGI code	Exp-1			Exp-2			Annotation
	Protein ion intensity	Unique peptide number	Sequence coverage	Protein ion intensity	Unique peptide number	Sequence coverage	
AT2G31400	1.94E+09	51	63.9	3.85E+09	44	55.1	GUN1
AT4G24280	3.13E+07	3	19.8	3.11E+08	5	28.1	cpHSC70-1
AT3G11630	1.65E+07	4	24.8	1.80E+08	3	37.6	2-Cys peroxiredoxin
ATCG01110	6.80E+06	3	12	1.12E+08	9	25.7	NdhH
AT5G10160	4.50E+06	2	7.3	3.06E+08	5	30.1	3-hydroxyacyl-ACP dehydratase
AT4G13670	2.48E+06	2	7.8	9.18E+07	5	21.7	PTAC5

AT1G03630	2.08E+06	3	9.5	1.97E+07	3	12.2	POR C
AT2G39670	1.38E+06	2	7.4	6.06E+07	6	23	Radical SAM domain-containing protein
AT3G45140	1.33E+06	2	2.7	4.15E+07	7	10.8	LOX2

---

**Supplementary Table 4. qRT-PCR analysis of PhANG expression in ClpD and ClpD-GFP overexpression lines in the wild-type (C-ClpD) and the *gun1-101* (g-ClpD) background.**

Gene expression was analyzed by qRT-PCR and normalized to actin mRNA levels. The relative expression of each gene in the different genotypes was compared to the wild type (WT) under the same condition (Lin or NF). The data are presented as means  $\pm$  s.d. ( $n=3$  biologically independent samples).

Lin								
	WT	C-ClpD-1	C-ClpD-5	C-ClpD-GFP-12	<i>gun1-101</i>	<i>g</i> -ClpD-4	<i>g</i> -ClpD-5	<i>g</i> -ClpD-GFP-14
<i>LHCB1.2</i>	1	2.13 $\pm$ 0.14	2.09 $\pm$ 0.16	2.89 $\pm$ 0.07	13.74 $\pm$ 0.99	24.6 $\pm$ 2.26	31.58 $\pm$ 1.72	39.67 $\pm$ 1.25
<i>LHCB2.2</i>	1	2.77 $\pm$ 0.24	2.23 $\pm$ 0.14	2.71 $\pm$ 0.17	13.41 $\pm$ 1.14	25.21 $\pm$ 1.29	26.44 $\pm$ 1.85	42.74 $\pm$ 4.35
<i>RBCS2B</i>	1	2.62 $\pm$ 0.30	2.23 $\pm$ 0.26	2.20 $\pm$ 0.10	3.58 $\pm$ 0.50	5.19 $\pm$ 0.58	6.07 $\pm$ 0.63	10.68 $\pm$ 0.70
NF								
	WT	C-ClpD-1	C-ClpD-5	C-ClpD-GFP-12	<i>gun1-101</i>	<i>g</i> -ClpD-4	<i>g</i> -ClpD-5	<i>g</i> -ClpD-GFP-14
<i>LHCB1.2</i>	1	2.57 $\pm$ 0.43	2.07 $\pm$ 0.14	1.41 $\pm$ 0.06	2.16 $\pm$ 0.14	3.92 $\pm$ 0.31	3.7 $\pm$ 0.31	3.99 $\pm$ 0.14
<i>LHCB2.2</i>	1	4.12 $\pm$ 0.35	2.76 $\pm$ 0.13	1.57 $\pm$ 0.05	12.16 $\pm$ 0.86	17.3 $\pm$ 1.11	14.06 $\pm$ 1.05	18.76 $\pm$ 0.58
<i>RBCS2B</i>	1	1.45 $\pm$ 0.03	1.16 $\pm$ 0.05	1.31 $\pm$ 0.09	1.43 $\pm$ 0.04	1.62 $\pm$ 0.15	1.59 $\pm$ 0.06	2.01 $\pm$ 0.09

**Supplementary Table 5. List of all oligonucleotides used in this study for genotyping, cloning, qPCR and northern blot analyses.**

Restriction sites used for cloning are underlined in the sequences.

Oligonucleotide	Sequence (5'-3')	Description and usage
Tic40-S	GAGGGCCGGGTTTATCTGTA	Forward primer for <i>tic40-4</i> T-DNA insertion mutant identification
Tic40-A	TCCTGGGAAGAGCTGCGATA	Reverse primer for <i>tic40-4</i> T-DNA insertion mutant identification
HSC-70.1-2S	CGAAGAGTGGTGATAGGCTTG	Forward primer for <i>cphsc70-1</i> T-DNA insertion mutant identification
HSC-70.1-2A	TCTGCTGCCTCTGTAAACCTC	Reverse primer for <i>cphsc70-1</i> T-DNA insertion mutant identification
ClpD-S	CTGTTTGGAGTATTTGGGACG	Forward primer for <i>clpd-1</i> and <i>clpd-2</i> T-DNA insertion mutants identification
ClpD-A	GGGCTTTGTCCTTCTCAAACCT	Reverse primer for <i>clpd-1</i> and <i>clpd-2</i> T-DNA insertion mutant identification
ClpR1-S	GCCTTGCTCTACTGTTCCCTA	Forward primer for <i>clpr1-2</i> T-DNA insertion mutant identification
ClpR1-A	TGGGCTTTGTTGGGTTATCAT	Reverse primer for <i>clpr1-2</i> T-DNA insertion mutant identification
ClpD-2S	CTCAAGCTTCGAATTCTGATGGAGGTGTTATCTACTTCC	Forward primer for amplifying full length <i>ClpD</i> or the transit peptide sequence of <i>ClpD</i> , including an EcoRI site
ClpD-2A	GGCAGCAGCCGGATCCCGCTATGCGATCGATGTTTTGTCTGT	Reverse primer for amplifying full length <i>ClpD</i> , including a BamHI site
ClpD-3A	GGCAGCAGCCGGATCCCGTCTGATCGCTCGTTCGGTG	Reverse primer for amplifying the transit peptide of <i>ClpD</i> , including a BamHI site
ClpD-3S	GACCGCGATCGCCATGGAGGTGTTATCTACTTCCT	Forward primer for amplifying the full length <i>ClpD</i> for <i>in vitro</i> translation, including a SgfI site
ClpD-4S	CTAAGCGATCGCCATGGCTATAATCTTCTCTCAGAAGG	Forward primer for amplifying the mature <i>ClpD</i> for <i>in vitro</i> translation, including a SgfI site
ClpD-4A	GTCGGTTTAAACCTATGCGATCGATGTTTTGTCT	Reverse primer for amplifying <i>ClpD</i> for <i>in vitro</i> translation including a PmeI site
ClpD-5A	GGCAGCAGCCGGATCCCGTGCATCGATGTTTTGTCTGT	Reverse primer for amplifying full length <i>ClpD</i> for fusion with GFP, including a BamHI site
GUN1-gateway-S	CACCATGGCGTCAACGCCGCCTC	Forward primer for amplifying full length <i>GUN1</i> for gateway entry cloning

GUN1-gateway-A	CAAAAGAAGAGGCTGTAAAGC	Reverse primer for amplifying full length <i>GUN1</i> for gateway entry cloning
ClpC-gateway-S	CACCATGGCTATGGCCACAAGGGT	Forward primer for amplifying full length <i>CLPC1</i> for gateway entry cloning
ClpC-gateway-A	AGCAACAGGGAGAGAATCTTC	Reverse primer for amplifying full length <i>CLPC1</i> for gateway entry cloning
Tic110-gateway-S	CACCATGAATCCCTCACTCGTCAC	Forward primer for amplifying full length <i>Tic110</i> for gateway entry cloning
Tic110-gateway-A	AAAGACGAAATTGCCCTCTTC	Reverse primer for amplifying full length <i>Tic110</i> for gateway entry cloning
ClpD-gateway-S	CACCATGGAGGTGTTATCTACTTCC	Forward primer for amplifying full length <i>ClpD</i> for gateway entry cloning
ClpD-gateway-A	TGCGATCGATGTTTTGTCTGT	Reverse primer for amplifying full length <i>ClpD</i> for gateway entry cloning
HSC70.1-gateway-S	CACCATGGCATCTTCAGCCGCC	Forward primer for amplifying full length <i>cpHSC70-1</i> for gateway entry cloning
HSC70.1-gateway-A	TTGGCTGTCTGTGAAGTCAG	Reverse primer for amplifying full length <i>cpHSC70-1</i> for gateway entry cloning
rpoB-qS	ATGGTGCTGTACAGTTGGT	Forward primer for quantification of ptDNA
rpoB-qA	AGGACCTTGGGTGTCACAT	Reverse primer for quantification of ptDNA
AT2G36250-qS	CGAGTAACTACAATGAGGCG	Forward primer of nuclear control gene for quantification of ptDNA
AT2G36250-qA	CTATTATCAGGCAAAACAGGAG	Reverse primer of nuclear control gene for quantification of ptDNA
LHCB1.2-qS	GCCGATCCAGTCAACAACA	Forward primer for qRT-PCR analysis for <i>LHCB1.2</i>
LHCB1.2-qA	AAAGTCTCAAACCATCACATAC	Reverse primer for qRT-PCR analysis for <i>LHCB1.2</i>
LHCB1.2-2S	GAGACTACGGATGGGACAC	Forward primer for amplifying <i>LHCB1.2</i> northern blot probe (with LHCB1.2-qA)
LHCB2.2-qS	CAACGCCTGGTCTTACGCT	Forward primer for qRT-PCR analysis for <i>LHCB1.2</i>
LHCB2.2-qA	AAGTGCCAAATTCACATCAAAC	Reverse primer for qRT-PCR analysis for <i>LHCB1.2</i>
RBCS2B-qS	ATACTATGATGGACGATACTGG	Forward primer for qRT-PCR analysis for <i>RBCS2B</i>
RBCS2B-qA	CGAATCCGATGATCCTAATGA	Reverse primer for qRT-PCR analysis for <i>RBCS2B</i>
PDH1-qS	GCTCAACACCTTACAACGCTA	Forward primer for qRT-PCR analysis for <i>PDH1</i>
PDH1-qA	GGGTCTGACCATTCTGCTT	Reverse primer for qRT-PCR analysis for <i>PDH1</i>
P3	TCTACAATGCCCTAACTGACA	Forward primer for qRT-PCR analysis for <i>GUN1</i>

P4	AGACAATGGAGCGTATGTTTA	Reverse primer for qRT-PCR analysis for <i>GUN1</i>
P338	GTGGCTACTAAACATACGCTC	Forward primer for qRT-PCR analysis for <i>GUN1</i>
P339	AAAAGAACTTCAACCGCTCGT	Reverse primer for qRT-PCR analysis for <i>GUN1</i>
P365	TCGTTTGCTTTACAGCCTCTT	Forward primer for qRT-PCR analysis for <i>GUN1</i>
P366	AACTTGTGGCCGTTTACGTC	Reverse primer for qRT-PCR analysis for <i>GFP</i> (coding sequence)
P367	TCAATCGAGTTGCTTTGTTACA	Reverse primer for qRT-PCR analysis for <i>GUN1</i> (3' UTR)
Hygromycin-S	TCGTTATGTTTATCGGCACTTT	Forward primer for qRT-PCR analysis for hygromycin resistance gene
Hygromycin-A	GCGGGAGATGCAATAGGTC	Reverse primer for qRT-PCR analysis for hygromycin resistance gene
HSP90-qS	AAGAGAGCTCCTTTTGATCTC	Forward primer for qRT-PCR analysis for cytosolic <i>HSP90</i> gene family
HSP90-qA	TCTTCACAGTTGTCCATGATG	Reverse primer for qRT-PCR analysis for cytosolic <i>HSP90</i> gene family
ClpD-qS	AGTTTCACCATTTGGAGGATTG	Forward primer for qRT-PCR analysis for <i>ClpD</i>
ClpD-qA	CTCACGGACTAATCACTATGT	Reverse primer for qRT-PCR analysis for <i>ClpD</i>
ClpP4-qS	CTACGAGGAGATTAGCAAGG	Forward primer for qRT-PCR analysis for <i>ClpP4</i>
ClpP4-qA	AATACCAGTAACCGCAGAAGA	Reverse primer for qRT-PCR analysis for <i>ClpP4</i>
Actin-qS	CCGGTATTGTGCTCGATTCTG	Forward primer for qRT-PCR analysis for <i>Actin</i>
Actin-qA	TTCCCGTTCTGCGGTAGTGG	Reverse primer for qRT-PCR analysis for <i>Actin</i>
clpP-S	GAAGGAGATACATCTTGGGTT	Forward primer for amplifying the <i>clpP</i> northern blot probe
clpP-A	GTGAGGGAATGCTATACGTTT	Reverse primer for amplifying the <i>clpP</i> northern blot probe
psbJ-S	ATGGCTGATACTACTGGAAG	Forward primer for amplifying the <i>psbJ</i> northern blot probe
psbJ-A	CTACAGGGATGAACCTAATC	Reverse primer for amplifying the <i>psbJ</i> northern blot probe
rpoB-S	AAGTGGCTTTAGATTCAAGG	Forward primer for amplifying the <i>rpoB</i> northern blot probe
rpoB-A	AGCATAGGAGGATTCTTTTCG	Reverse primer for amplifying the <i>rpoB</i> northern blot probe
ndhG-S	GATTTGCCTGGACCAATACAT	Forward primer for amplifying the <i>ndhG</i> northern blot probe

ndhG-A	AGCCACAGAAATTGCACCTAT	Reverse primer for amplifying the <i>ndhG</i> northern blot probe
psaJ-S	ATGCGAGATCTAAAAACATATCT	Forward primer for amplifying the <i>psaJ</i> northern blot probe
psaJ-A	CTAGAATGAAAAAAGGGAAATG	Reverse primer for amplifying the <i>psaJ</i> northern blot probe

---